ELECTRONIC SUPPLEMENTARY INFORMATION

Identification of New Oxospiro Chromane Quinoline-Carboxylate Antimalarials that Arrest Parasite Growth at Ring Stage

Ehtesham Jameel[a,†], Hari Madhav[a,†], Prakhar Agrawal[b], Md. Kausar Raza[c], Saiema Ahmedi[d], Abdur Rahman[a], Nida Shahid[e], Kashfa Shaheen[a], Chhaya Haresh Gajra[b], Ashma Khan[f], Md. Zubbair Malik[g], Md Ali Imam[h], Md. Kalamuddin[d], Jitendra Kumar[i], Dinesh Gupta[b], Shahid M. Nayeem[f], Nikhat Manzoor[c], Asif Mohammad[b], Pawan Malhotra[b,*] and Nasimul Hoda[a,*]

[a]Drug Design and Synthesis Laboratory, Department of Chemistry, Jamia Millia Islamia, New Delhi, India-110025
[b]International Centre for Genetic Engineering and Biotechnology (ICGEB), Aruna Asaf Ali Marg, New Delhi, India-110067
[c]Department of Chemistry and Chemical Engineering, California Institute of Technology (Caltech), Pasadena, CA 91125-7200
[d]Medical Mycology Lab, Department of Biosciences, Jamia Millia Islamia, New Delhi, India-110025
[e]Department of Chemistry, Jamia Millia Islamia, New Delhi-110025
[f]Department of Chemistry, Aligarh Muslim University, Aligarh, Uttar Pradesh, India-202002
[g]School of Computational Biology, Jawaharlal Nehru University, JNU Campus Road, New Delhi, India-110067
[h]Centre for Interdisciplinary Research in Basic Sciences, Jamia Millia Islamia, New Delhi, India-110025
[i]Department of Chemistry, Sardar Vallabhbhai Patel College, Bhabua, Kaimur- 821101, V. K. S. U., Ara, Bihar, India-802301

[†]Joint First Authors (These authors contributed equally to the article).

[*]Corresponding Authors

Dr. Nasimul Hoda
Professor,
Drug Design and Synthesis Laboratory,
Department of Chemistry,
Jamia Millia Islamia, New Delhi,
India -110025.
Email: nhoda@jmi.ac.in

Dr. Pawan Malhotra
Group Leader, Malaria Biology
International Centre for Genetic Engineering and Biotechnology,
New Delhi, India - 110067.
Email: pawanmal@gmail.com;
pawanm@icgeb.res.in

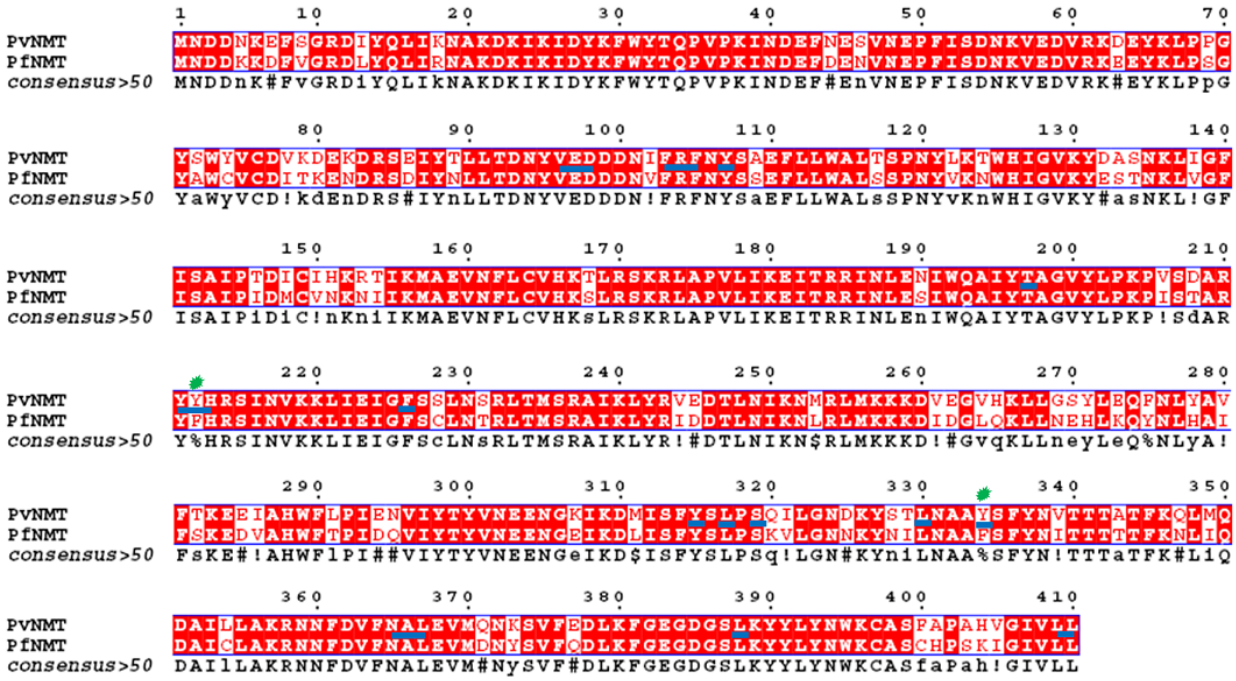

Figure S1: Sequence alignment of *Pv*NMT and *Pf*NMT. Adopted with permission from Supplementary Information of Yu, *et al*. [J. Med. Chem. 2012, 55, 20, 8879–8890]. Copyright 2012 American Chemical Society.

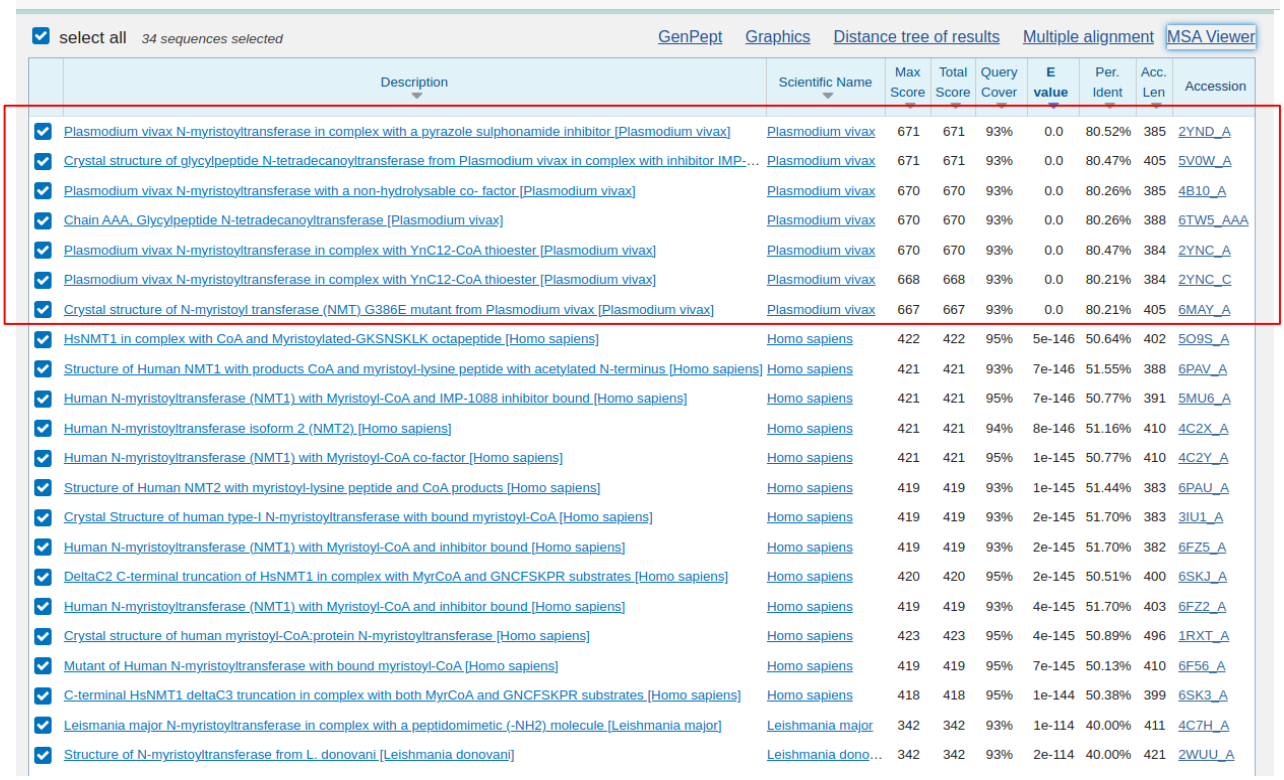

select all 34 sequences selected | GenPept | Graphics | Distance tree of results | Multiple alignment | MSA Viewer

Description	Scientific Name	Max Score	Total Score	Query Cover	E value	Per. Ident	Acc. Len	Accession
Plasmodium vivax N-myristoyltransferase in complex with a pyrazole sulphonamide inhibitor [Plasmodium vivax]	Plasmodium vivax	671	671	93%	0.0	80.52%	385	2YND_A
Crystal structure of glycylpeptide N-tetradecanoyltransferase from Plasmodium vivax in complex with inhibitor IMP-...	Plasmodium vivax	671	671	93%	0.0	80.47%	405	5V0W_A
Plasmodium vivax N-myristoyltransferase with a non-hydrolysable co- factor [Plasmodium vivax]	Plasmodium vivax	670	670	93%	0.0	80.26%	385	4B10_A
Chain AAA, Glycylpeptide N-tetradecanoyltransferase [Plasmodium vivax]	Plasmodium vivax	670	670	93%	0.0	80.26%	388	6TW5_AAA
Plasmodium vivax N-myristoyltransferase in complex with YnC12-CoA thioester [Plasmodium vivax]	Plasmodium vivax	670	670	93%	0.0	80.47%	384	2YNC_A
Plasmodium vivax N-myristoyltransferase in complex with YnC12-CoA thioester [Plasmodium vivax]	Plasmodium vivax	668	668	93%	0.0	80.21%	384	2YNC_C
Crystal structure of N-myristoyl transferase (NMT) G386E mutant from Plasmodium vivax [Plasmodium vivax]	Plasmodium vivax	667	667	93%	0.0	80.21%	405	6MAY_A
HsNMT1 in complex with CoA and Myristoylated-GKSNSKLK octapeptide [Homo sapiens]	Homo sapiens	422	422	95%	5e-146	50.64%	402	5O9S_A
Structure of Human NMT1 with products CoA and myristoyl-lysine peptide with acetylated N-terminus [Homo sapiens]	Homo sapiens	421	421	93%	7e-146	51.55%	388	6PAV_A
Human N-myristoyltransferase (NMT1) with Myristoyl-CoA and IMP-1088 inhibitor bound [Homo sapiens]	Homo sapiens	421	421	95%	7e-146	50.77%	391	5MU6_A
Human N-myristoyltransferase isoform 2 (NMT2) [Homo sapiens]	Homo sapiens	421	421	94%	8e-146	51.16%	410	4C2X_A
Human N-myristoyltransferase (NMT1) with Myristoyl-CoA co-factor [Homo sapiens]	Homo sapiens	421	421	95%	1e-145	50.77%	410	4C2Y_A
Structure of Human NMT2 with myristoyl-lysine peptide and CoA products [Homo sapiens]	Homo sapiens	419	419	93%	1e-145	51.44%	383	6PAU_A
Crystal Structure of human type-I N-myristoyltransferase with bound myristoyl-CoA [Homo sapiens]	Homo sapiens	419	419	93%	2e-145	51.70%	383	3IU1_A
Human N-myristoyltransferase (NMT1) with Myristoyl-CoA and inhibitor bound [Homo sapiens]	Homo sapiens	419	419	93%	2e-145	51.70%	382	6FZ5_A
DeltaC2 C-terminal truncation of HsNMT1 in complex with MyrCoA and GNCFSKPR substrates [Homo sapiens]	Homo sapiens	420	420	95%	2e-145	50.51%	400	6SKJ_A
Human N-myristoyltransferase (NMT1) with Myristoyl-CoA and inhibitor bound [Homo sapiens]	Homo sapiens	419	419	93%	4e-145	51.70%	403	6FZ2_A
Crystal structure of human myristoyl-CoA:protein N-myristoyltransferase [Homo sapiens]	Homo sapiens	423	423	95%	4e-145	50.89%	496	1RXT_A
Mutant of Human N-myristoyltransferase with bound myristoyl-CoA [Homo sapiens]	Homo sapiens	419	419	95%	7e-145	50.13%	410	6F56_A
C-terminal HsNMT1 deltaC3 truncation in complex with both MyrCoA and GNCFSKPR substrates [Homo sapiens]	Homo sapiens	418	418	95%	1e-144	50.38%	399	6SK3_A
Leismania major N-myristoyltransferase in complex with a peptidomimetic (-NH2) molecule [Leishmania major]	Leishmania major	342	342	93%	1e-114	40.00%	411	4C7H_A
Structure of N-myristoyltransferase from L. donovani [Leishmania donovani]	Leishmania dono...	342	342	93%	2e-114	40.00%	421	2WUU_A

Figure S2: Blast result against PDB database for Q8ILW6, NMT_PLAF7 Glycylpeptide N-tetradecanoyltransferase of *Plasmodium falciparum*.

```
Percent Identity  Matrix - created by Clustal2.1


  1: tr|A0A0J9SLR4|A0A0J9SLR4_PLAVI  100.00  100.00  100.00  100.00  100.00  100.00
  2: tr|A0A0J9TQB4|A0A0J9TQB4_PLAVI  100.00  100.00  100.00  100.00  100.00  100.00
  3: tr|A0A0J9S6C3|A0A0J9S6C3_PLAVI  100.00  100.00  100.00  100.00  100.00  100.00
  4: tr|A0A0J9T6X6|A0A0J9T6X6_PLAVI  100.00  100.00  100.00  100.00  100.00  100.00
  5: tr|A0A1G4HIY1|A0A1G4HIY1_PLAVI  100.00  100.00  100.00  100.00  100.00  100.00
  6: tr|A5K1A2|A5K1A2_PLAVS          100.00  100.00  100.00  100.00  100.00  100.00
```

Figure S3: Multiple Alignment Sequence using Clustal Omega (other amino acid sequence of *Pv*NMT from the organism *Plasmodium vivax* Brazil I, *Plasmodium vivax* North Korean, *Plasmodium vivax* India VII, *Plasmodium vivax* Mauritania I, *Plasmodium vivax* (malaria parasite *P. Vivax*) and *Plasmodium vivax* (strain Salvador I) respectively) showing 100% identity.

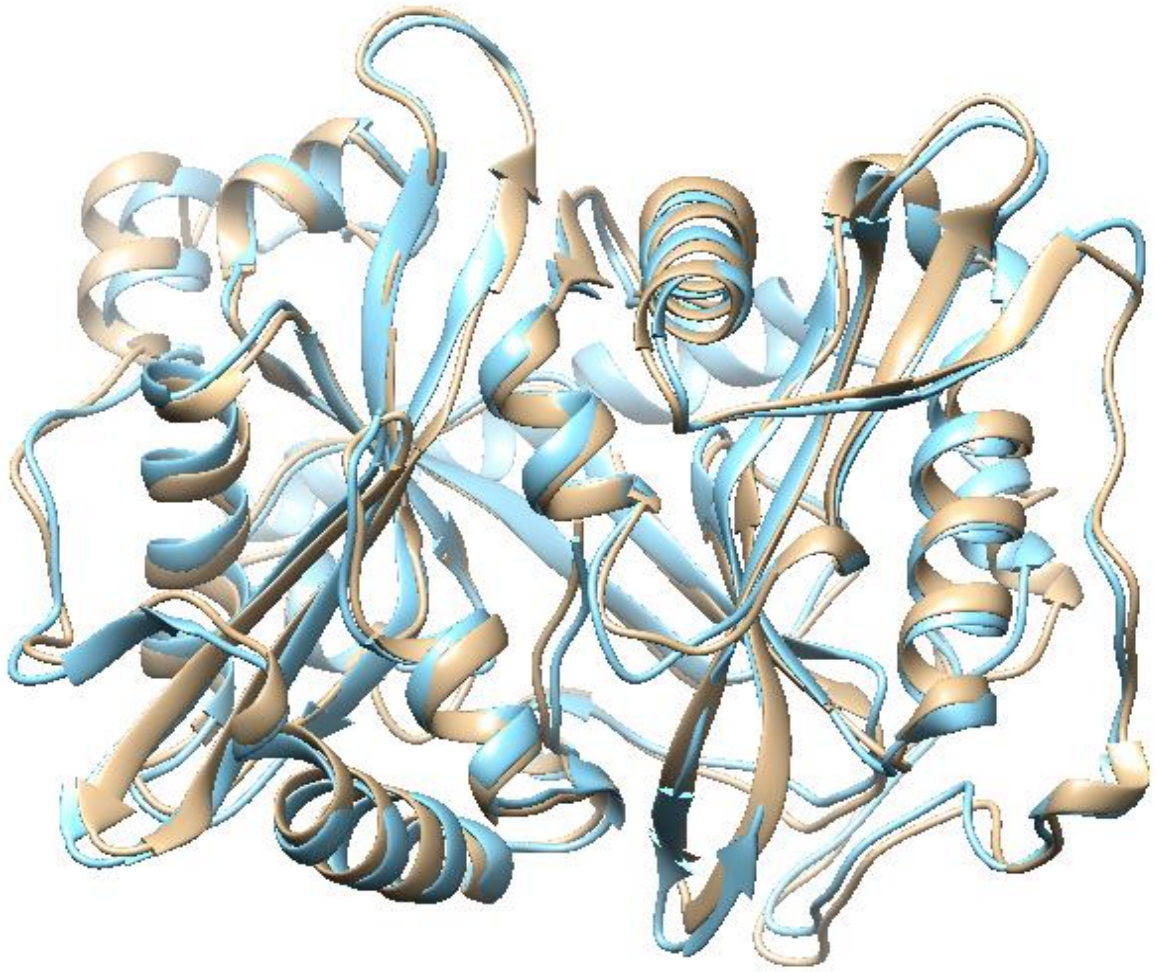

Figure S4: RMSD between 4BBH (*Plasmodium vivax*) and Robbeta Model-1. RMSD between 344 pruned atom pairs is 0.995 angstroms; (across all 384 pairs: 1.304). Blue: Robetta Model-1 and Grey: 4BBH Chain A.

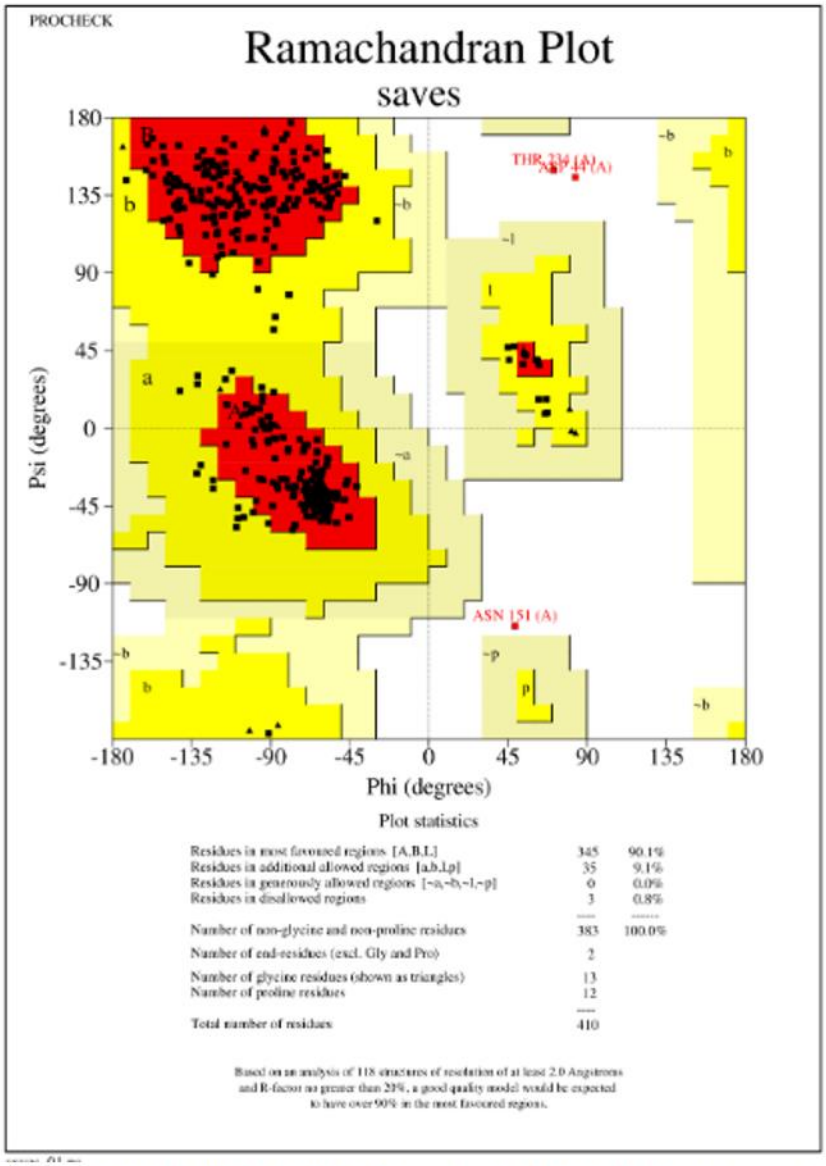


```
----------<<< P R O C H E C K    S U M M A R Y >>>----------

/var/www/SAVES/Jobs/996945/saves.pdb   1.5                  410 residues

Ramachandran plot:   90.1% core    9.1% allow    0.0% gener    0.8% disall

All Ramachandrans:    5 labelled residues (out of 408)
Chi1-chi2 plots:      1 labelled residues (out of 292)
Side-chain params:    5 better     0 inside      0 worse

Residue properties: Max.deviation:     5.8            Bad contacts:    0
                    Bond len/angle:    4.6    Morris et al class:  1  1  2

G-factors           Dihedrals:   0.17  Covalent:   0.32    Overall:   0.24

Planar groups:    98.8% within limits   1.2% highlighted
```

Figure S5: Ramachandran Plot for Robetta Model 1.

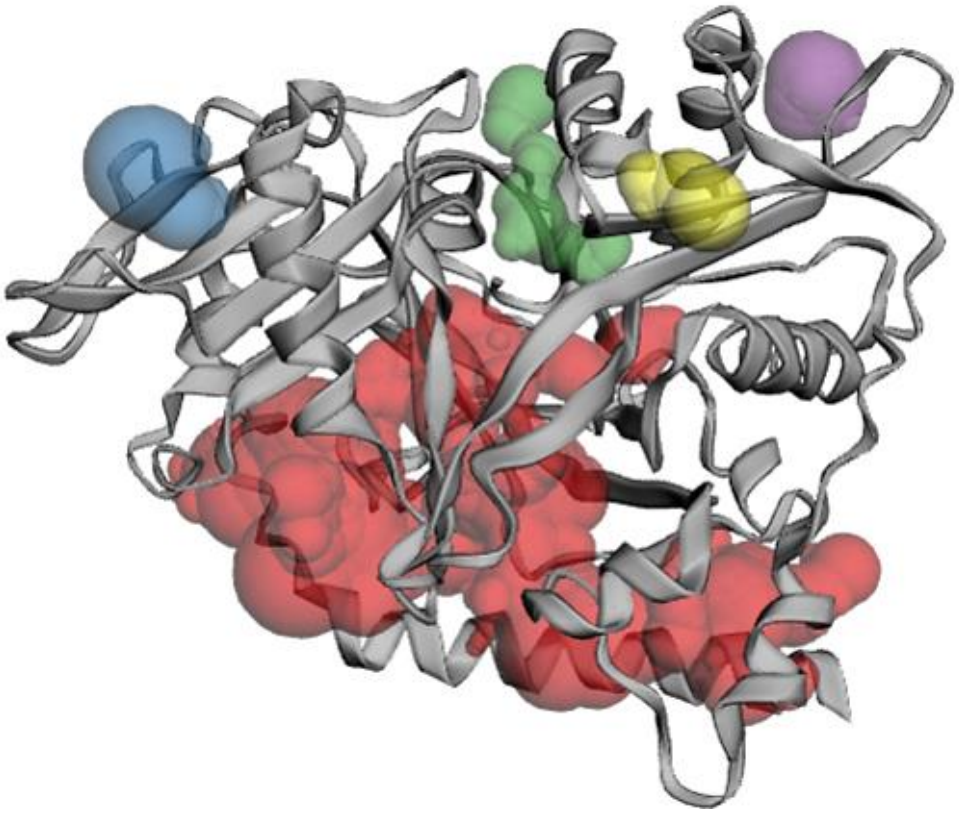

Figure S6: Validation for drugability of obtained protein model of *Pf*NMT was done using CASTp server and CavityPlus.

Table S1: CASTp Top five pockets are as:

PocketID	**Area (SA)Å^2**	**Volume (SA)Å^3**
1	1745.643	1091.244
2	55.026	33.704
3	104.186	28.978
4	27.757	20.361
5	36.067	15.956

Table S2: CAVITY to detect potential binding sites on the surface of a given protein structure and rank them based on drugability scores:

No.	Pred. Max pKd	Pred. Avg pKd	DrugScore	Drugability
1	11.72	6.84	3851.00	Strong
2	11.93	6.71	2812.00	Strong
3	10.93	6.36	465.00	Medium
4	10.67	6.27	809.00	Strong
5	8.34	5.48	-872.00	Weak

Table S3: CavPharm to predict pharmacophore class of Cavity1:

Pharmacophore class of Cavity1	x	y	z	Radius(Å)
Positive electrostatic center (POK 4.H)	13.00	10.00	-19.00	2.00
Positive electrostatic center (POK 4.H)	17.50	16.00	-17.00	2.00
H-bond donor center (POK 2.N)	19.50	18.00	-28.00	1.00
H-bond root (POK 3.F)	17.14	17.05	-27.32	1.50
H-bond donor center (POK 2.N)	16.00	7.00	-17.00	1.00
H-bond root (POK 3.F)	16.25	8.19	-19.13	1.50
H-bond acceptor center (POK 2.O)	18.00	25.50	-25.00	1.00
H-bond root (POK 3.F)	18.93	23.26	-26.25	1.50
H-bond donor center (POK 2.N)	12.50	11.00	-19.00	1.00
H-bond root (POK 3.F)	12.70	13.01	-16.92	1.50
H-bond acceptor center (POK 2.O)	20.50	20.50	-25.00	1.00
H-bond root (POK 3.F)	20.75	22.75	-24.98	1.50
H-bond donor center (POK 2.N)	10.00	7.50	-12.50	1.00
H-bond root (POK 3.F)	8.69	9.76	-12.40	1.50
H-bond acceptor center (POK 2.O)	17.00	19.50	-12.00	1.00
H-bond root (POK 3.F)	15.25	20.96	-10.51	1.50
H-bond acceptor center (POK 2.O)	9.00	7.50	-15.00	1.00
H-bond root (POK 3.F)	6.62	9.01	-14.71	1.50
H-bond acceptor center (POK 2.O)	18.50	18.50	-29.50	1.00

Pharmacophore class of Cavity1	x	y	z	Radius(Å)
H-bond root (POK 3.F)	16.89	17.11	-30.05	1.50
H-bond acceptor center (POK 2.O)	22.50	16.00	-26.50	1.00
H-bond root (POK 3.F)	23.93	17.65	-28.28	1.50
Hydrophobic center (POK 2.C)	17.50	24.50	-20.00	1.50
Hydrophobic center (POK 2.C)	24.00	25.00	-20.50	1.50
Hydrophobic center (POK 2.C)	20.00	19.50	-19.50	1.50
Hydrophobic center (POK 2.C)	9.50	23.00	-19.50	1.50
Hydrophobic center (POK 2.C)	2.50	22.00	-16.50	1.50
Hydrophobic center (POK 2.C)	20.50	28.50	-19.50	1.50
Hydrophobic center (POK 2.C)	7.50	16.00	-18.50	1.50
H-bond acceptor center (POK 2.O)	20.00	16.50	-22.00	1.00
H-bond root (POK 3.F)	19.87	15.10	-23.63	1.50
H-bond acceptor center (POK 2.O)	12.00	27.00	-21.50	1.00
H-bond root (POK 3.F)	10.13	25.75	-22.35	1.50
H-bond acceptor center (POK 2.O)	5.50	15.00	-20.50	1.00
H-bond root (POK 3.F)	3.43	14.43	-19.82	1.50
H-bond donor center (POK 2.N)	16.00	26.00	-24.50	1.00
H-bond root (POK 3.F)	14.36	28.27	-24.66	1.50
H-bond donor center (POK 2.N)	17.00	28.00	-20.00	1.00
H-bond root (POK 3.F)	14.91	29.21	-19.70	1.50
H-bond donor center (POK 2.N)	9.50	25.50	-19.50	1.00
H-bond root (POK 3.F)	10.13	25.75	-22.35	1.50
H-bond donor center (POK 2.N)	5.00	23.00	-19.50	1.00
H-bond root (POK 3.F)	2.22	22.07	-20.06	1.50
H-bond donor center (POK 2.N)	17.00	18.50	-19.50	1.00
H-bond root (POK 3.F)	15.43	17.59	-20.77	1.50
H-bond acceptor center (POK 2.O)	5.00	22.00	-19.00	1.00
H-bond root (POK 3.F)	6.57	21.66	-16.76	1.50
H-bond acceptor center (POK 2.O)	17.00	29.00	-19.50	1.00
H-bond root (POK 3.F)	14.91	29.21	-19.70	1.50
H-bond donor center (POK 2.N)	16.00	18.50	-14.50	1.00
H-bond root (POK 3.F)	15.73	20.75	-15.46	1.50
Negative electrostatic center (POK 4.S)	17.50	26.50	-25.50	2.00

Pharmacophore class of Cavity1	x	y	z	Radius(Å)
Negative electrostatic center (POK 4.S)	18.00	22.00	-23.00	2.00
Negative electrostatic center (POK 4.S)	21.00	16.50	-29.50	2.00
Negative electrostatic center (POK 4.S)	17.50	20.00	-13.00	2.00

The residues in pocket 1:

PHE:8:A, VAL:9:A, ASP:12:A, LEU:13:A, LEU:16:A, ILE:17:A, ARG:18:A, ASN:19:A, ALA:20:A, LYS:21:A, ASP:22:A, LYS:23:A, ILE:24:A, LYS:25:A, ILE:26:A, ASP:27:A, TYR:28:A, LYS:29:A, PHE:30:A, TRP:31:A, THR:92:A, ASP:93:A, ASN:94:A, TYR:95:A, VAL:96:A, GLU:97:A, ASP:98:A, ASP:99:A, ASP:100:A, ASN:101:A, VAL:102:A, PHE:103:A, ARG:104:A, PHE:105:A, ASN:106:A, TYR:107:A, PHE:111:A, LEU:112:A, ALA:115:A, VAL:160:A, ASN:161:A, PHE:162:A, LEU:163:A, CYS:164:A, VAL:165:A, HIS:166:A, LYS:167:A, SER:168:A, LEU:169:A, ARG:170:A, SER:171:A, LYS:172:A, ARG:173:A, LEU:174:A, ALA:175:A, PRO:176:A, LEU:178:A, ILE:179:A, TYR:196:A, THR:197:A, ALA:198:A, GLY:199:A, VAL:200:A, TYR:201:A, LEU:202:A, PRO:203:A, TYR:211:A, PHE:212:A, HIS:213:A, ILE:224:A, GLY:225:A, PHE:226:A, SER:227:A, CYS:228:A, TYR:242:A, TYR:315:A, LEU:317:A, PRO:318:A, SER:319:A, LYS:320:A, LEU:322:A, LEU:330:A, ASN:331:A, ALA:332:A, PHE:334:A, SER:335:A, PHE:336:A, VAL:363:A, PHE:364:A, ASN:365:A, ALA:366:A, LEU:367:A, GLU:368:A, PHE:381:A, GLY:382:A, GLU:383:A, GLY:384:A, ASP:385:A, GLY:386:A, SER:387:A, LEU:388:A, LYS:389:A, TYR:390:A, TYR:393:A, VAL:408:A, LEU:409:A, LEU:410:A

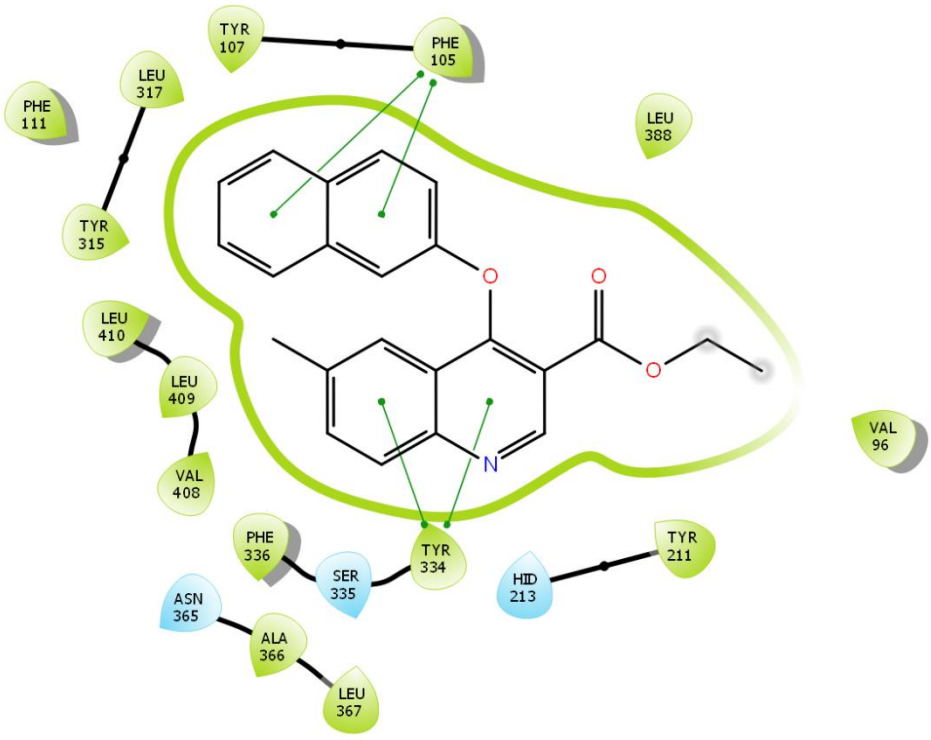

Figure S7: 2D interactions of compound **9a** with *Pv*NMT.

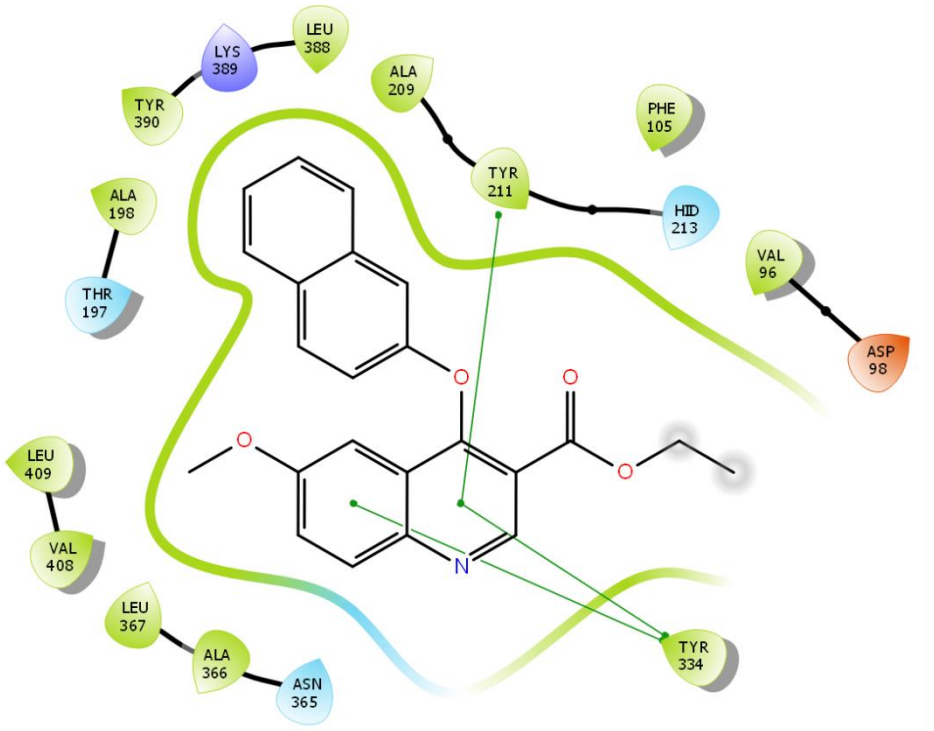

Figure S8: 2D interactions of compound **9b** with *Pv*NMT.

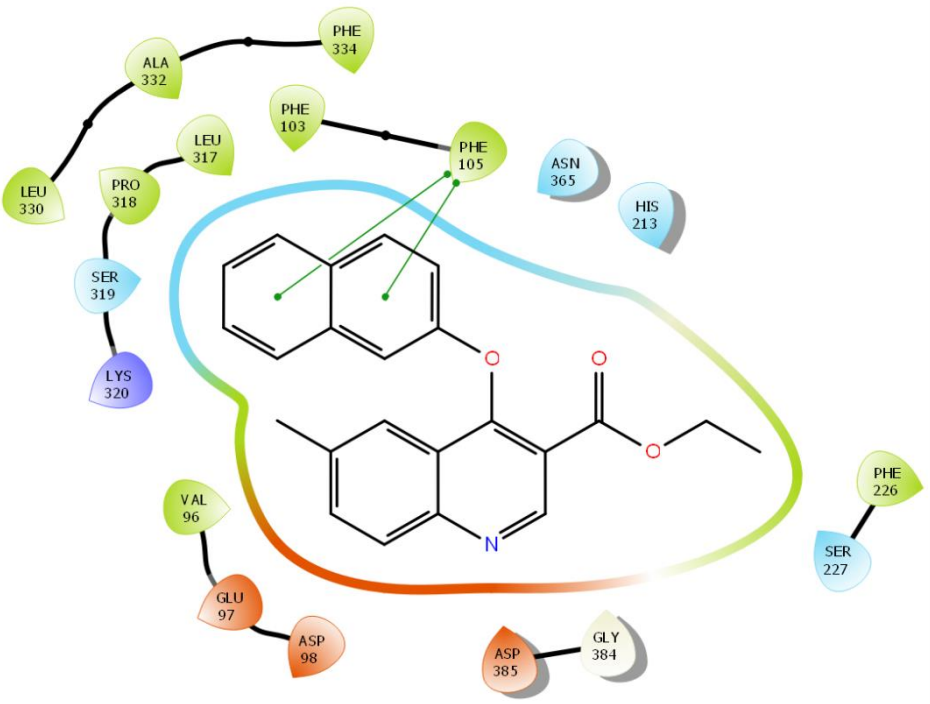

Figure S9: 2D interactions of compound **9a** with *Pf*NMT model protein.

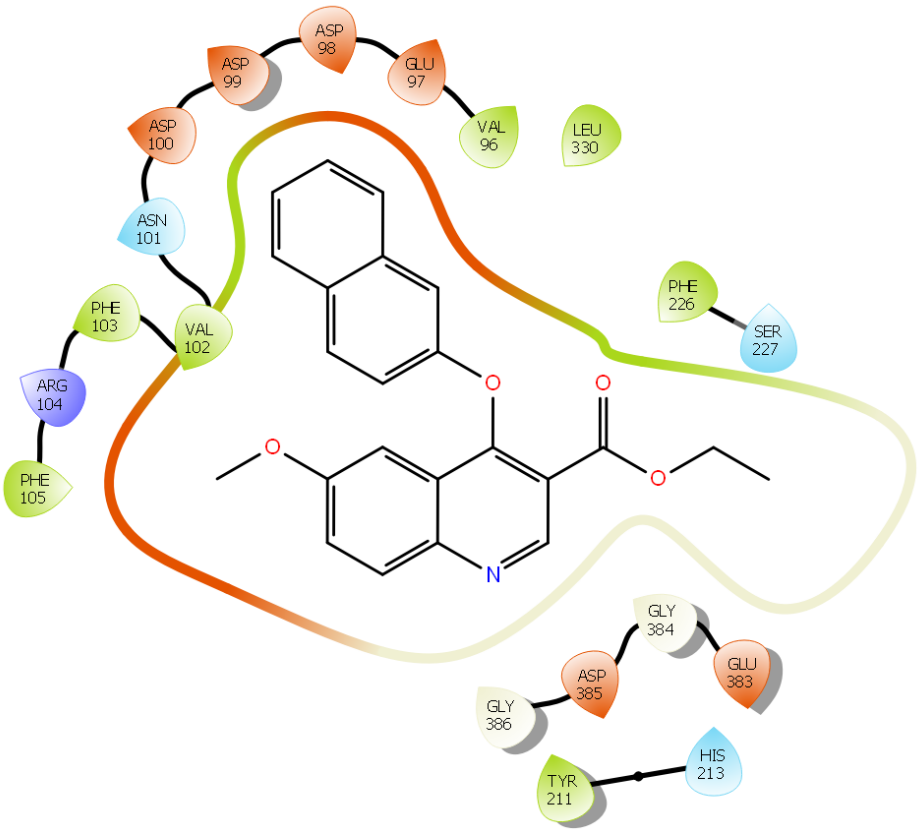

Figure S10: 2D interactions of compound **9b** with *Pf*NMT model protein.

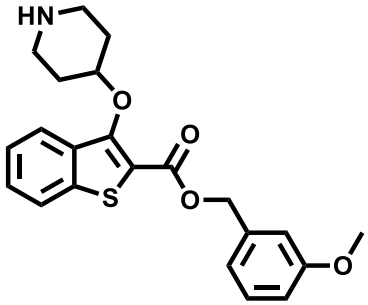

Figure S11: Molecular structure of crystal bound inhibitor, **E** of *Pv*NMT (PDB: 4BBH).

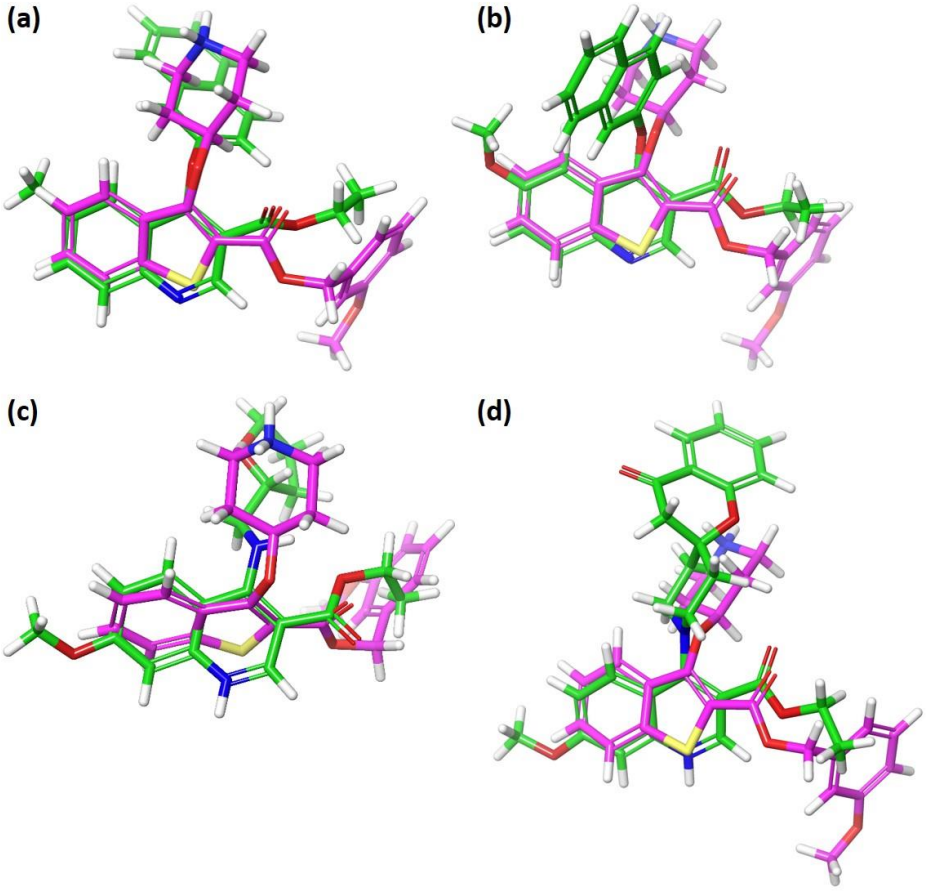

Figure S12: Superimposed docked images of the experimental ligands (green); (a) **9a**, (b) **9b**, (c) **9n**, and (d) **9o** with control inhibitor **E** (magenta) in *Pv*NMT.

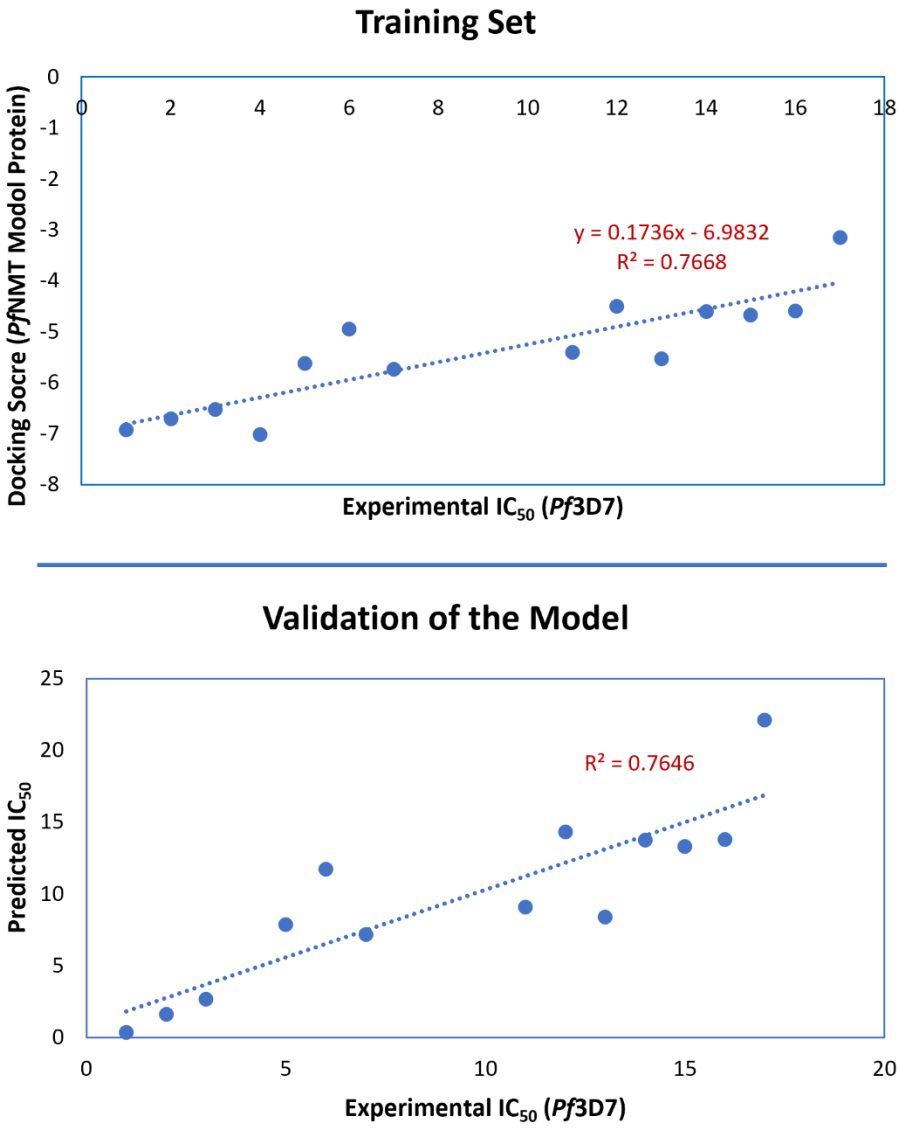

Figure S13: Correlation curve for validation of docking study. The variables in the equation of straight line defined as y = docking score; x = predicted IC_{50} value.

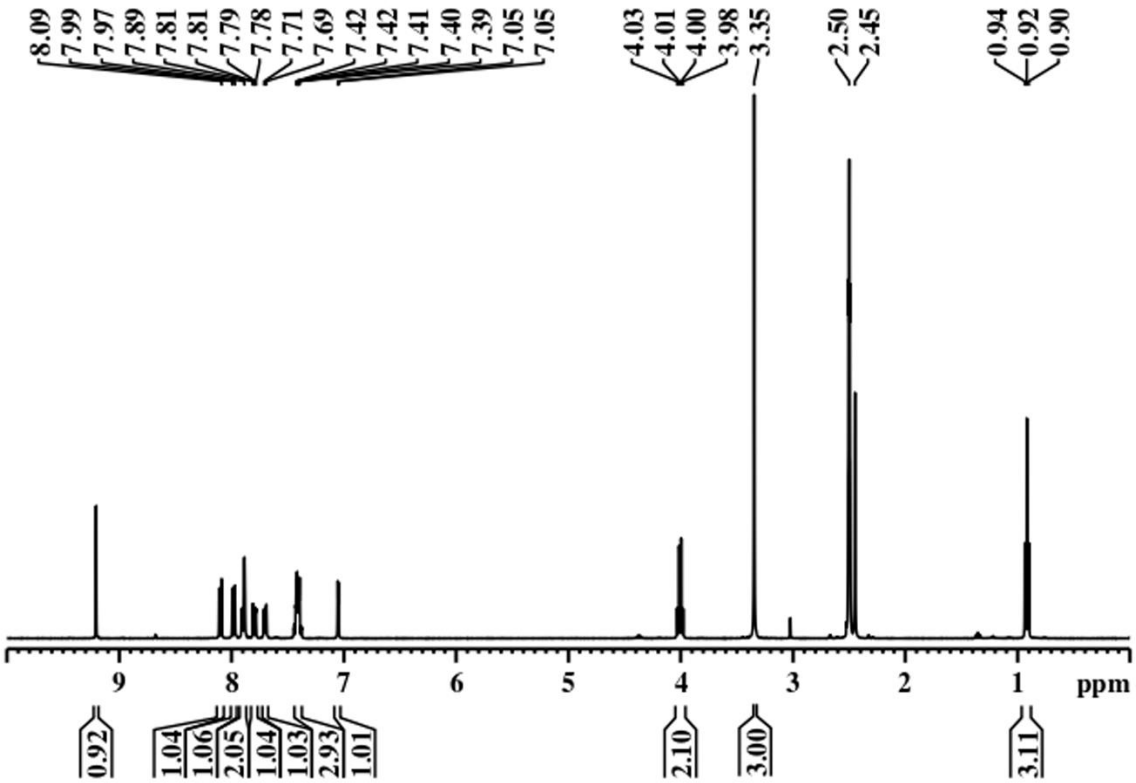

Figure S14: ^{1}H NMR of **9a** in d_6-DMSO.

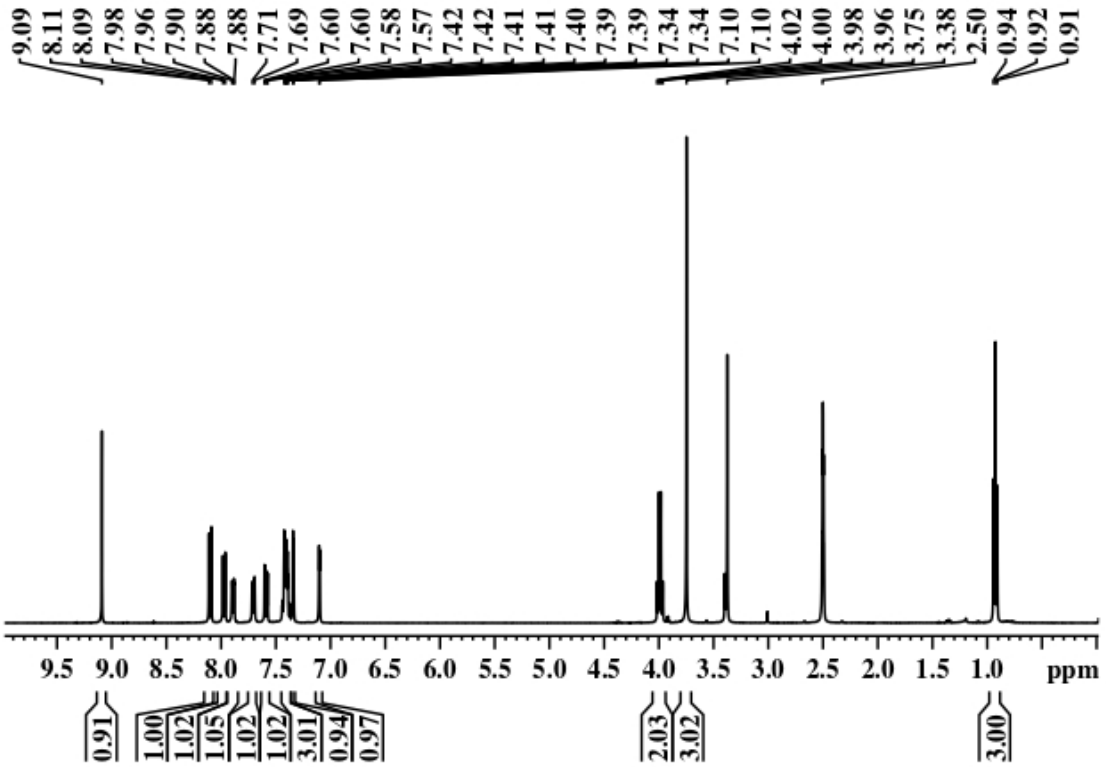

Figure S15: ^{1}H NMR of **9b** in d_6-DMSO.

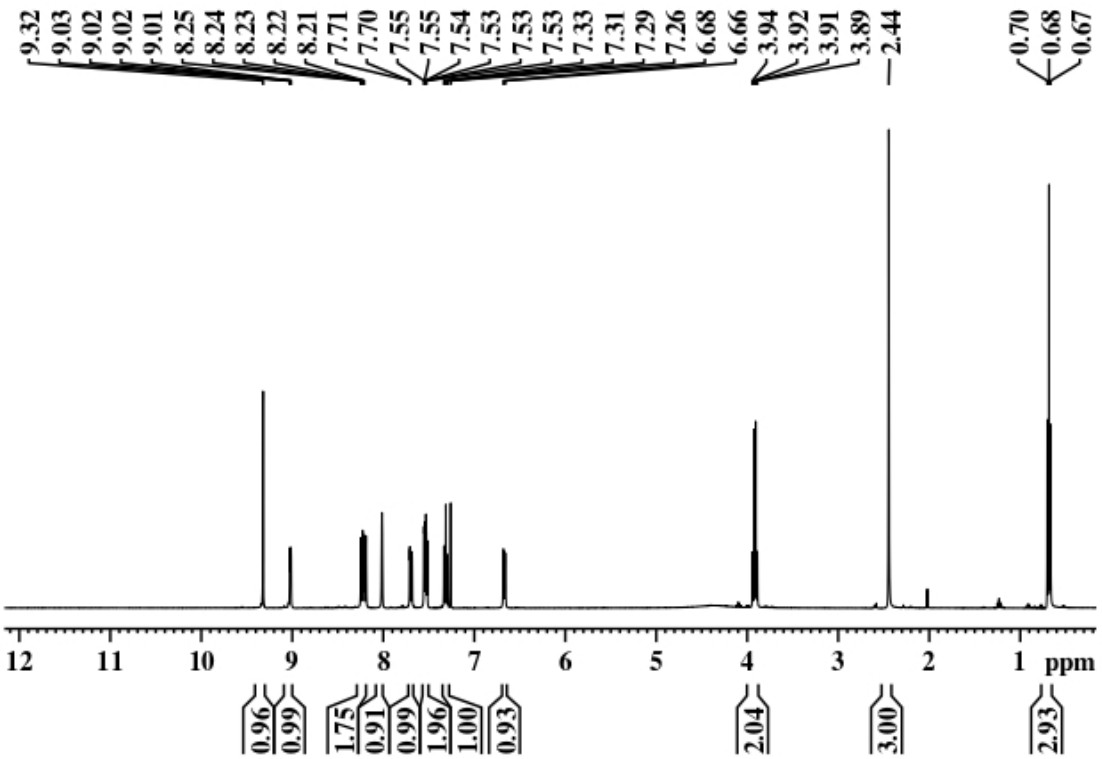

Figure S16: ^{1}H NMR of **9c** in $CDCl_3$.

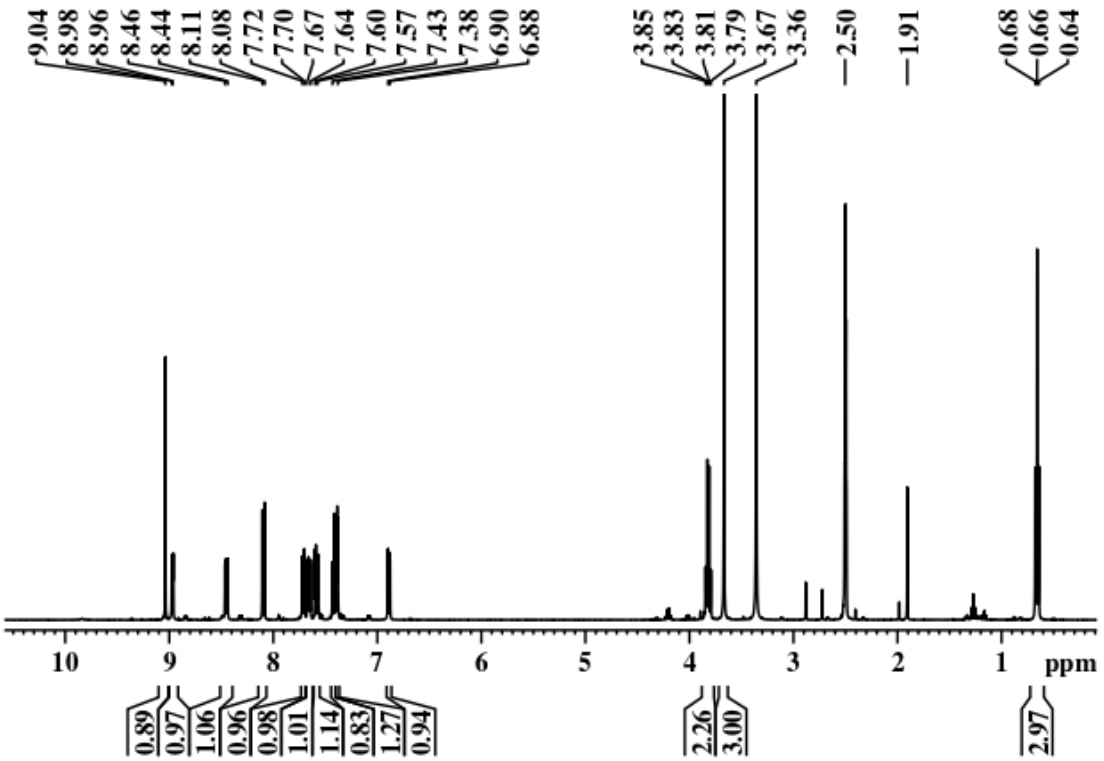

Figure S17: ^{1}H NMR of **9d** in d_6-DMSO.

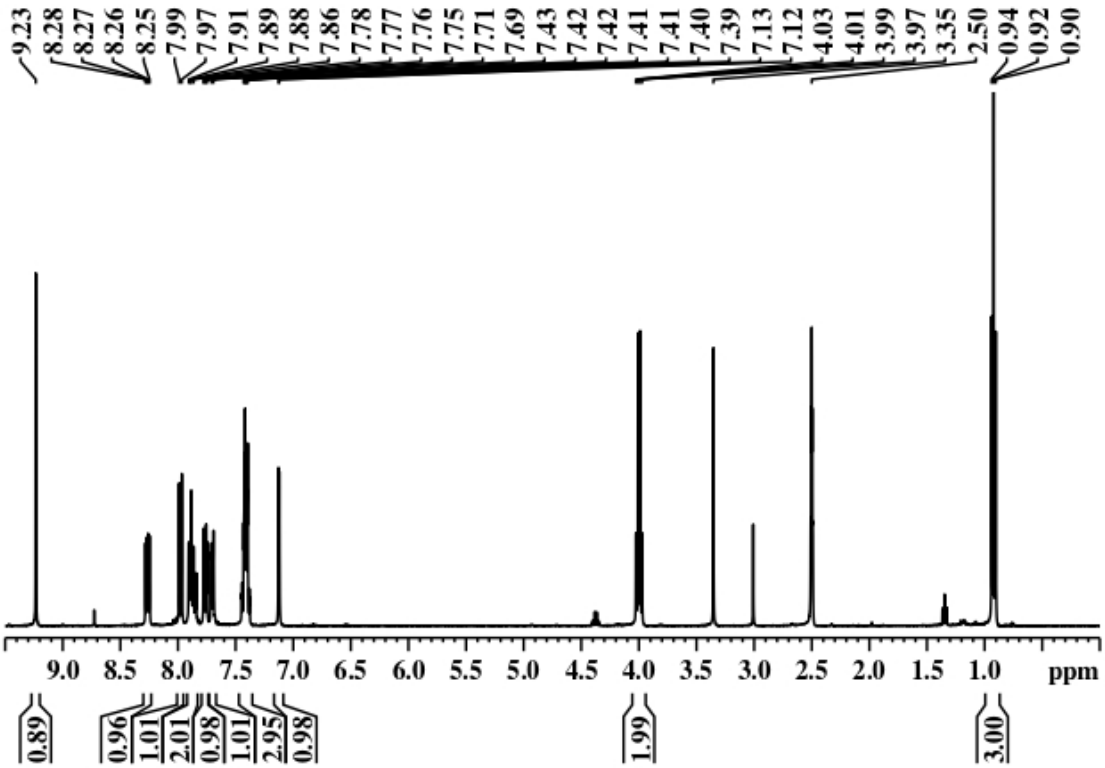

Figure S18: ^{1}H NMR of **9e** in d_6-DMSO.

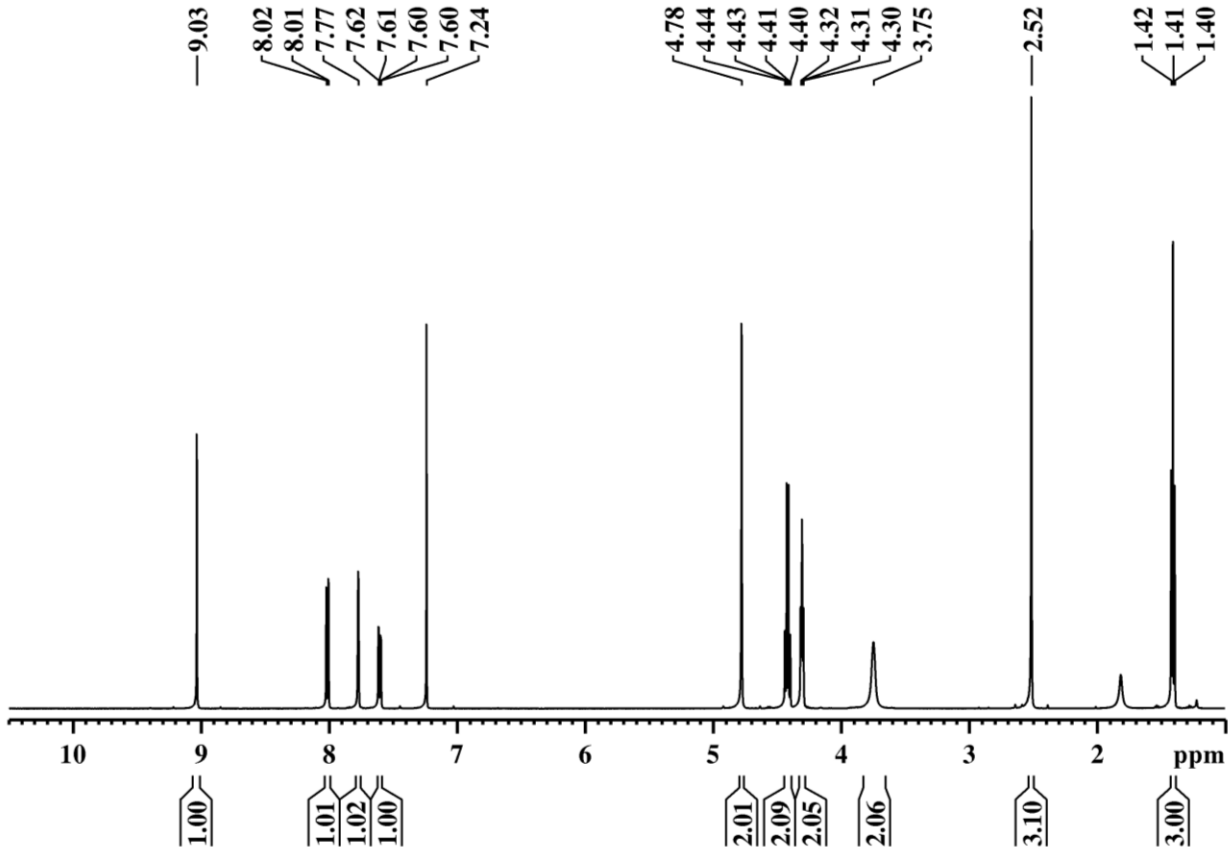

Figure S19: ^{1}H NMR of **9f** in $CDCl_3$.

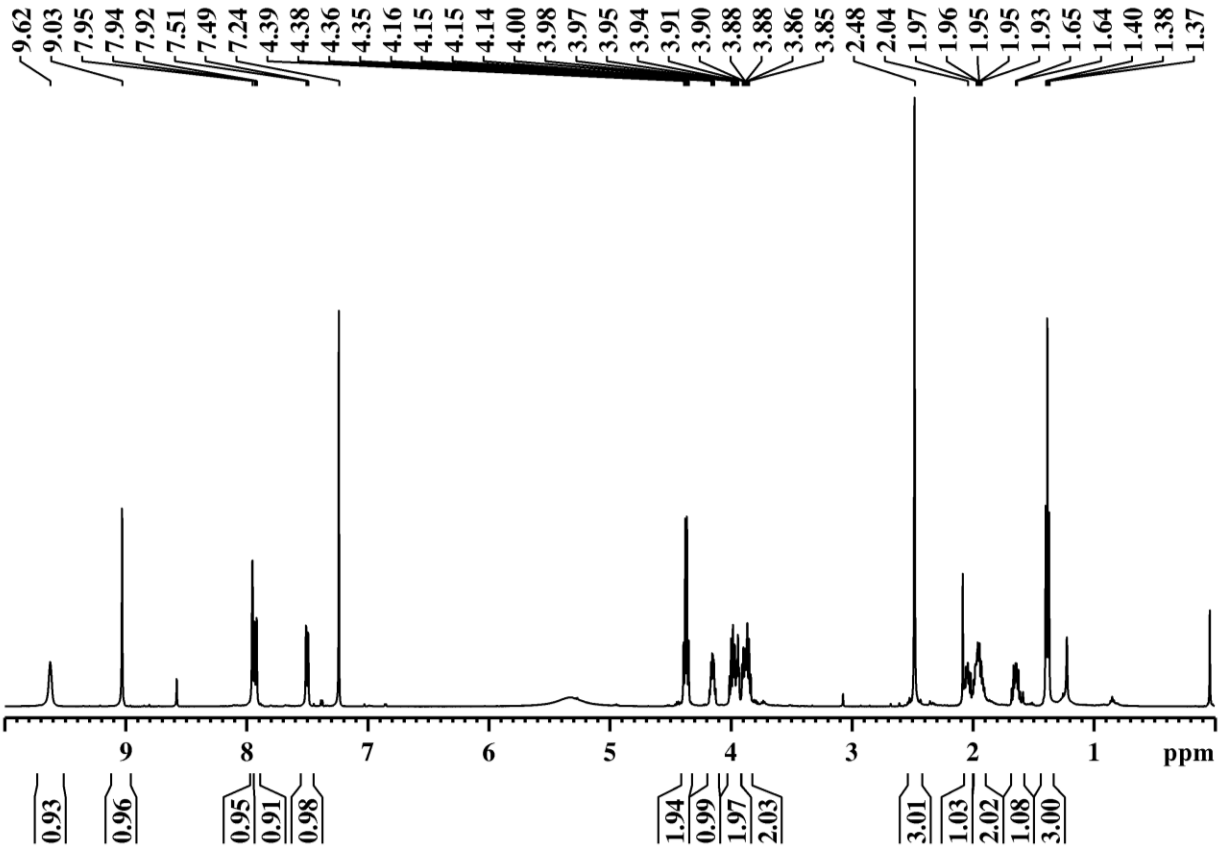

Figure S20: ^{1}H NMR of **9g** in $CDCl_3$.

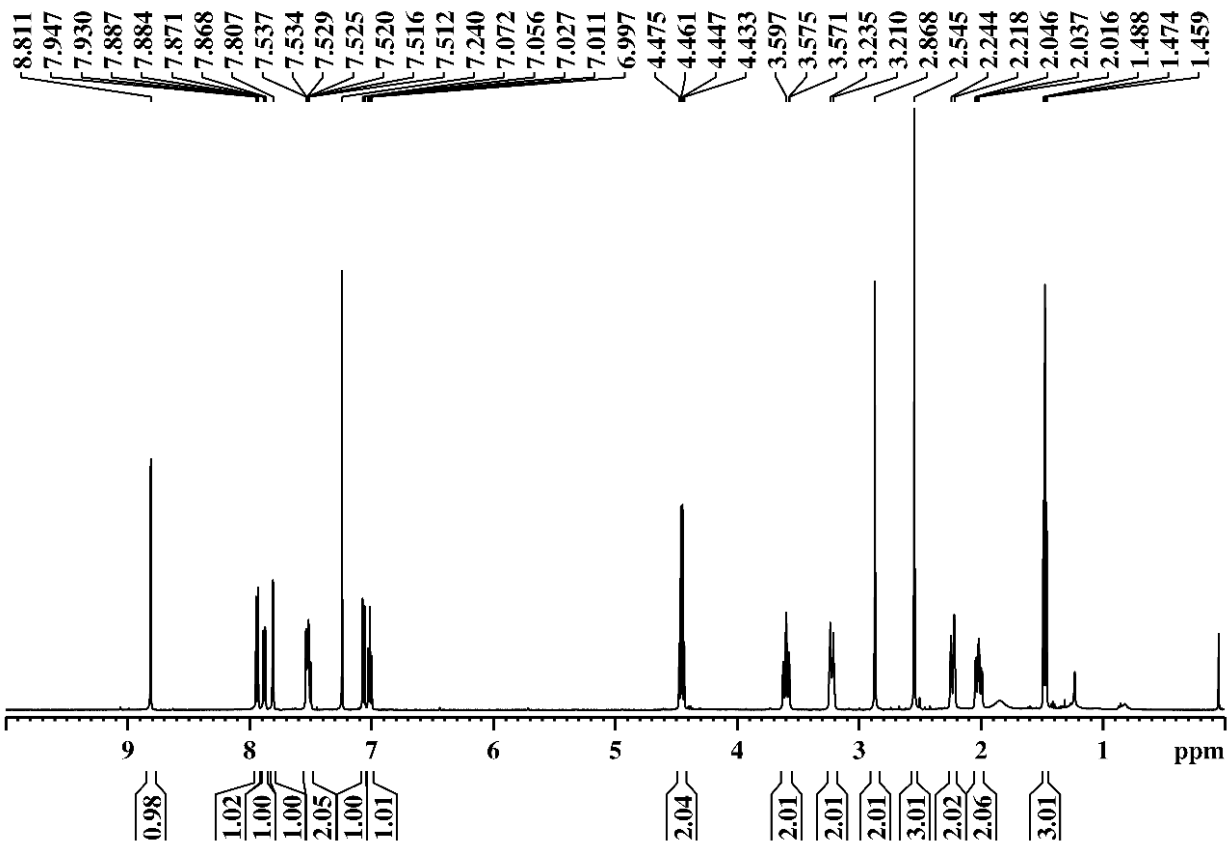

Figure S21: ^{1}H NMR of **9h** in $CDCl_3$.

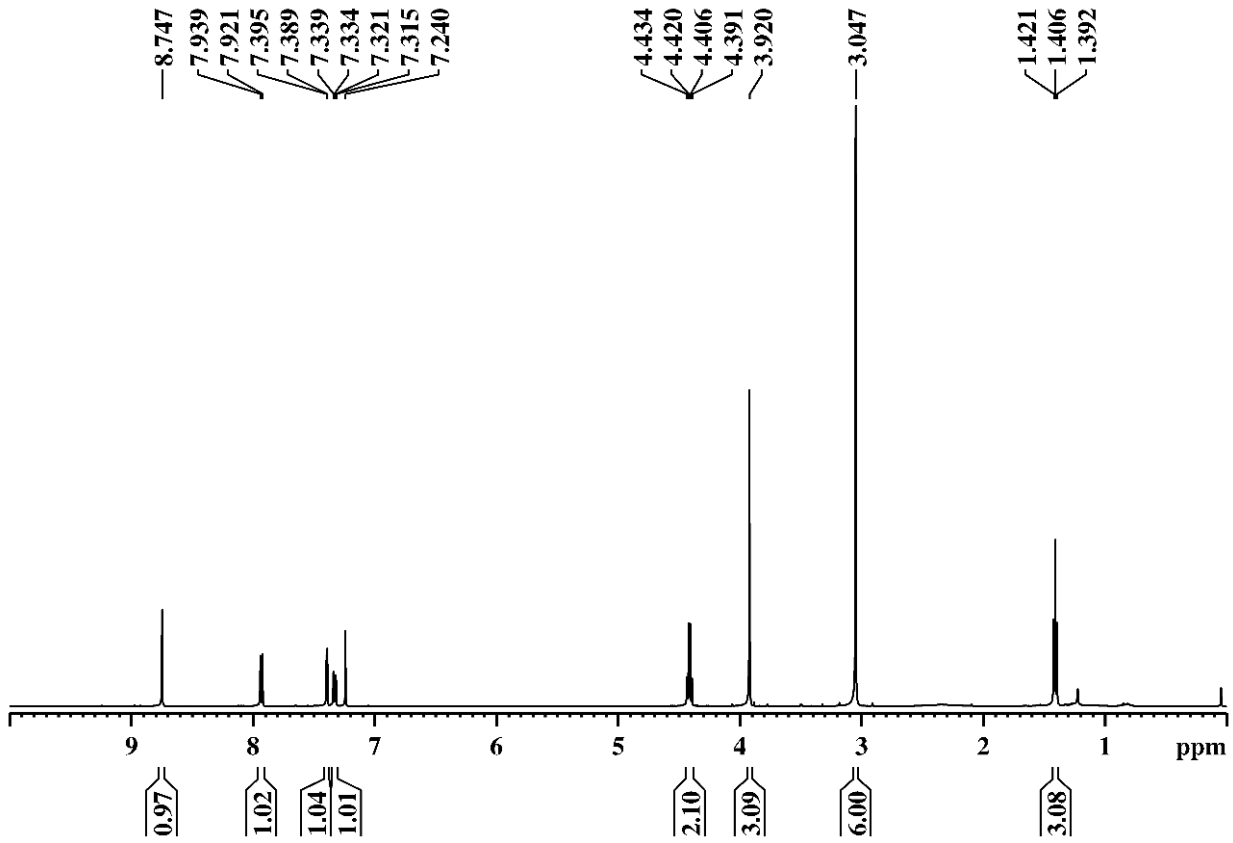

Figure S22: ^{1}H NMR of **9i** in $CDCl_3$.

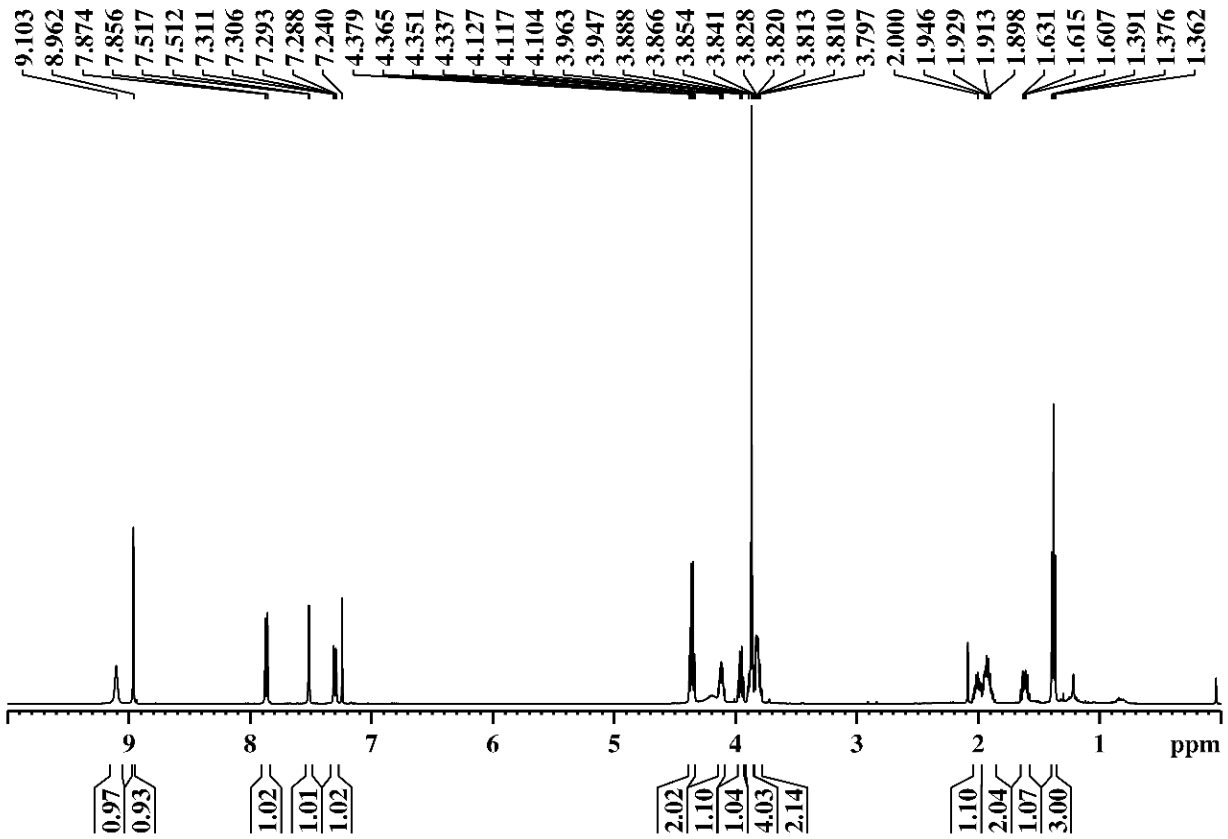

Figure S23: ^{1}H NMR of **9j** in $CDCl_3$.

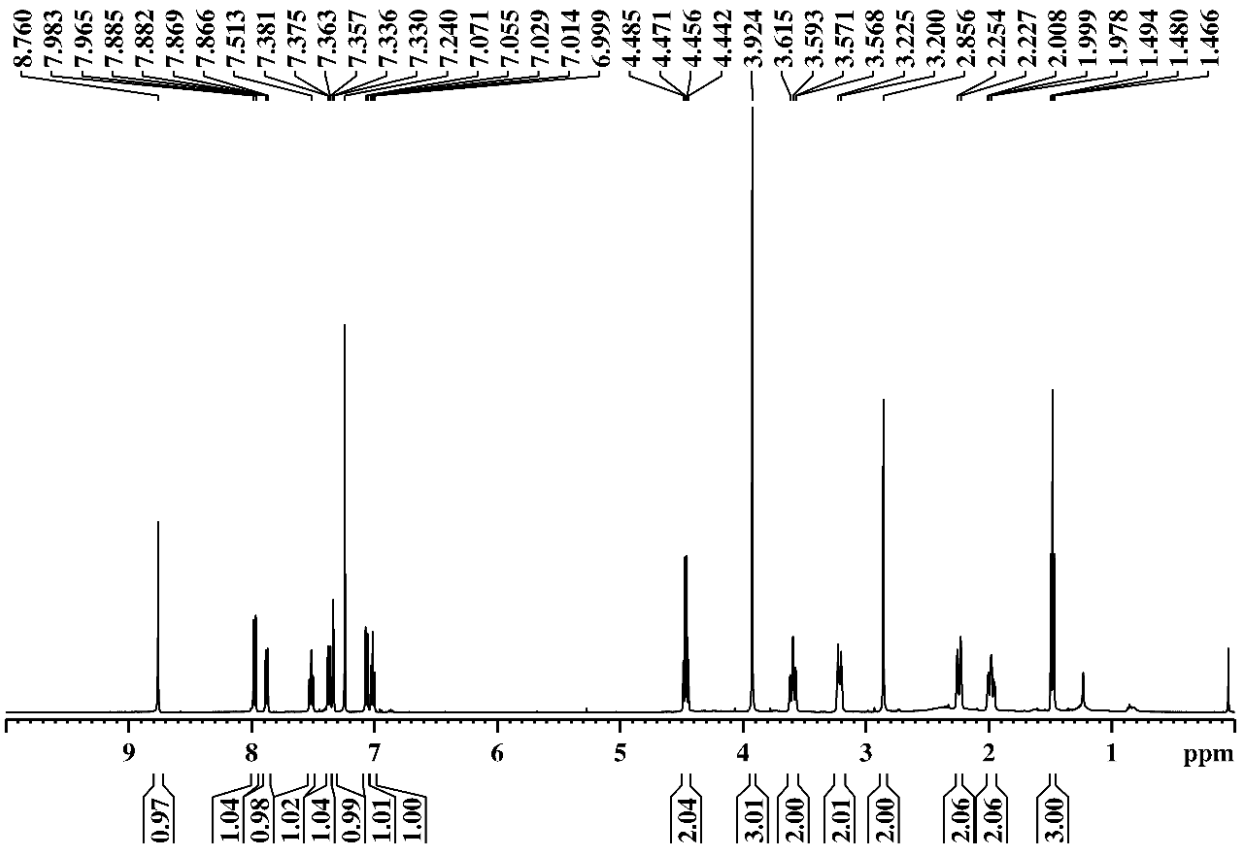

Figure S24: ^{1}H NMR of **9k** in $CDCl_3$.

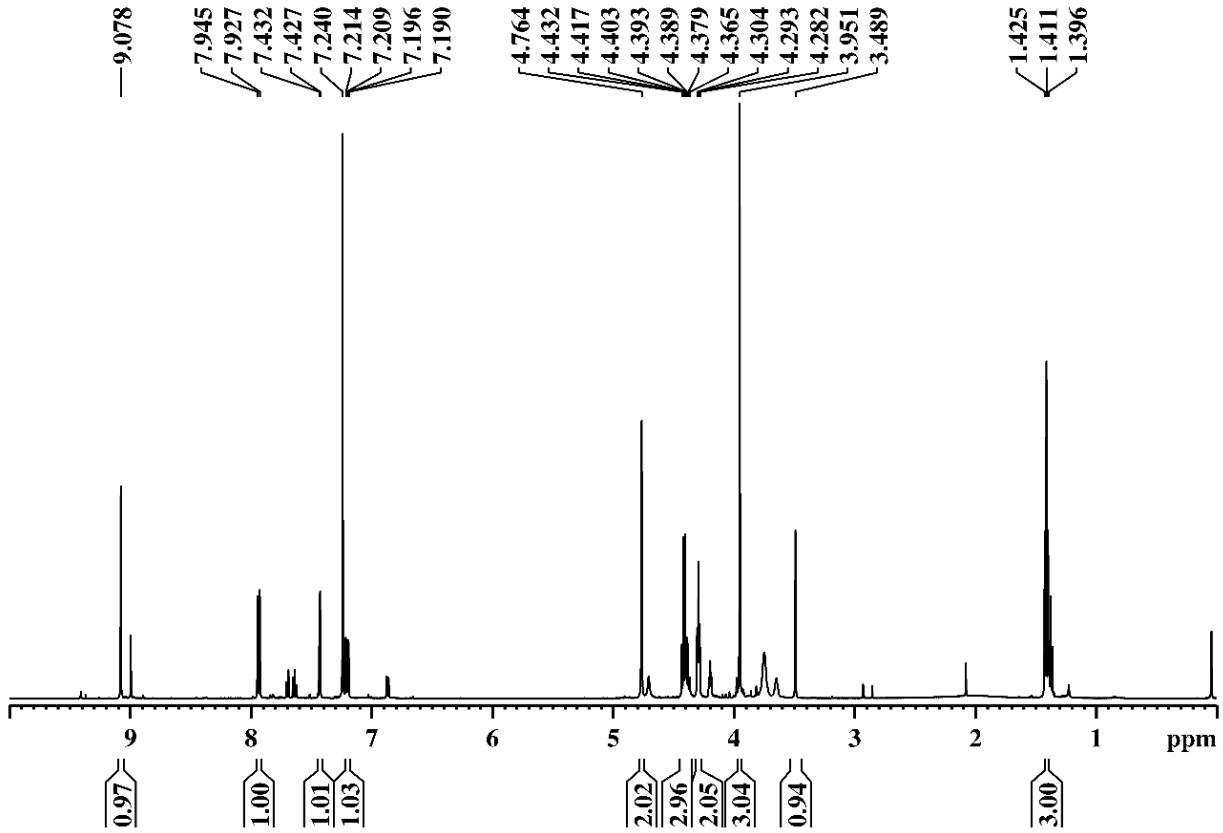

Figure S25: ^{1}H NMR of **9l** in $CDCl_3$.

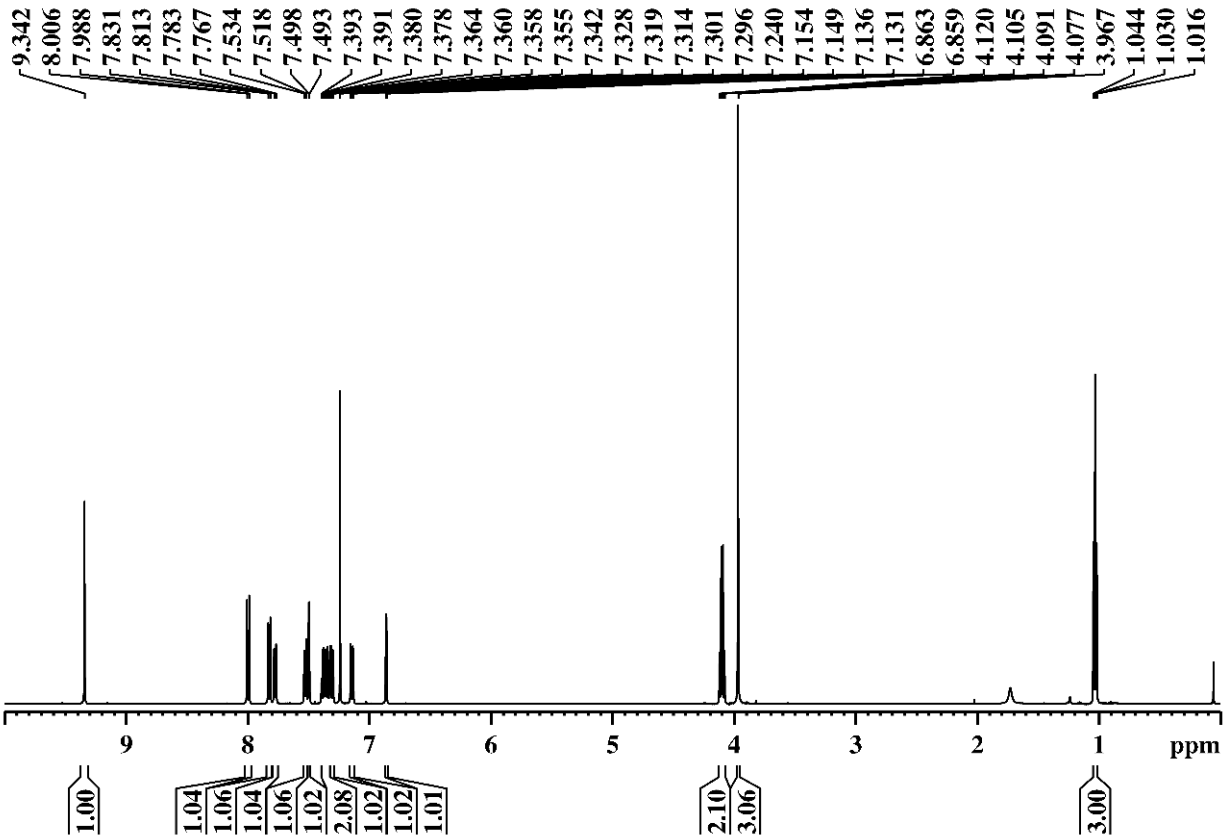

Figure S26: ^{1}H NMR of **9m** in $CDCl_3$.

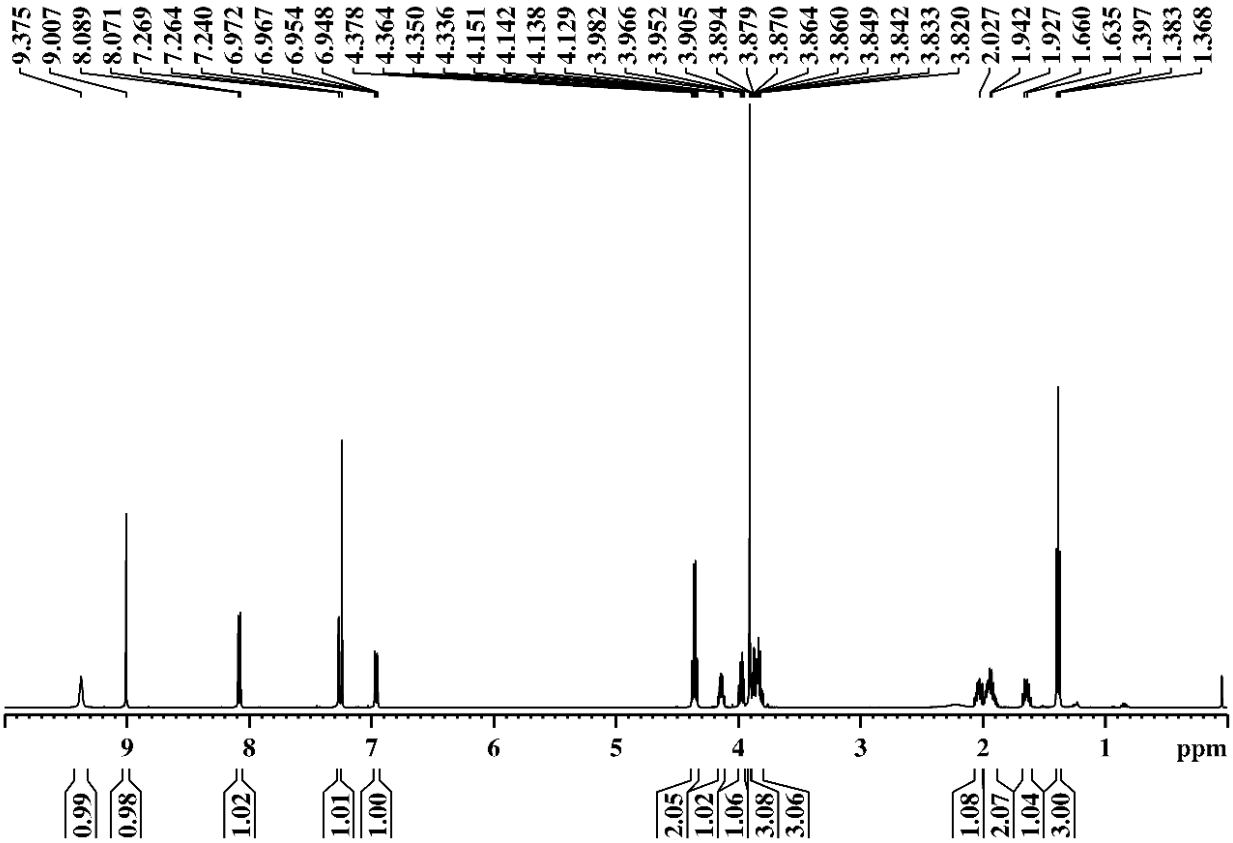

Figure S27: ^{1}H NMR of **9n** in $CDCl_3$.

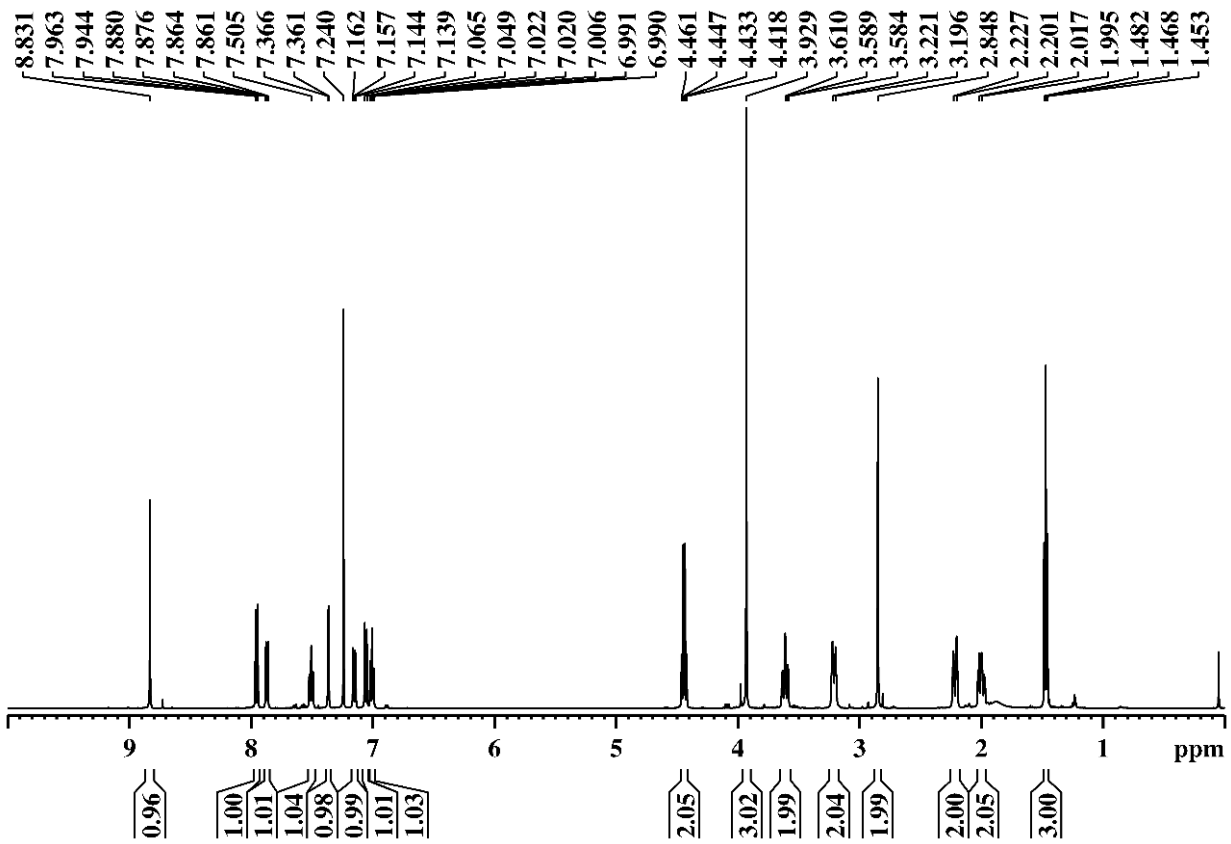

Figure S28: ^{1}H NMR of **9o** in $CDCl_3$.

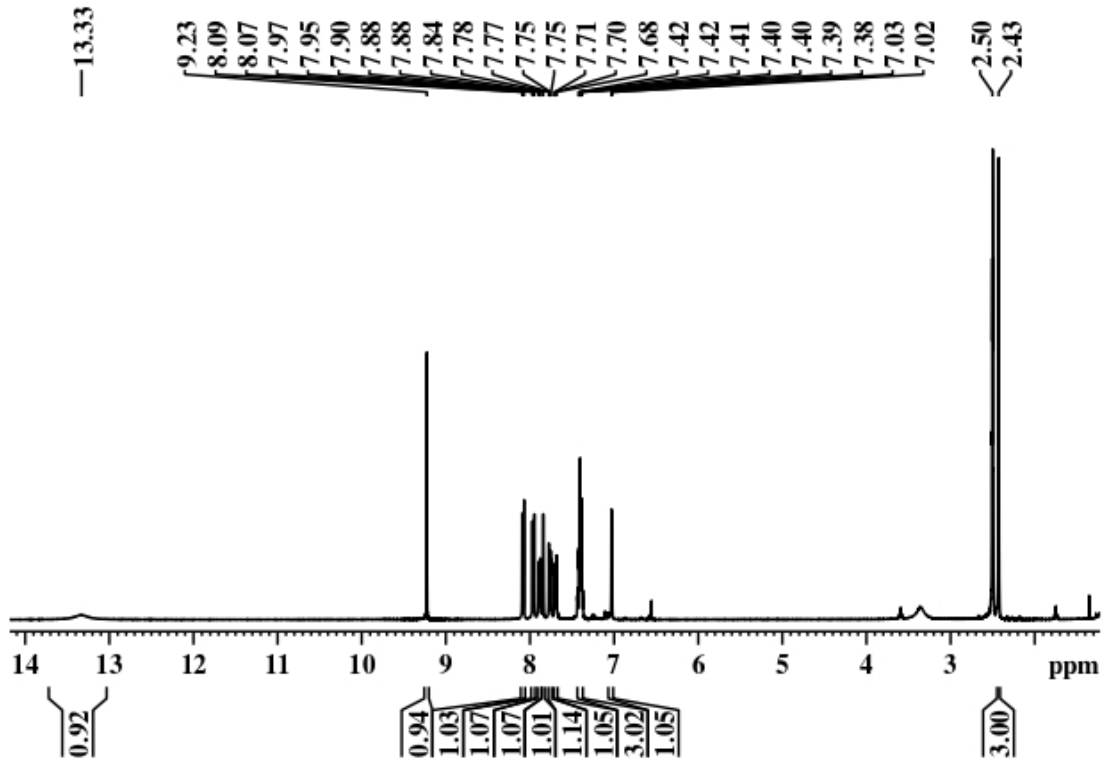

Figure S29: ^{1}H NMR of **10a** in d_6-DMSO**.**

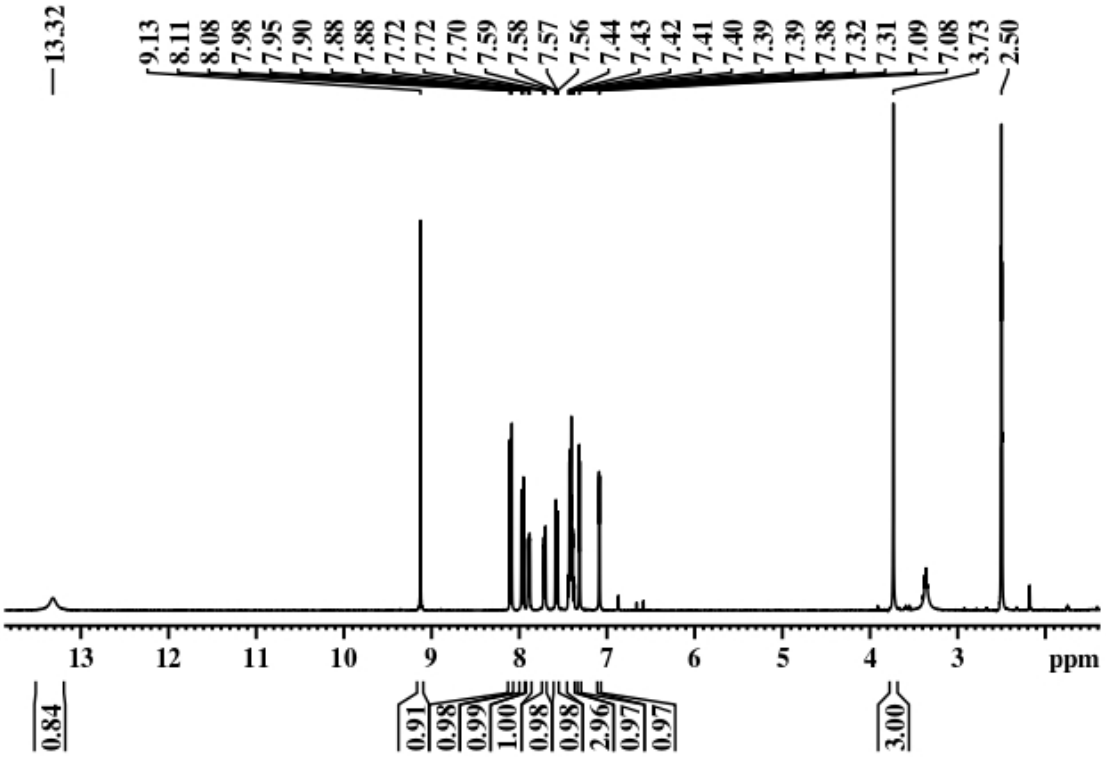

Figure S30: ^{1}H NMR of **10b** in d_6-DMSO.

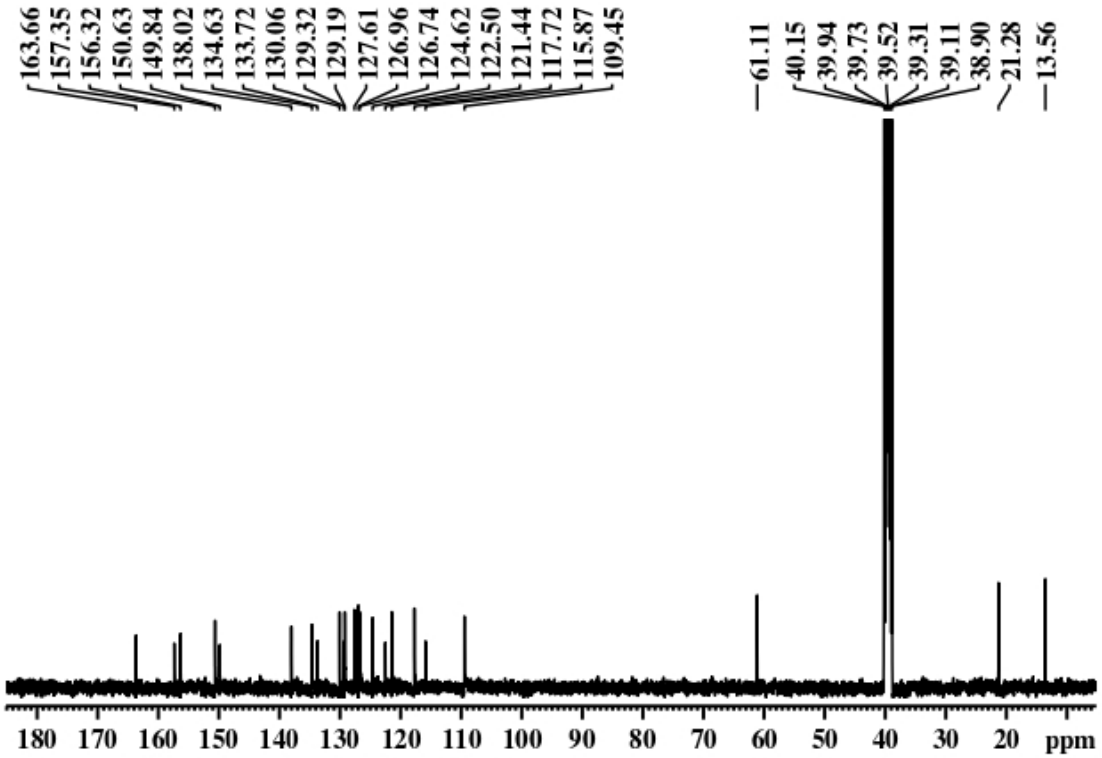

Figure S31: ^{13}C NMR of **9a** in d_6-DMSO.

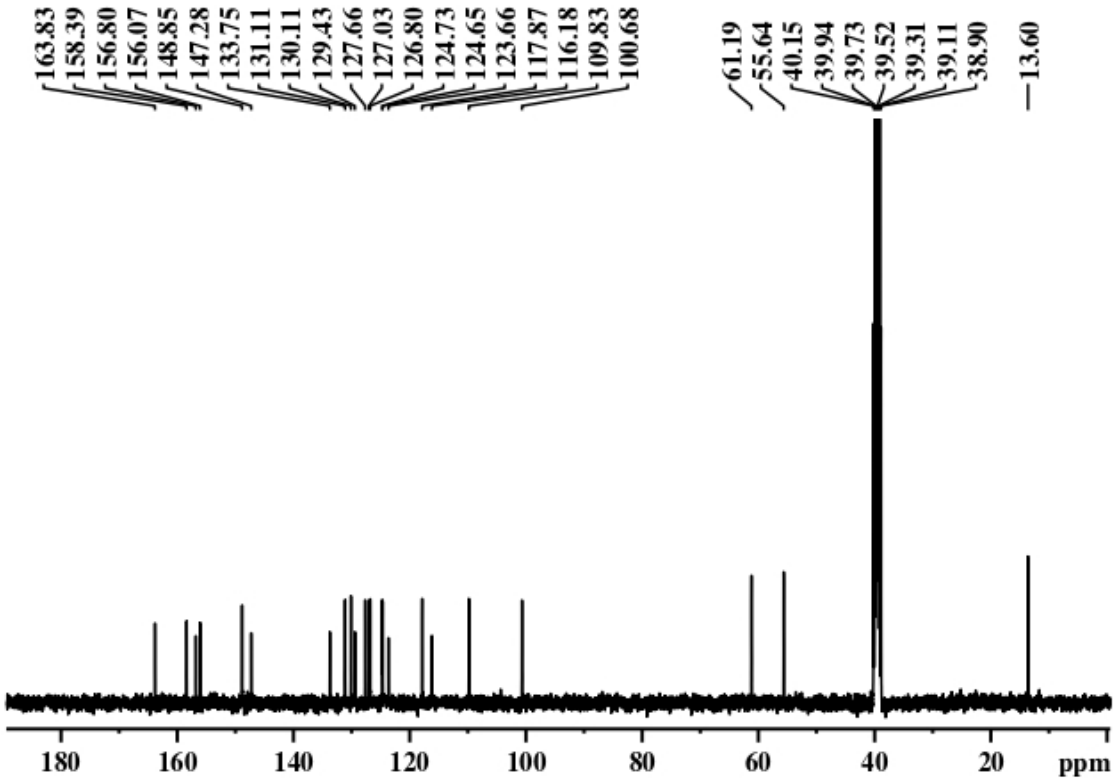

Figure S32: ^{13}C NMR of **9b** in d_6-DMSO.

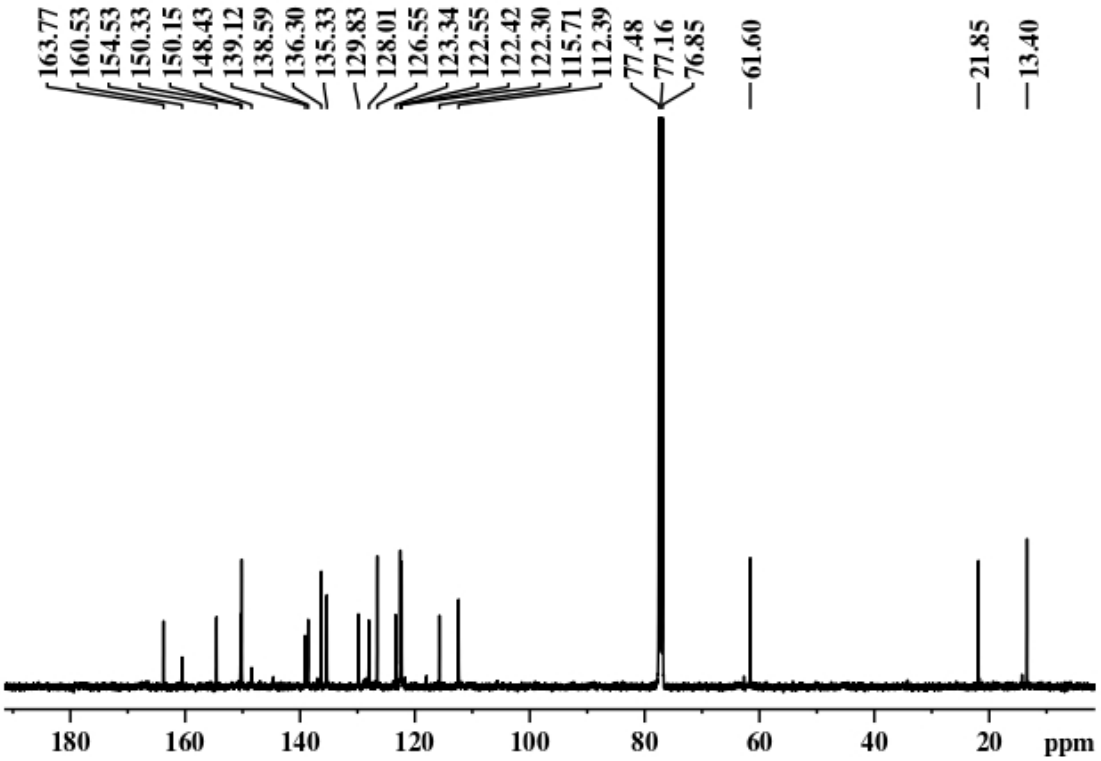

Figure S33: ^{13}C NMR of **9c** in $CDCl_3$.

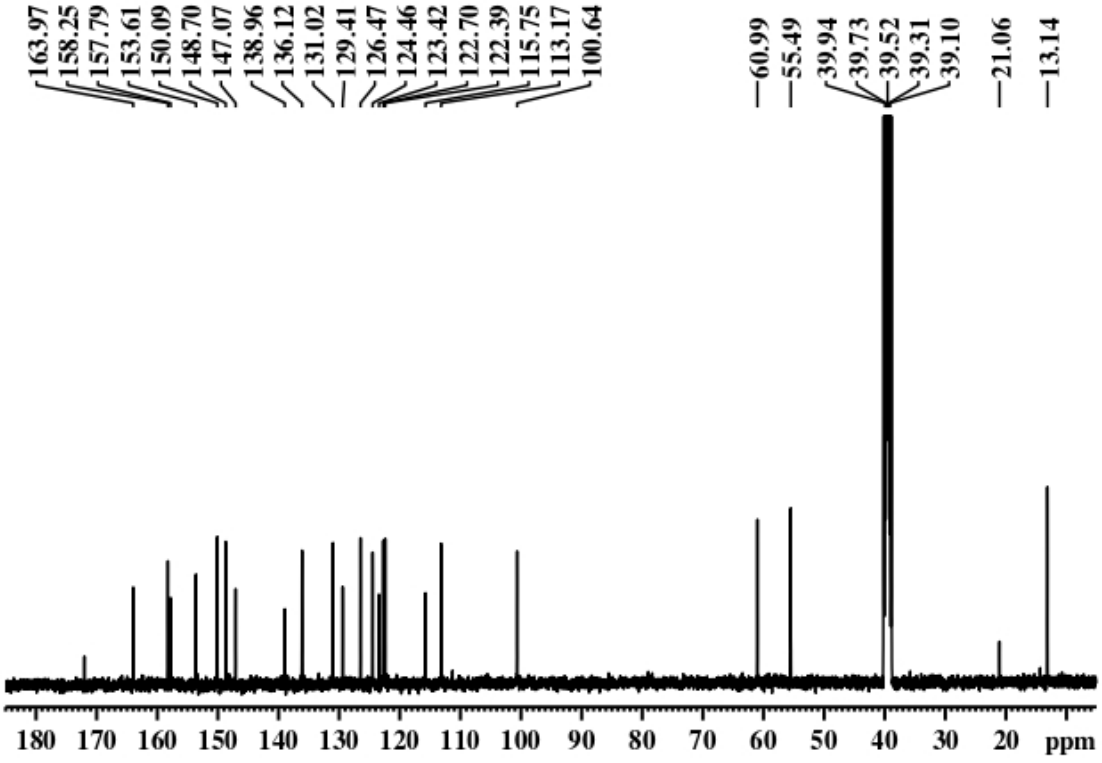

Figure S34: ^{13}C NMR of **9d** in d_6-DMSO.

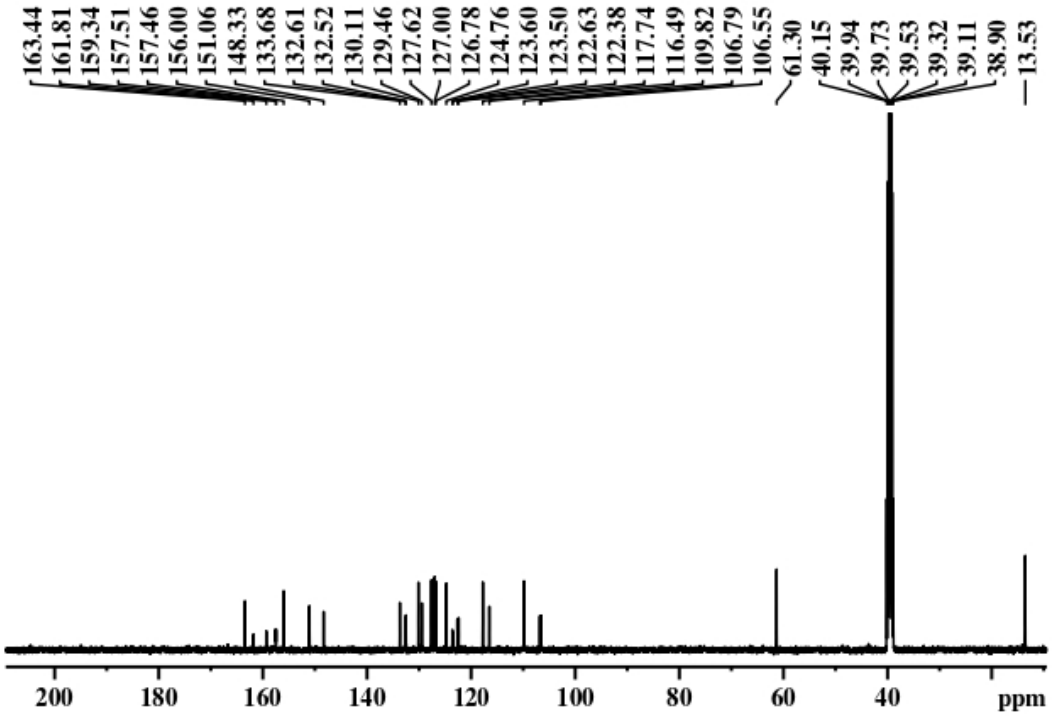

Figure S35: ^{13}C NMR of **9e** in d_6-DMSO.

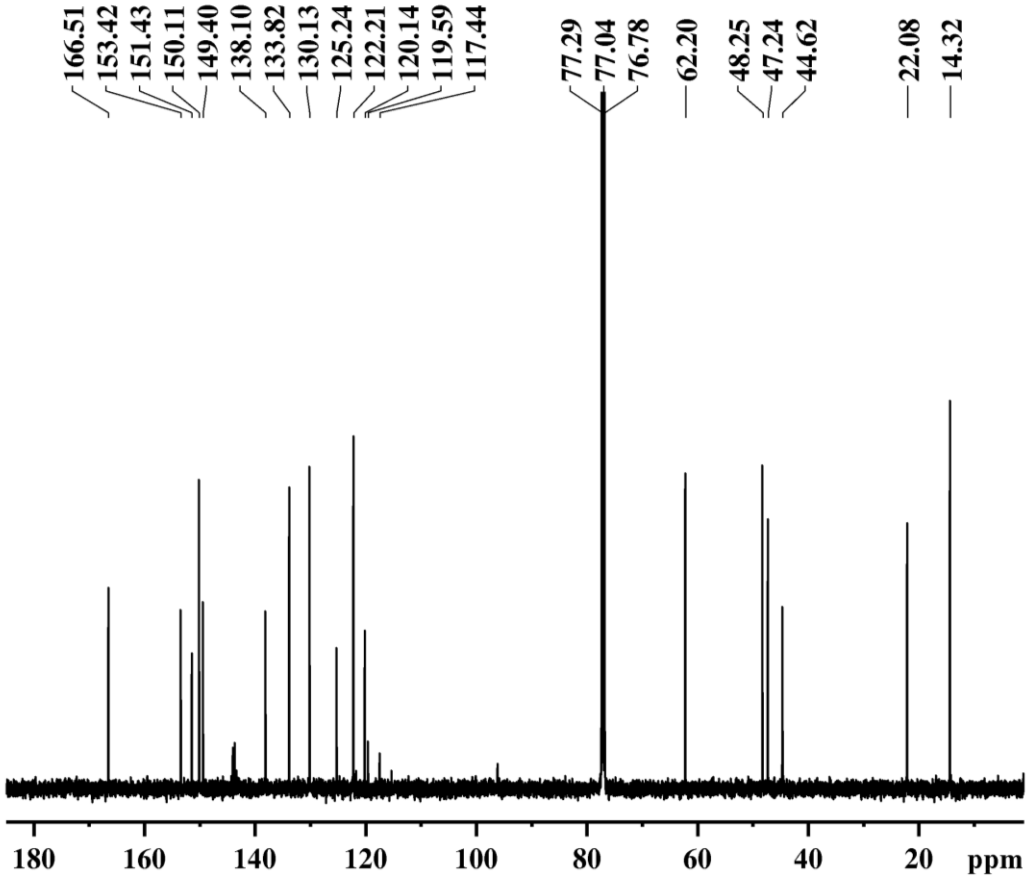

Figure S36: ^{13}C NMR of **9f** in $CDCl_3$.

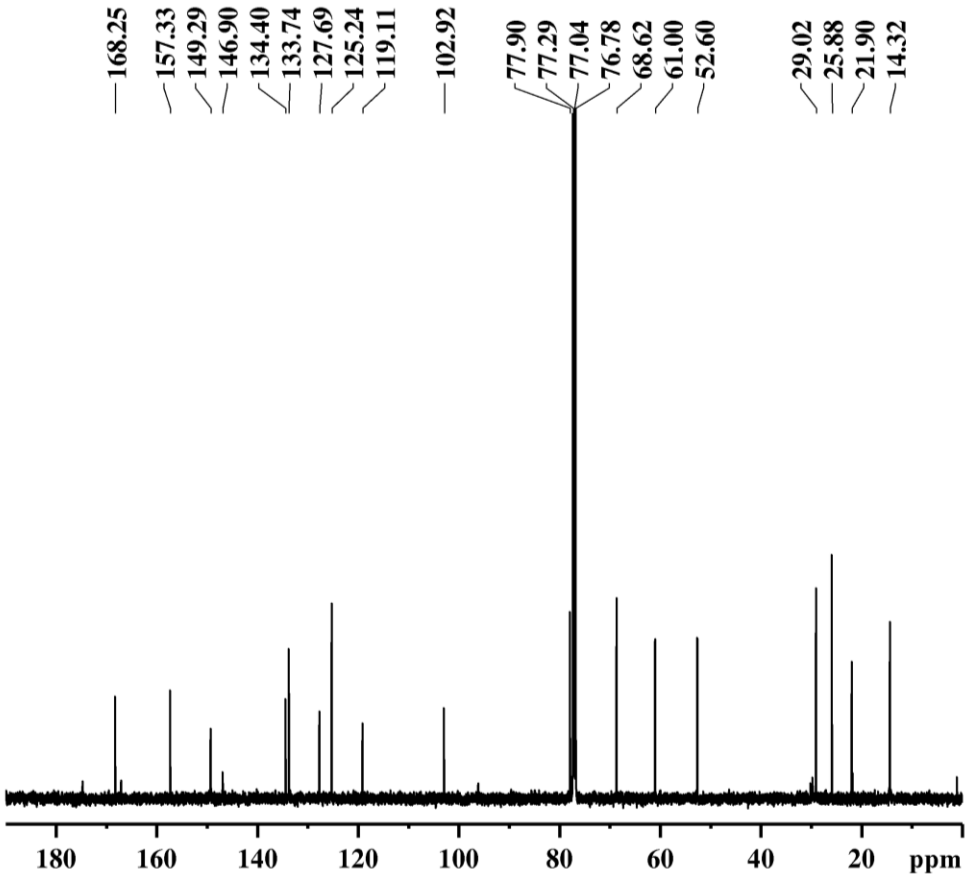

Figure S37: ^{13}C NMR of **9g** in $CDCl_3$.

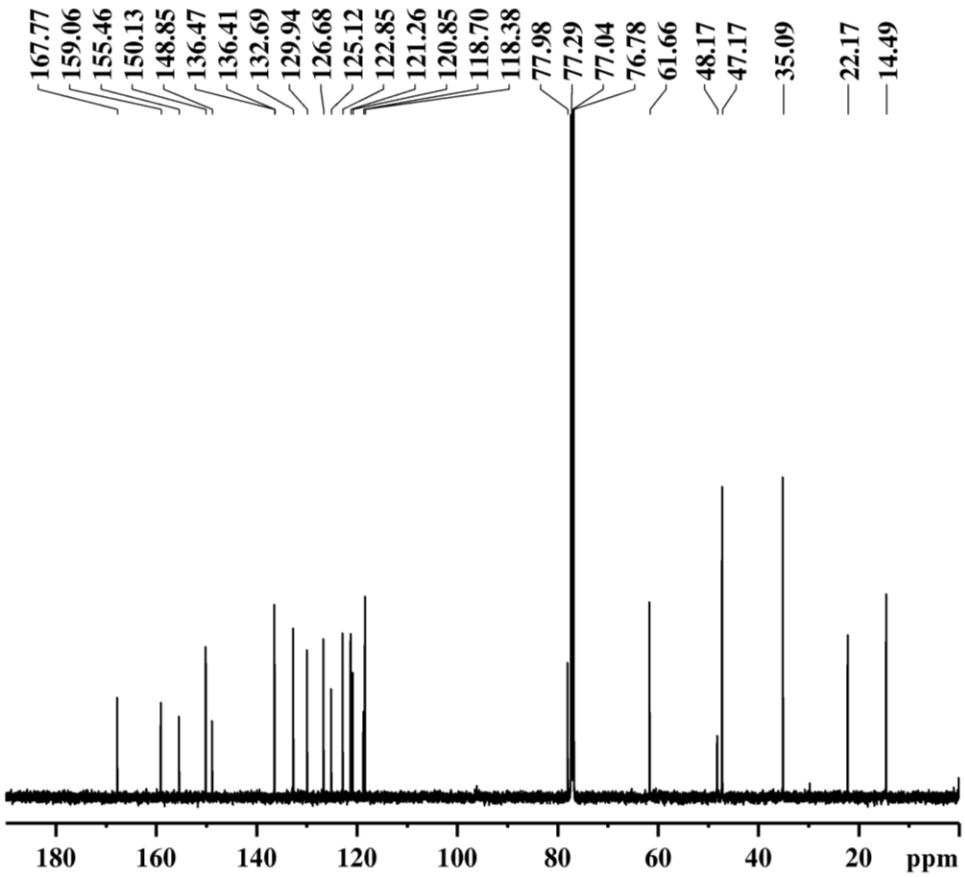

Figure S38: ^{13}C NMR of **9h** in $CDCl_3$.

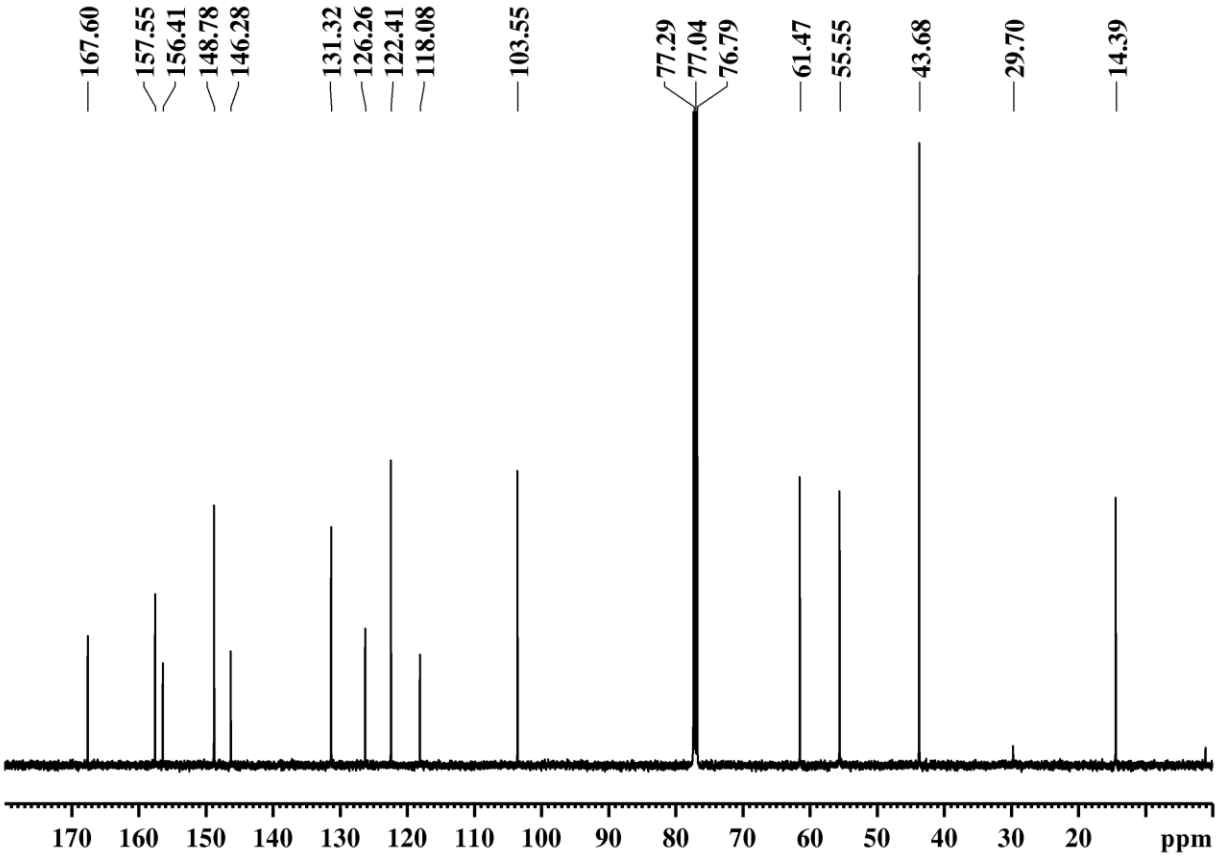

Figure S39: ^{13}C NMR of **9i** in $CDCl_3$.

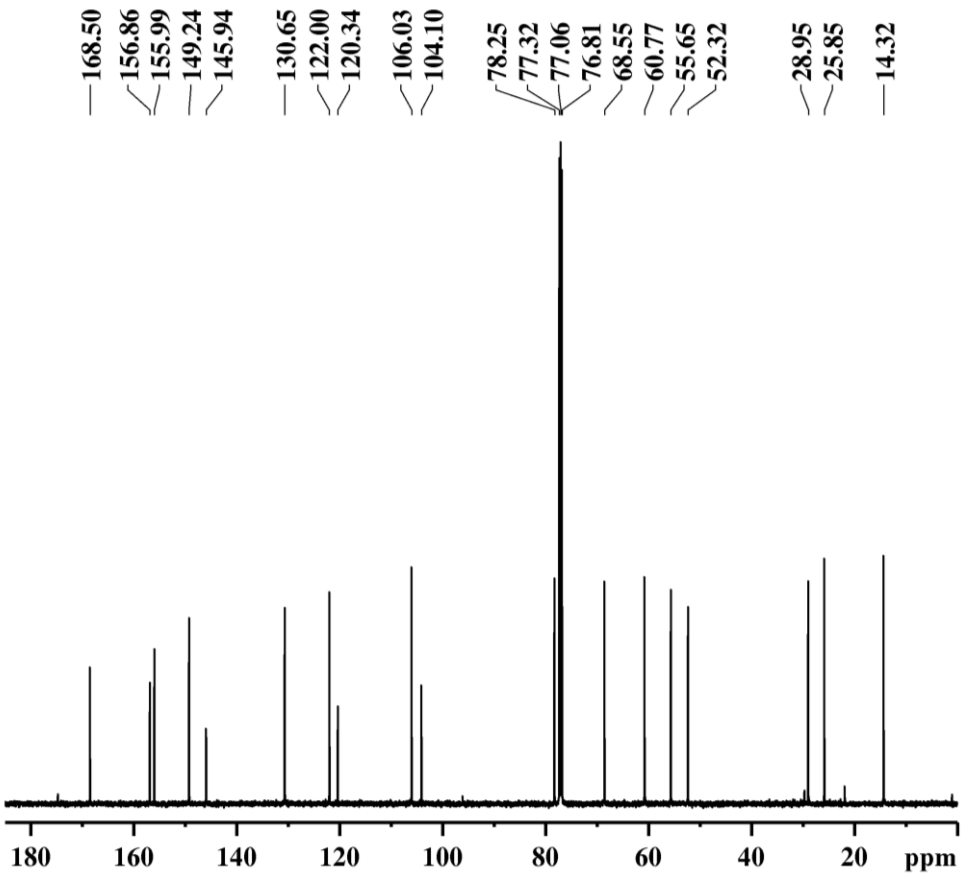

Figure S40: ^{13}C NMR of **9j** in $CDCl_3$.

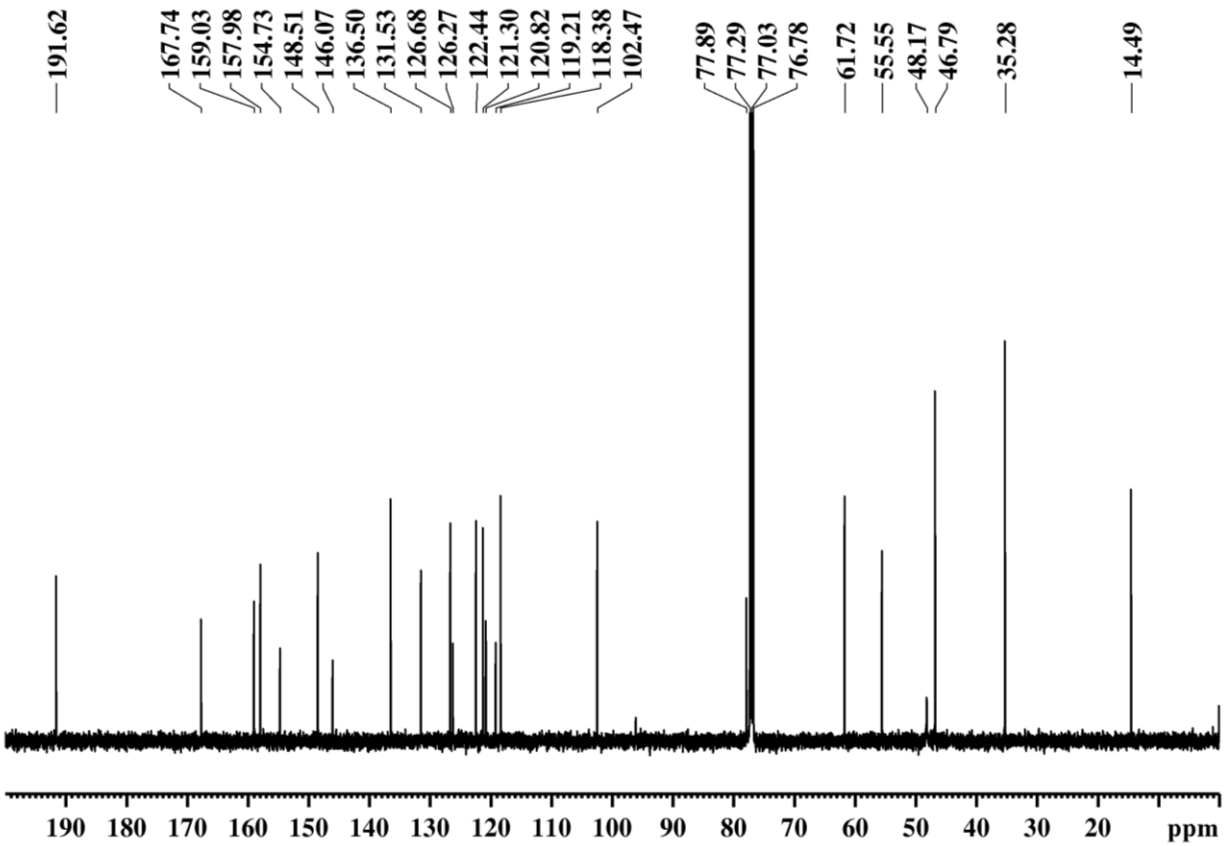

Figure S41: ^{13}C NMR of **9k** in $CDCl_3$.

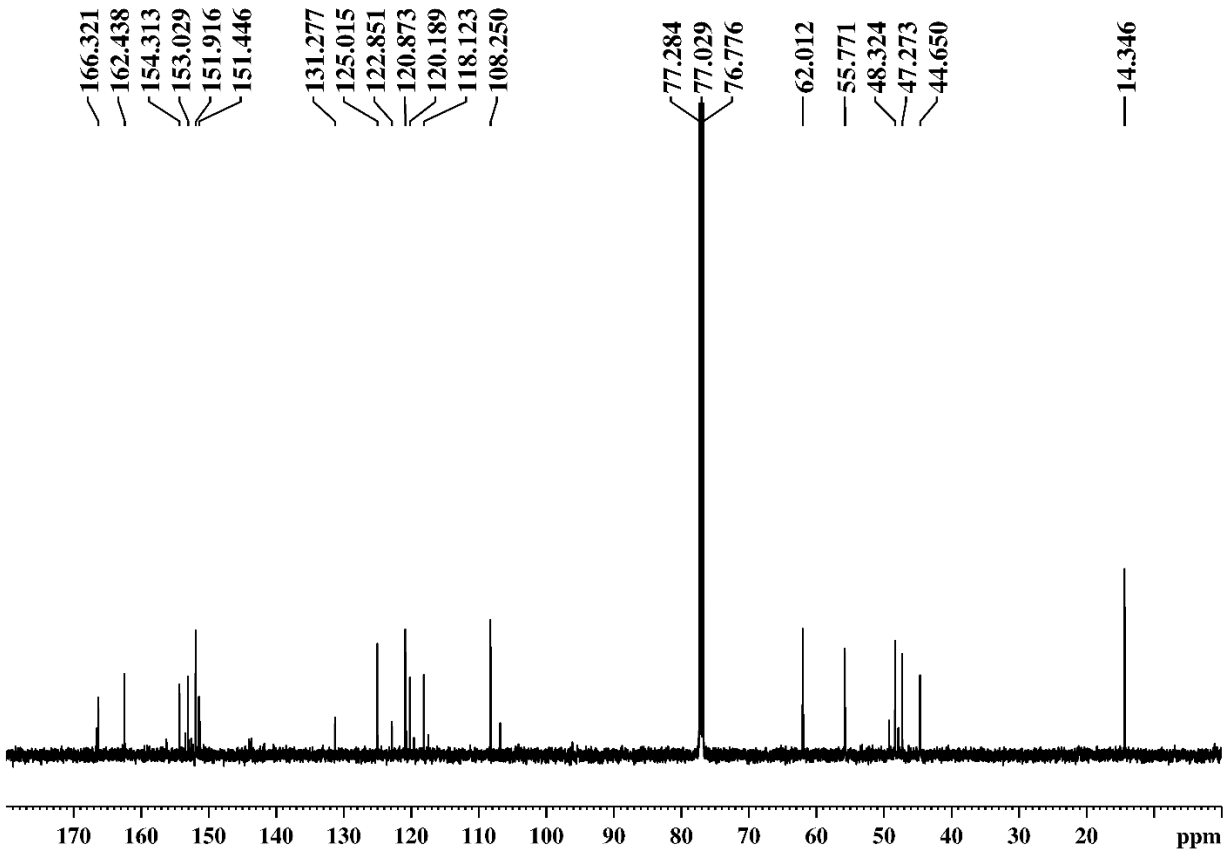

Figure S42: ^{13}C NMR of **9l** in $CDCl_3$.

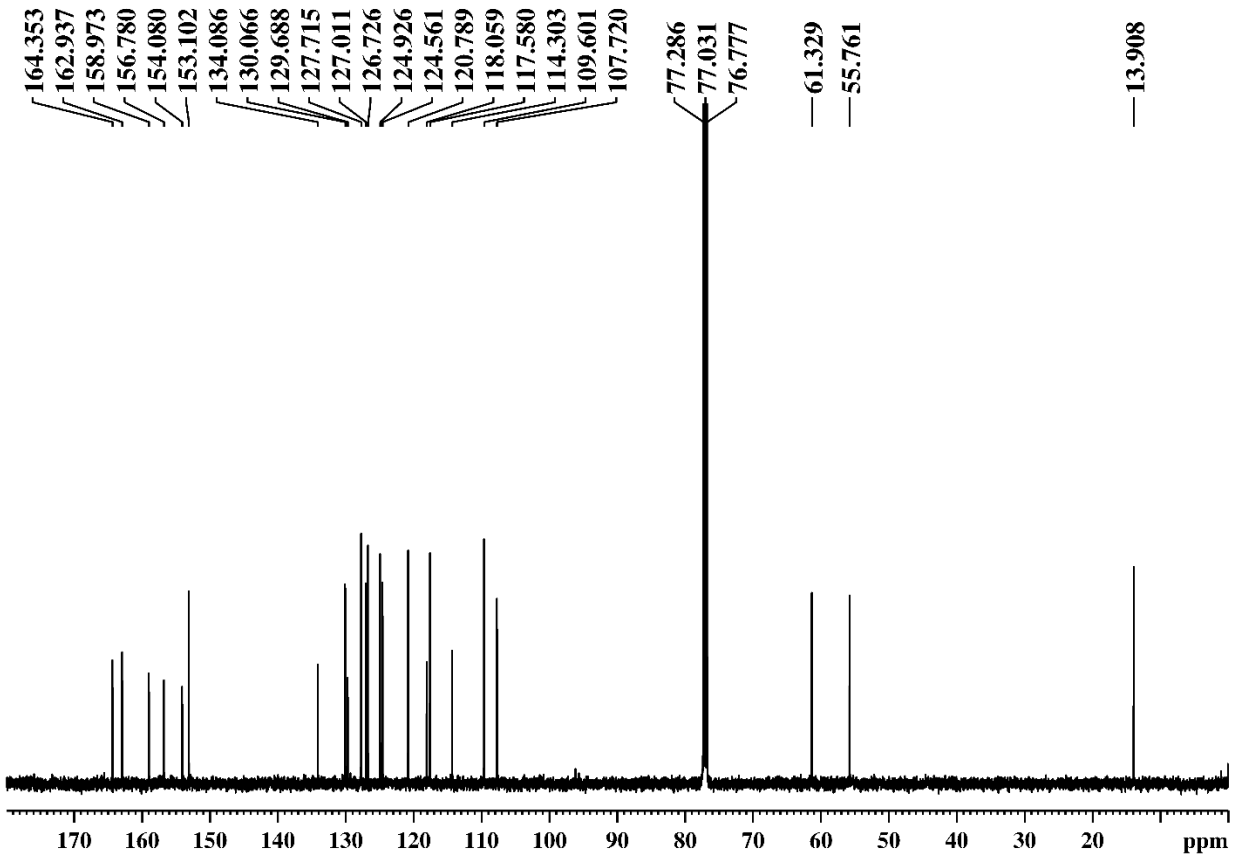

Figure S43: ^{13}C NMR of **9m** in $CDCl_3$.

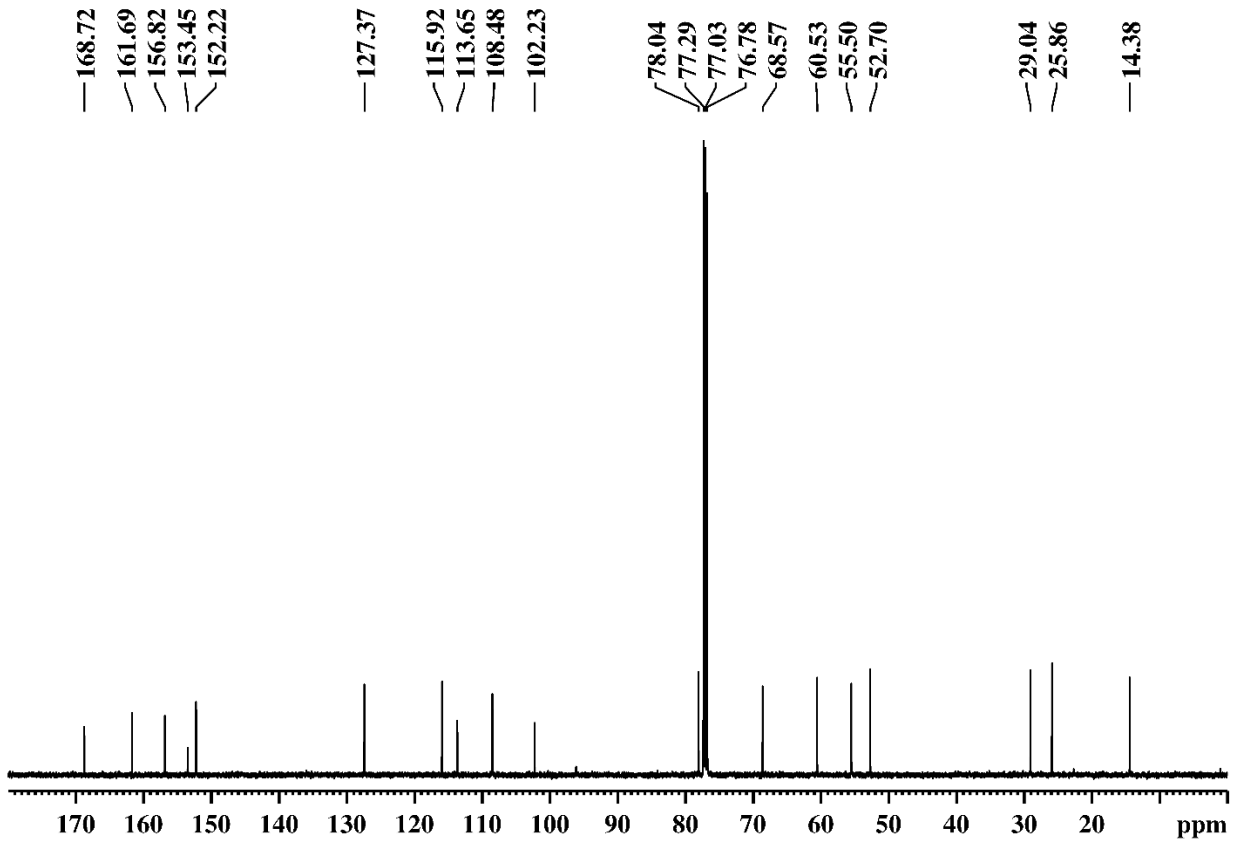

Figure S44: ^{13}C NMR of **9n** in $CDCl_3$.

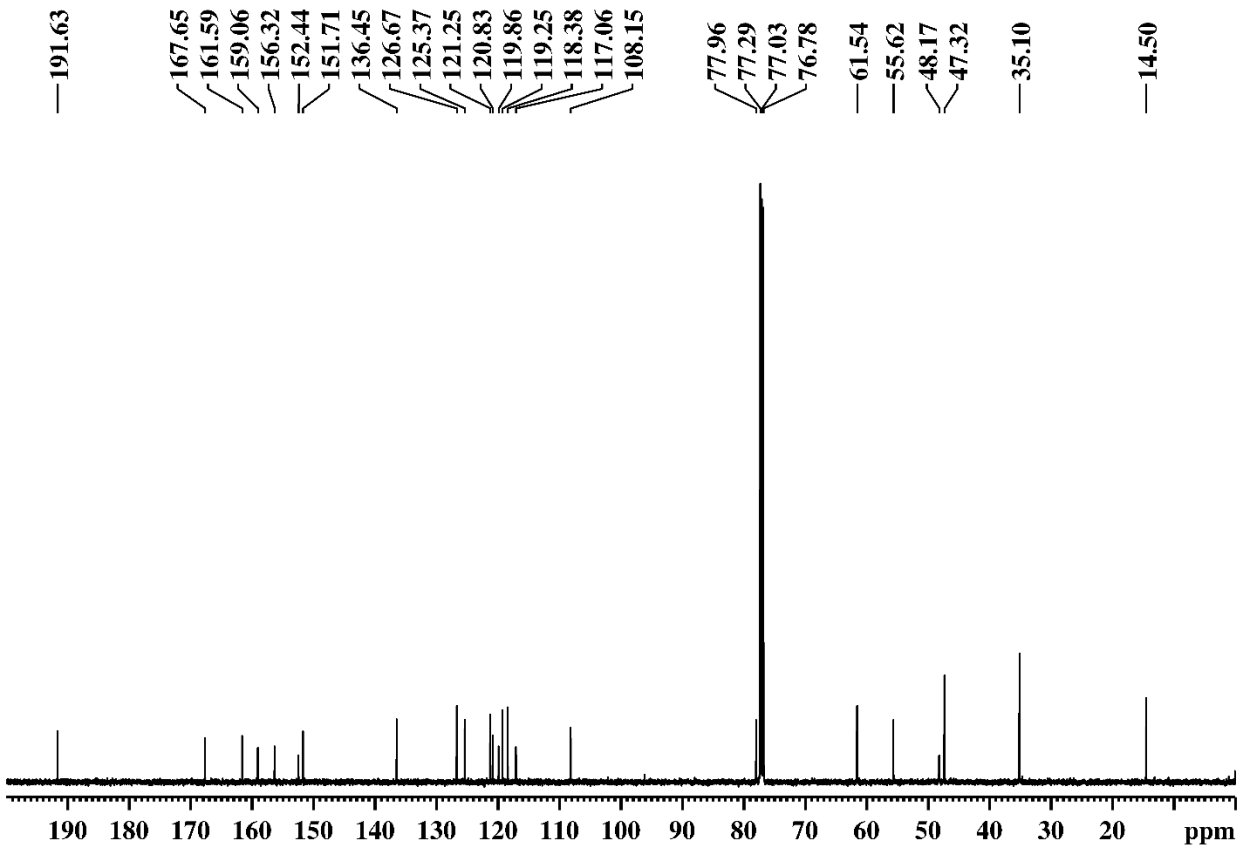

Figure S45: ^{13}C NMR of **9o** in $CDCl_3$.

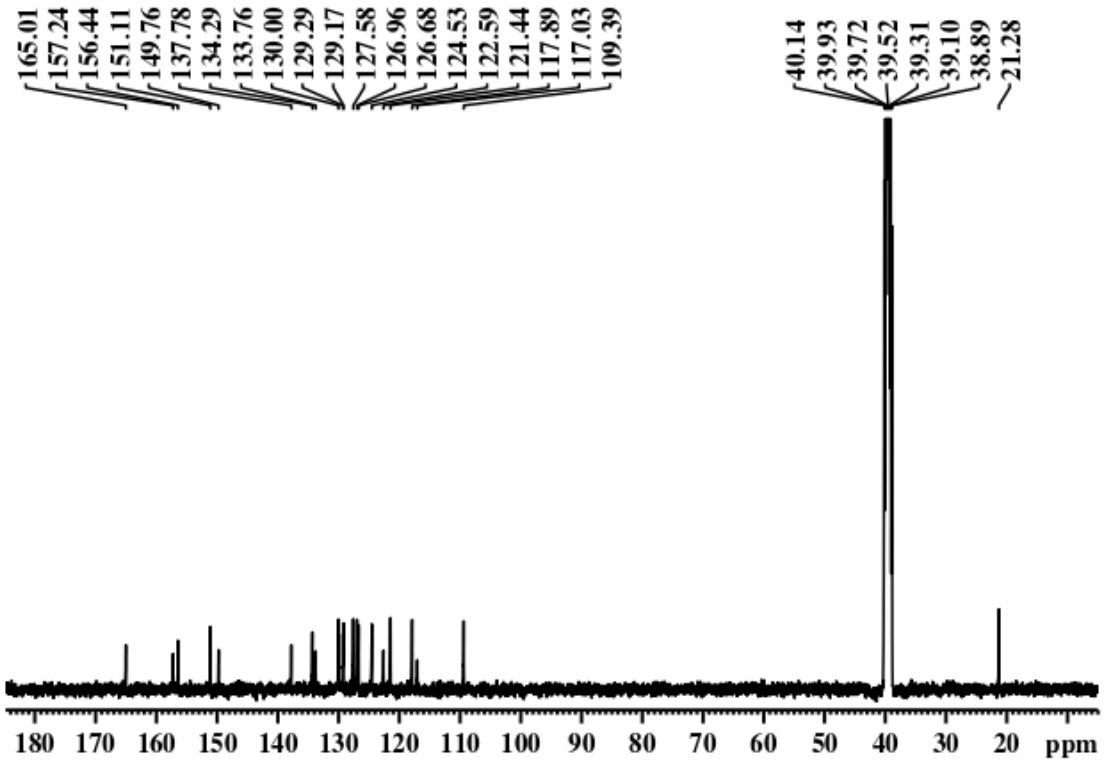

Figure S46: ^{13}C NMR of **10a** in d_6-DMSO.

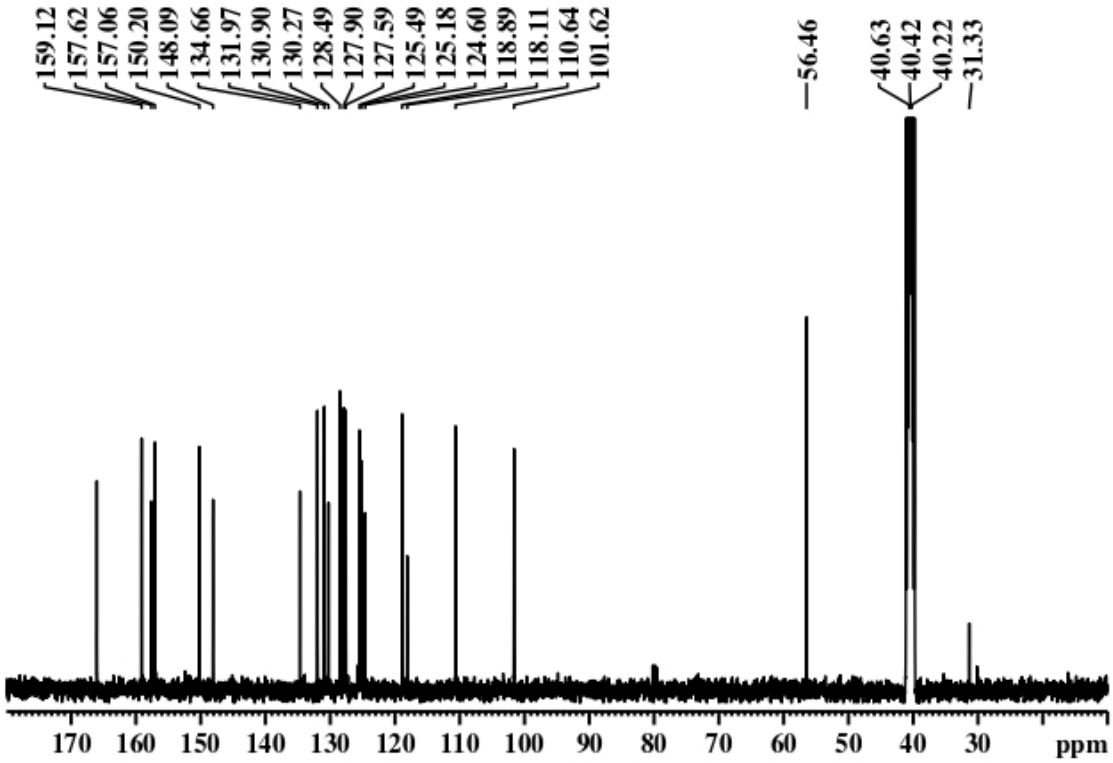

Figure S47: ^{13}C NMR of **10b** in d_6-DMSO.

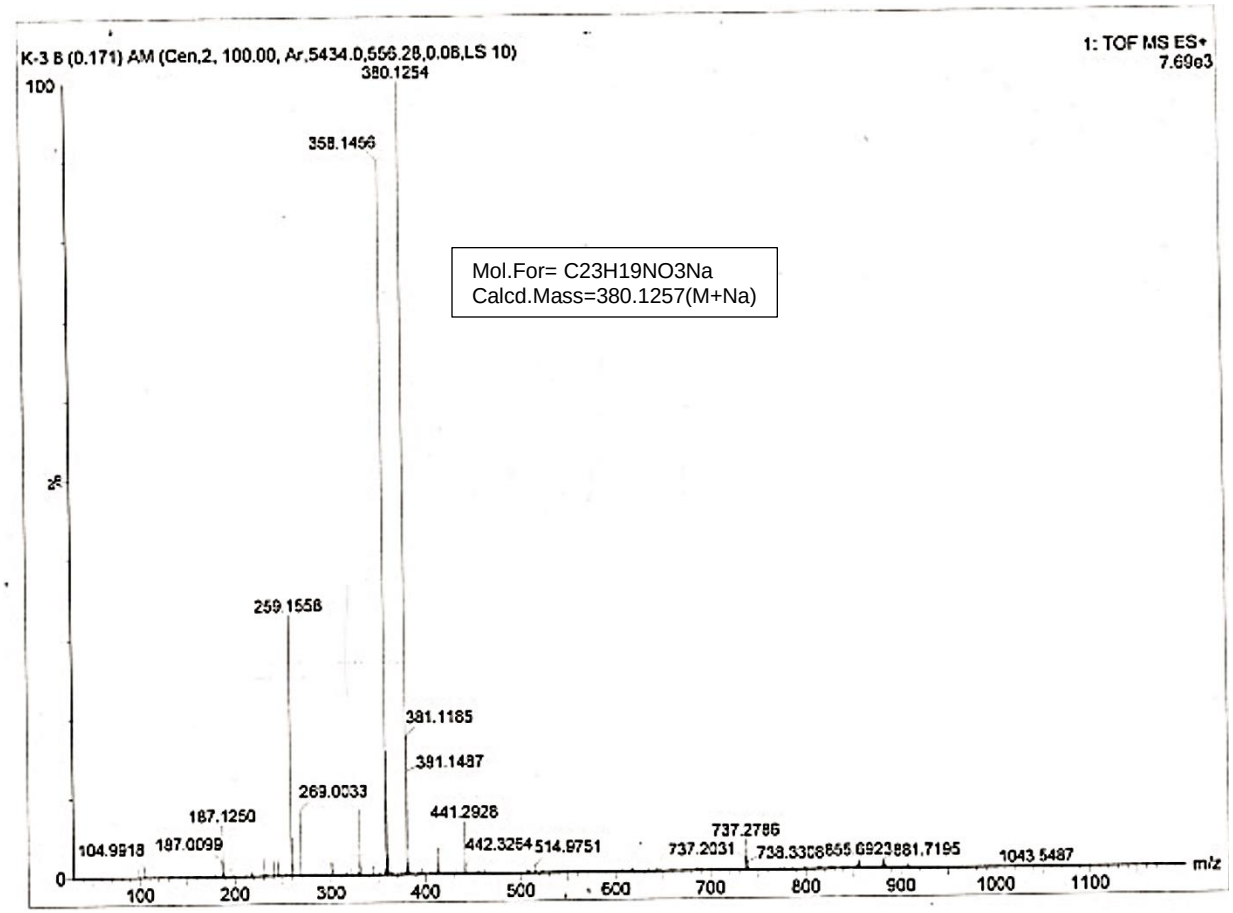

Figure S48: HRMS of **9a** showing molecular ion peak at 380.1254 (m/z) which corresponds to $[M+Na]^+$.

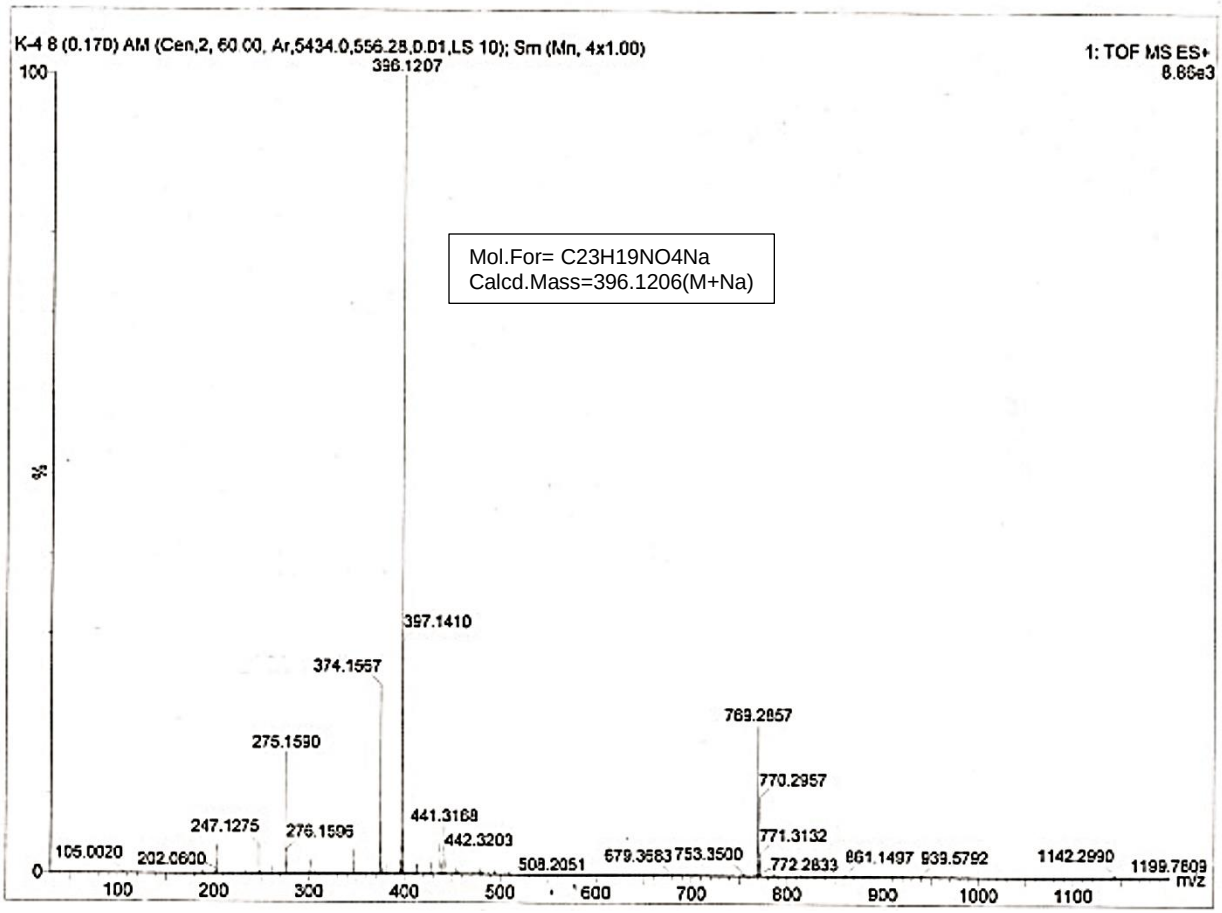

Figure S49: HRMS of **9b** showing molecular ion peak at 396.1207 (m/z) which corresponds to $[M+Na]^+$.

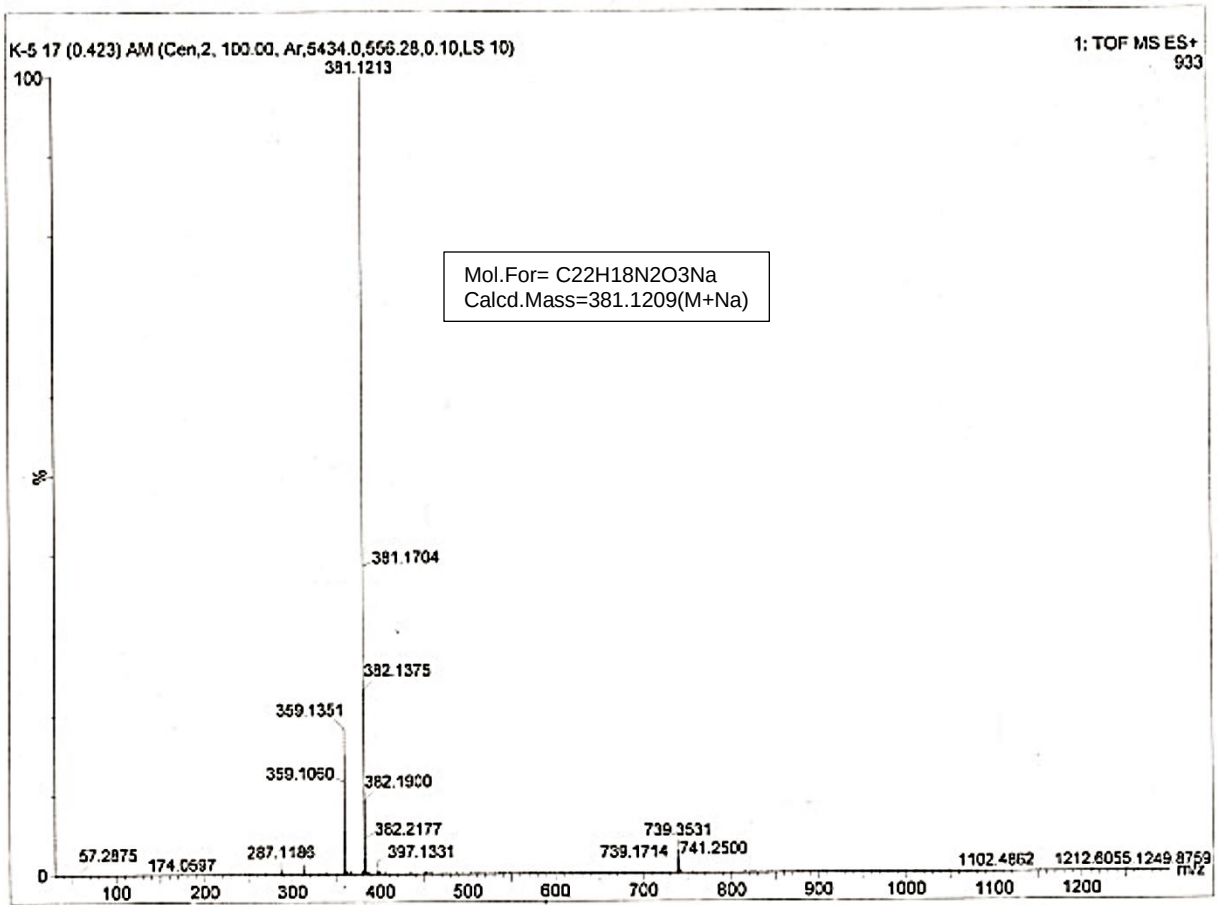

Figure S50: HRMS of **9c** showing molecular ion peak at 381.1213 (m/z) which corresponds to $[M+Na]^+$.

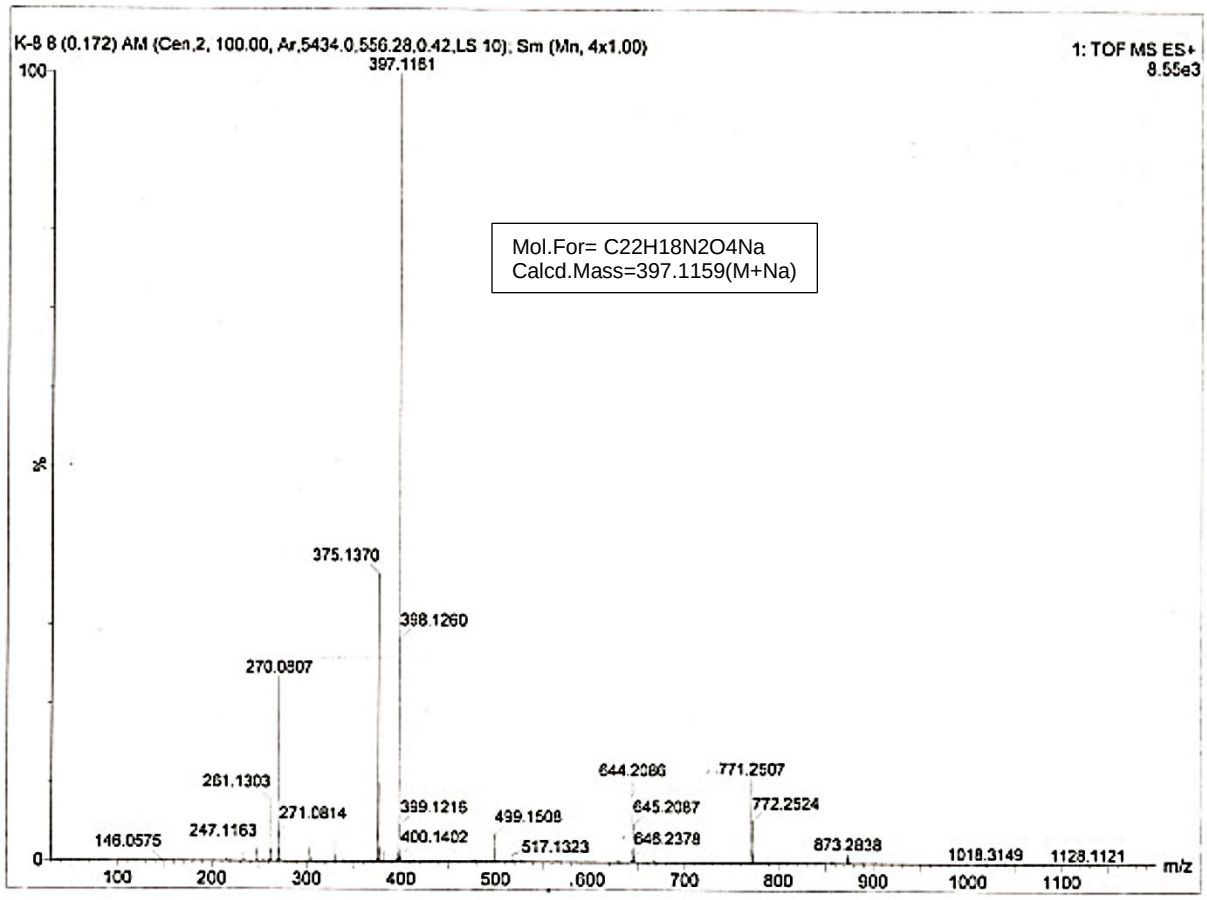

Figure S51: HRMS of **9d** showing molecular ion peak at 397.1161 (m/z) which corresponds to $[M+Na]^+$.

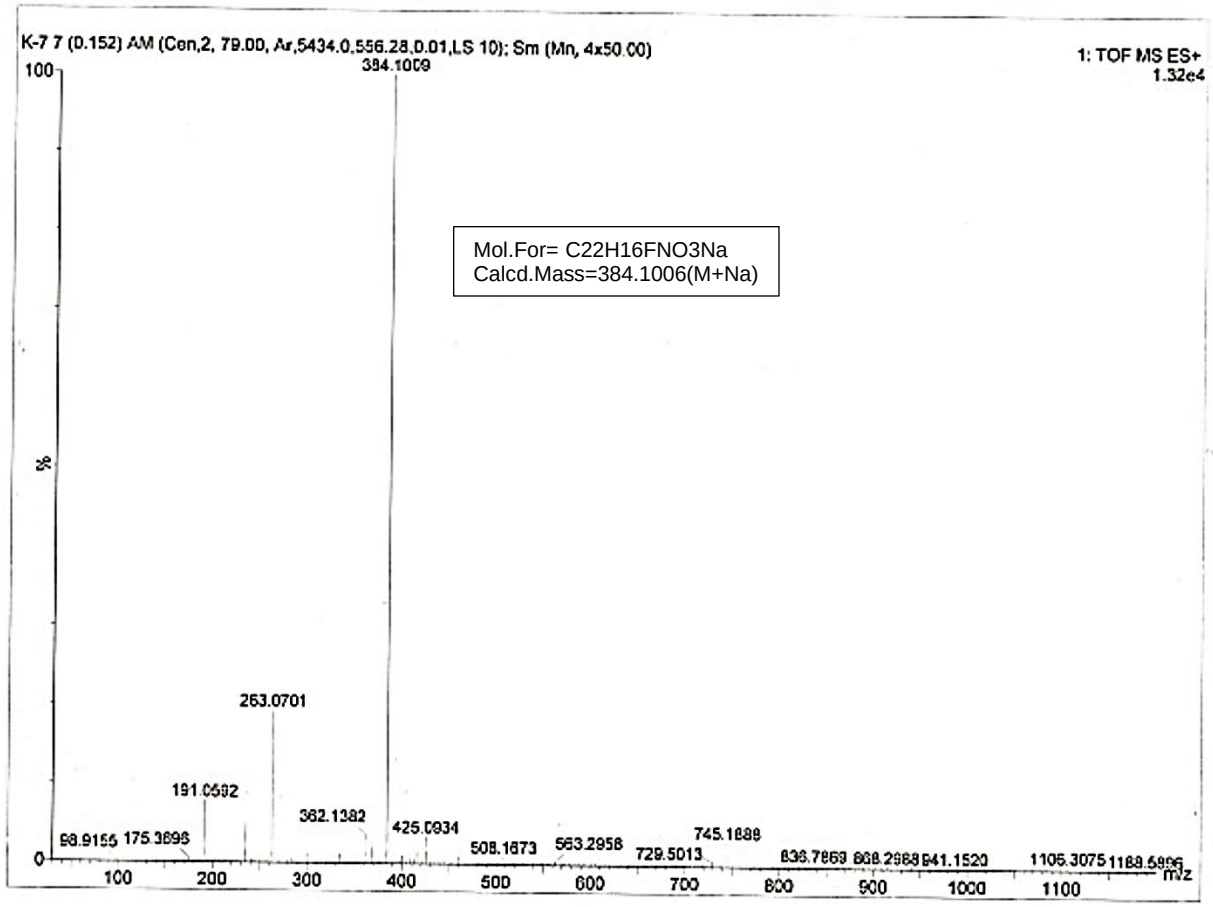

Figure S52: HRMS of **9e** showing molecular ion peak at 384.1009 (m/z) which corresponds to $[M+Na]^+$.

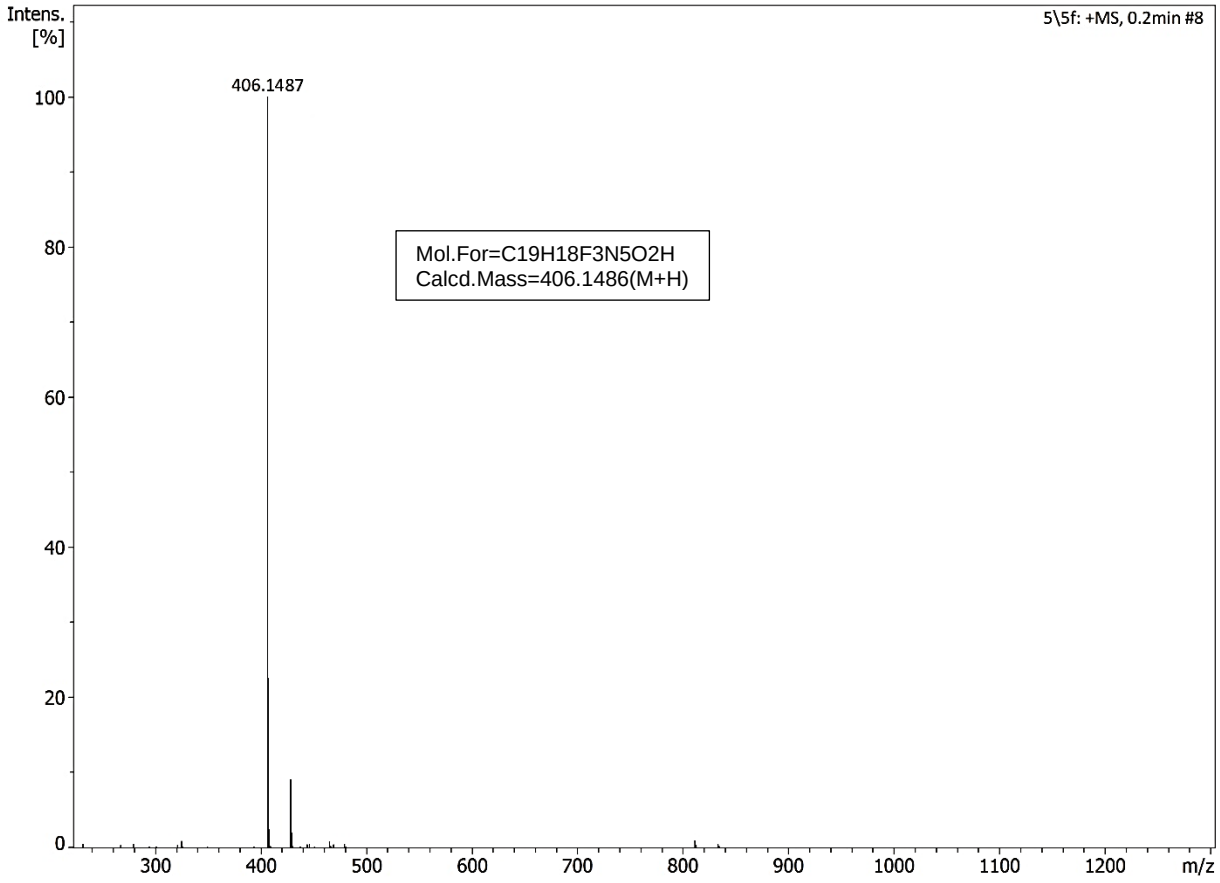

Figure S53: HRMS of **9f** showing molecular ion peak at 406.1487 (m/z) which corresponds to $[M+H]^+$.

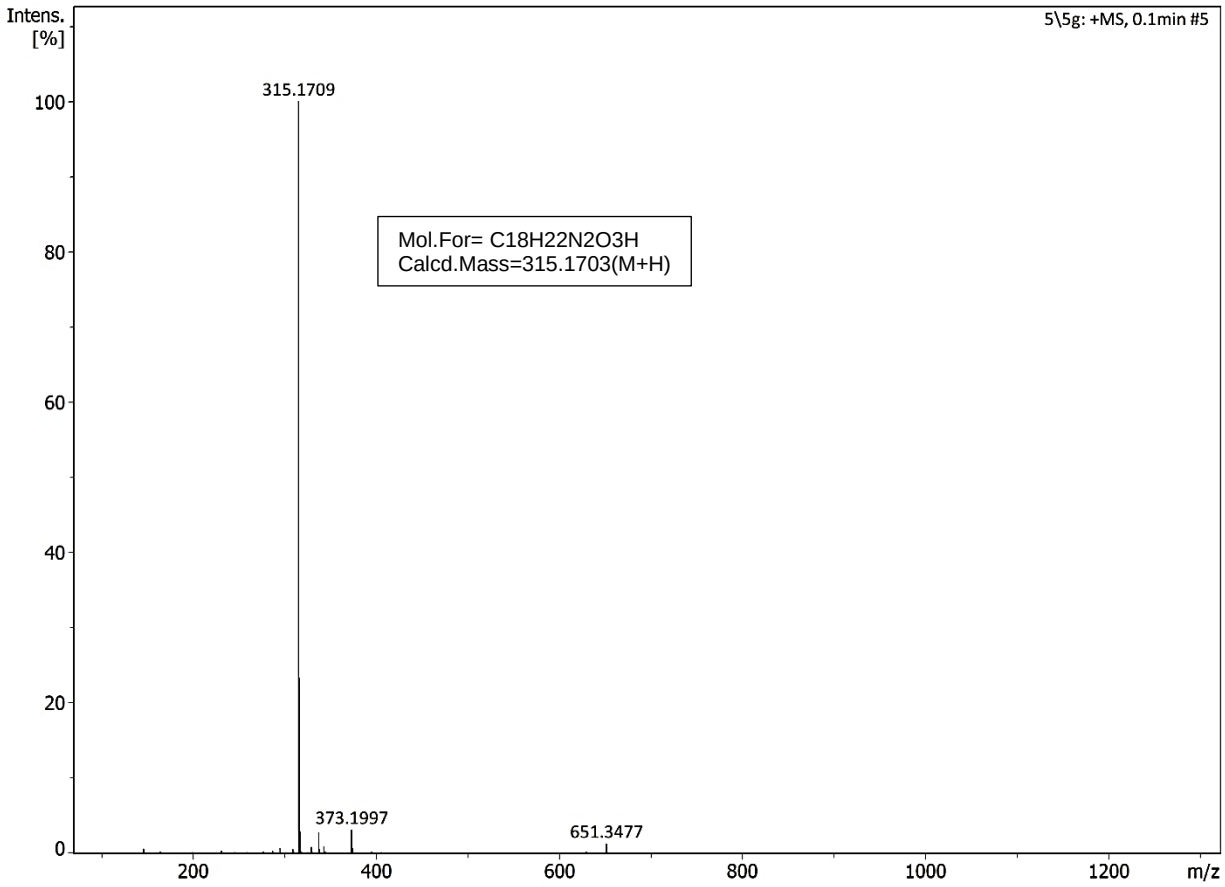

Figure S54: HRMS of **9g** showing molecular ion peak at 315.1709 (m/z) which corresponds to $[M+H]^+$.

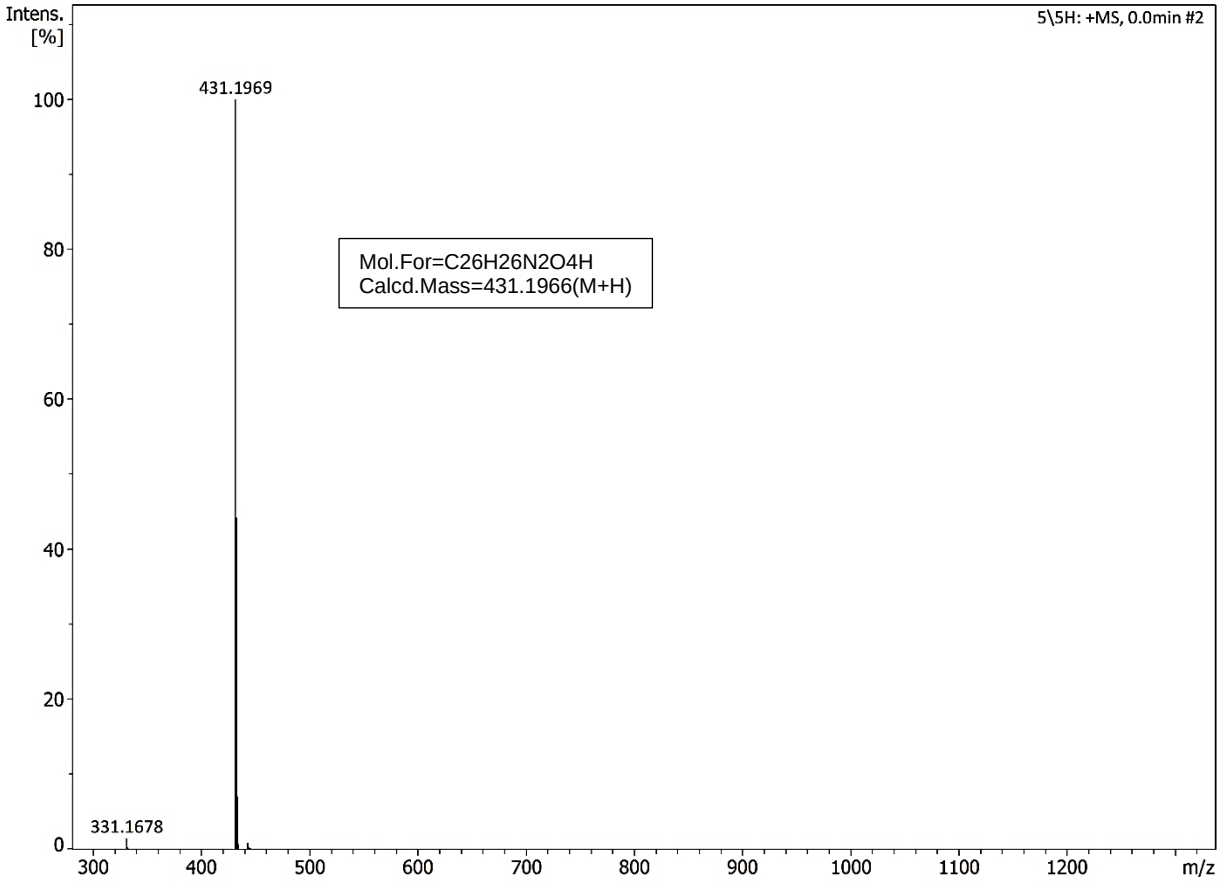

Figure S55: HRMS of **9h** showing molecular ion peak at 431.1969 (m/z) which corresponds to $[M+H]^+$.

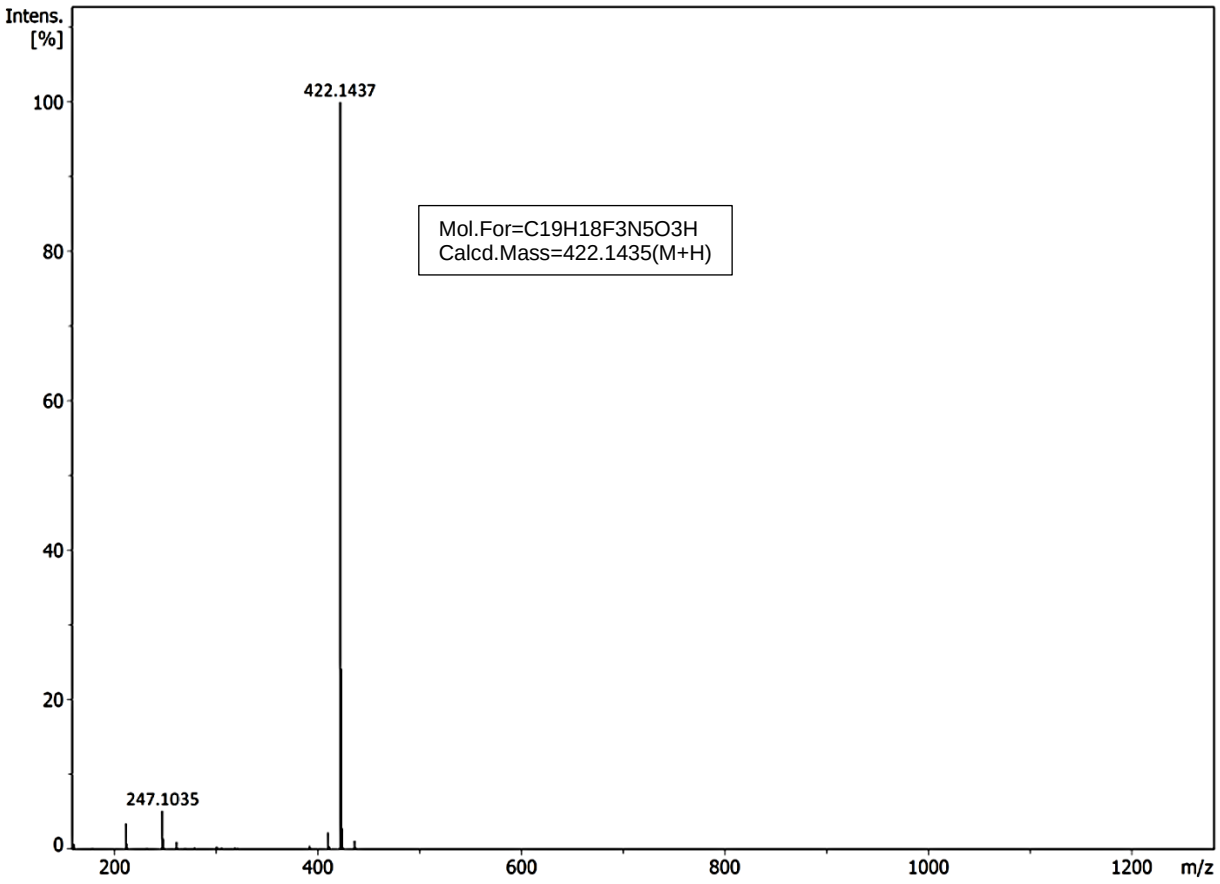

Figure S56: HRMS of **9i** showing molecular ion peak at 422.1437 (m/z) which corresponds to $[M+H]^+$.

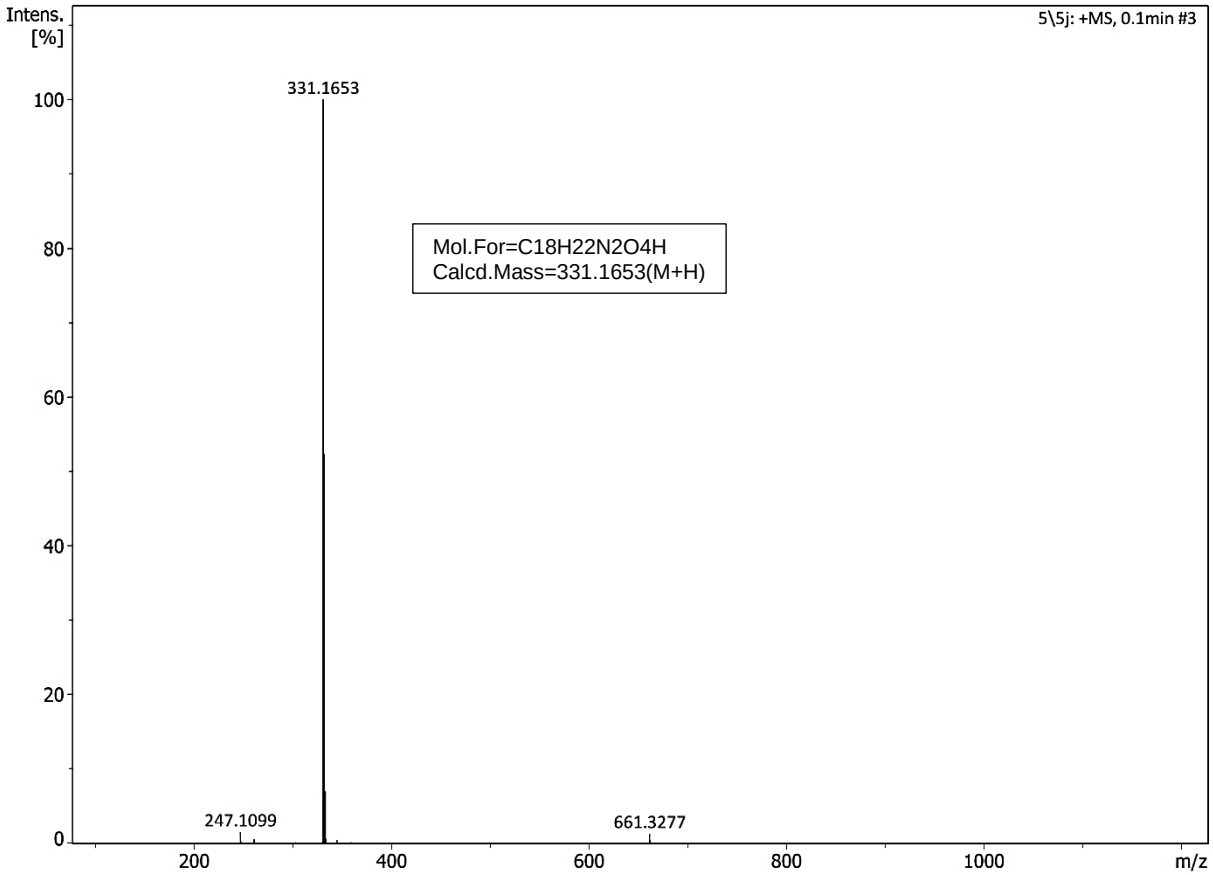

Figure S57: HRMS of **9j** showing molecular ion peak at 331.1653 (m/z) which corresponds to $[M+H]^+$.

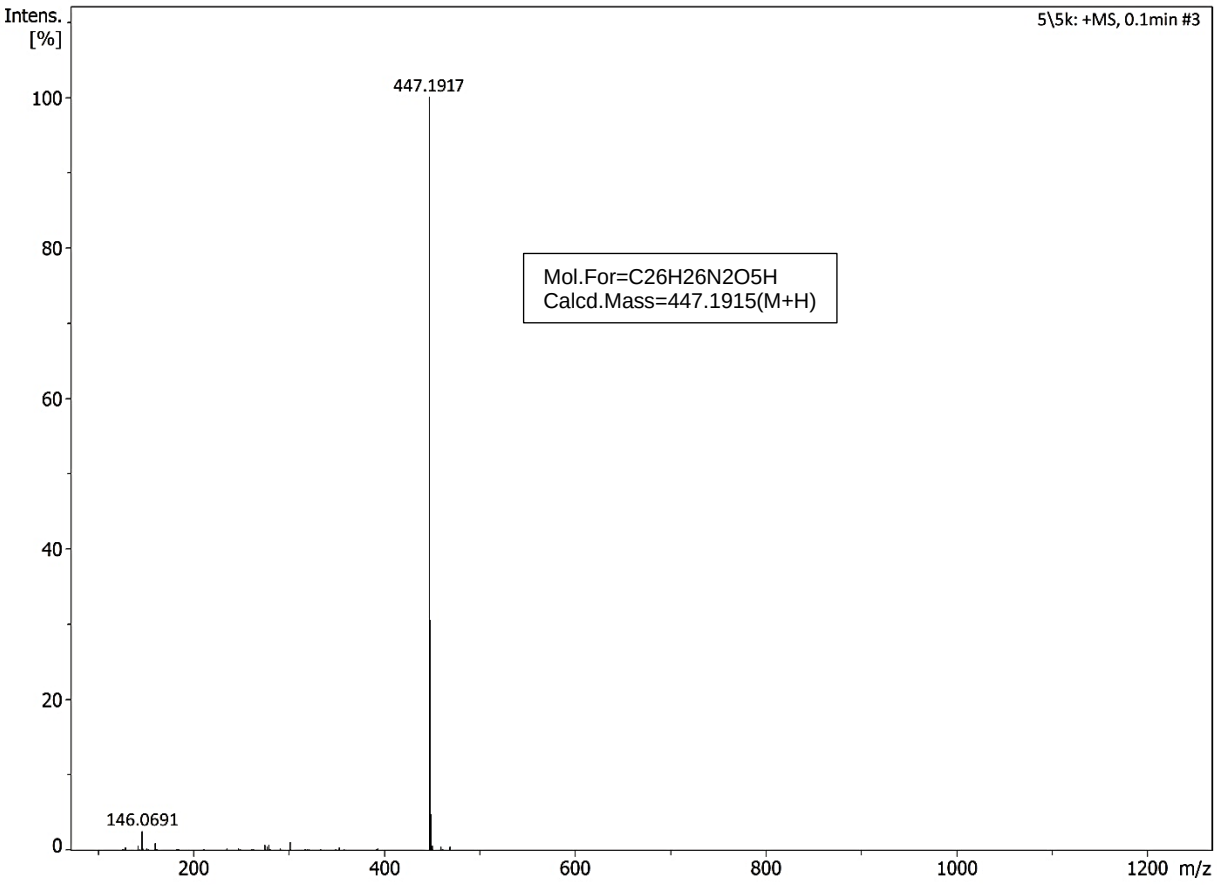

Figure S58: HRMS of **9k** showing molecular ion peak at 447.1917 (m/z) which corresponds to $[M+H]^+$.

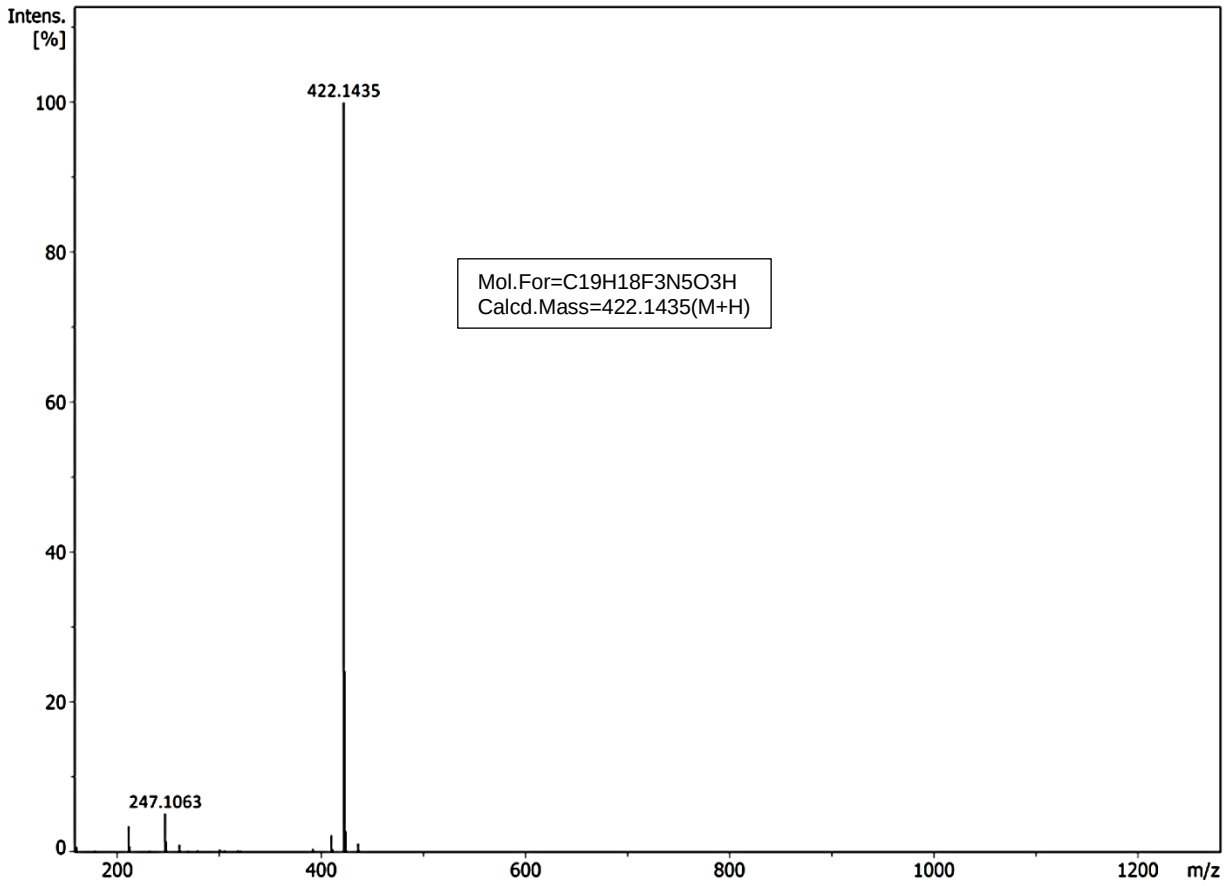

Figure S59: HRMS of **9l** showing molecular ion peak at 422.1435 (m/z) which corresponds to $[M+H]^+$.

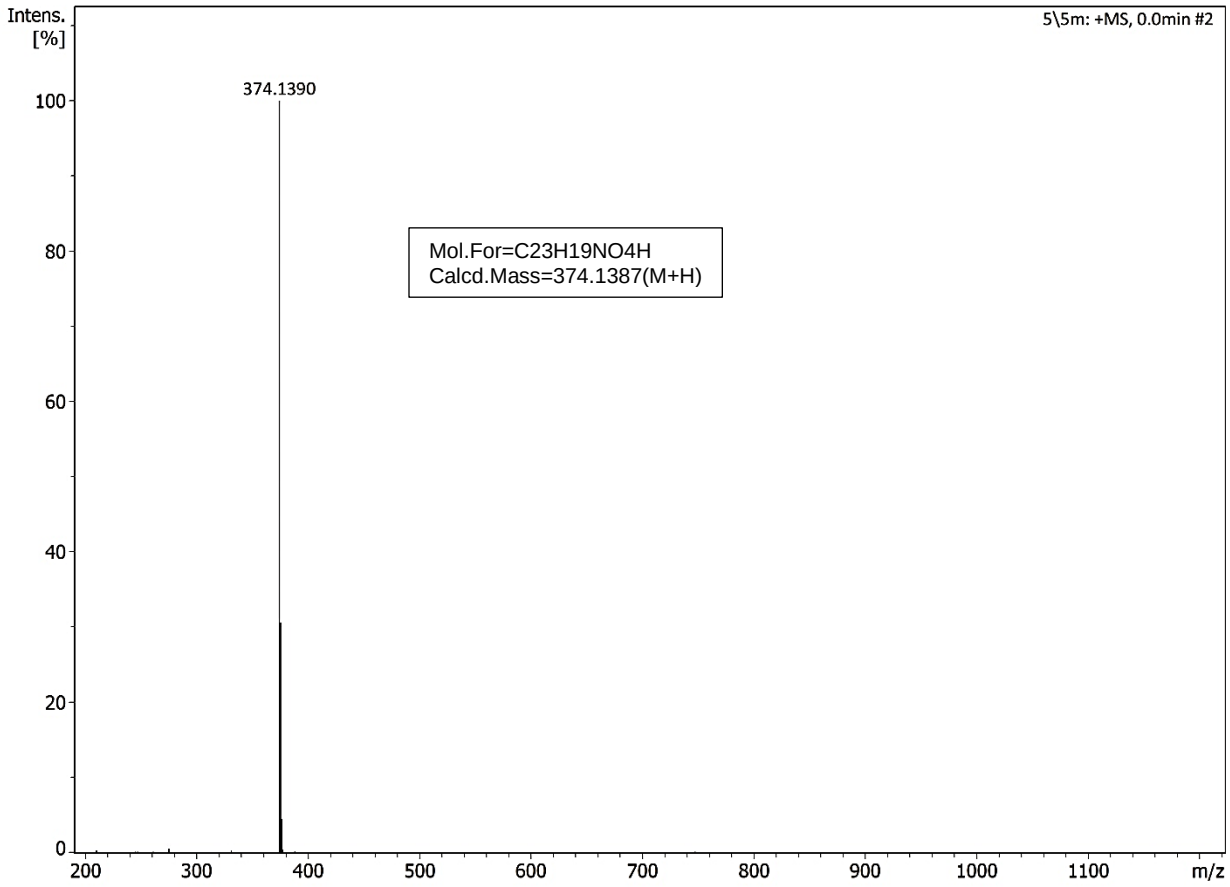

Figure S60: HRMS of **9m** showing molecular ion peak at 374.1390 (m/z) which corresponds to $[M+H]^+$.

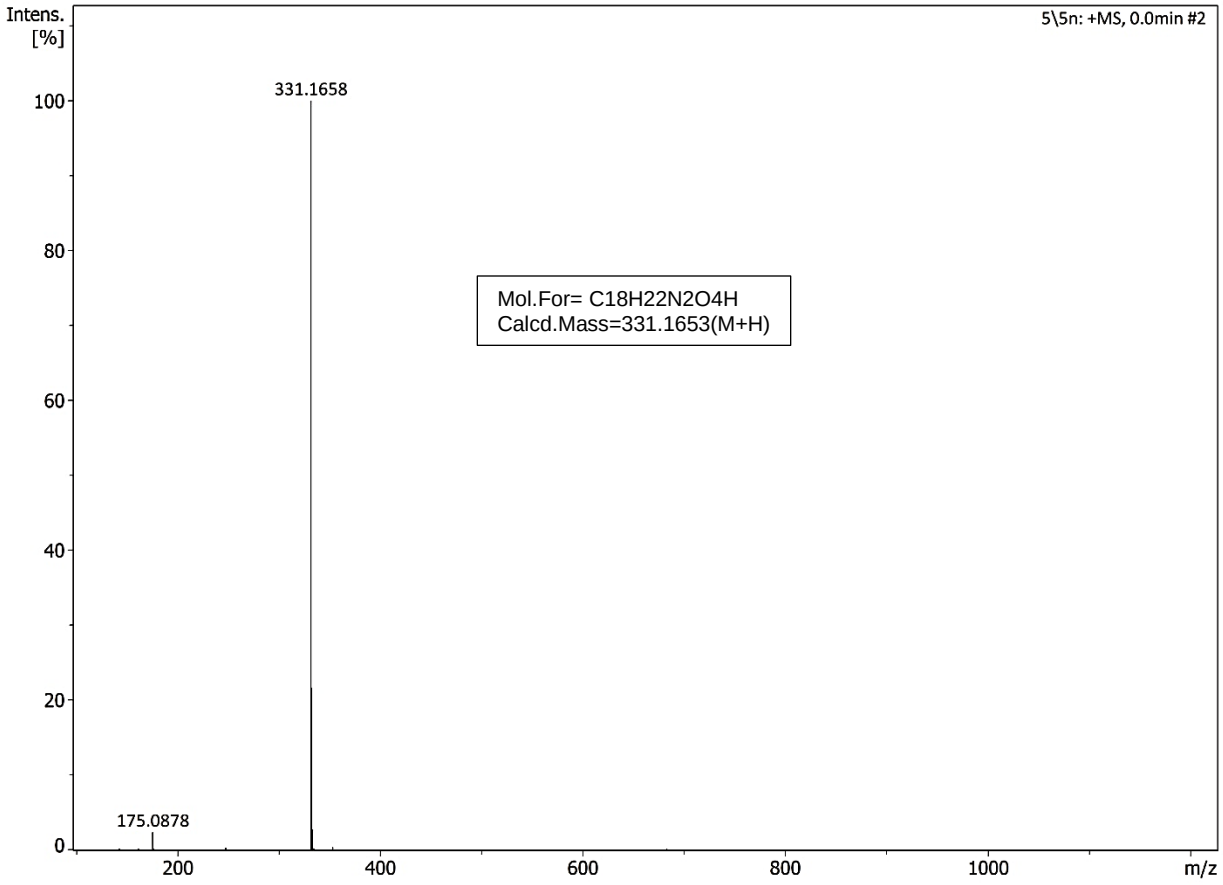

Figure S61: HRMS of **9n** showing molecular ion peak at 331.1658 (m/z) which corresponds to $[M+H]^+$.

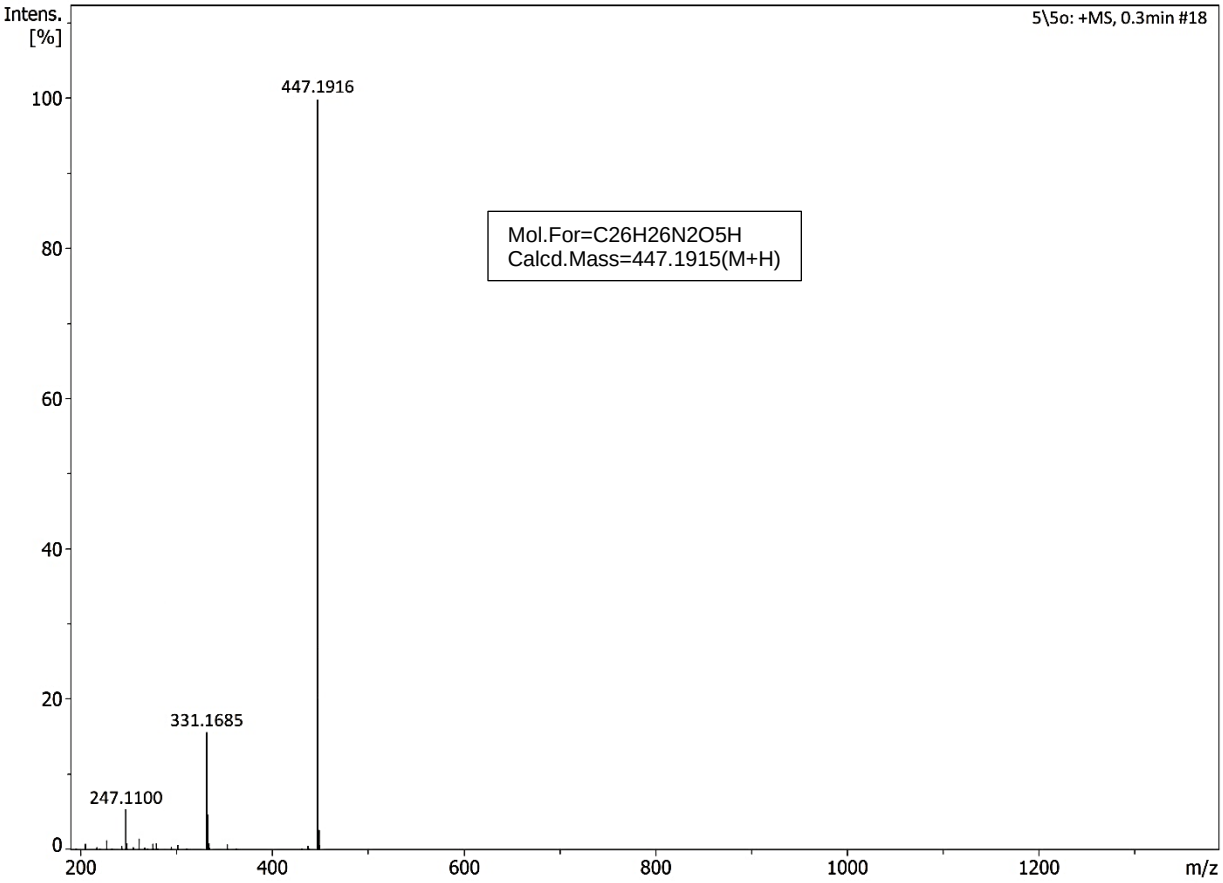

Figure S62: HRMS of **9o** showing molecular ion peak at 447.1916 (m/z) which corresponds to $[M+H]^+$.

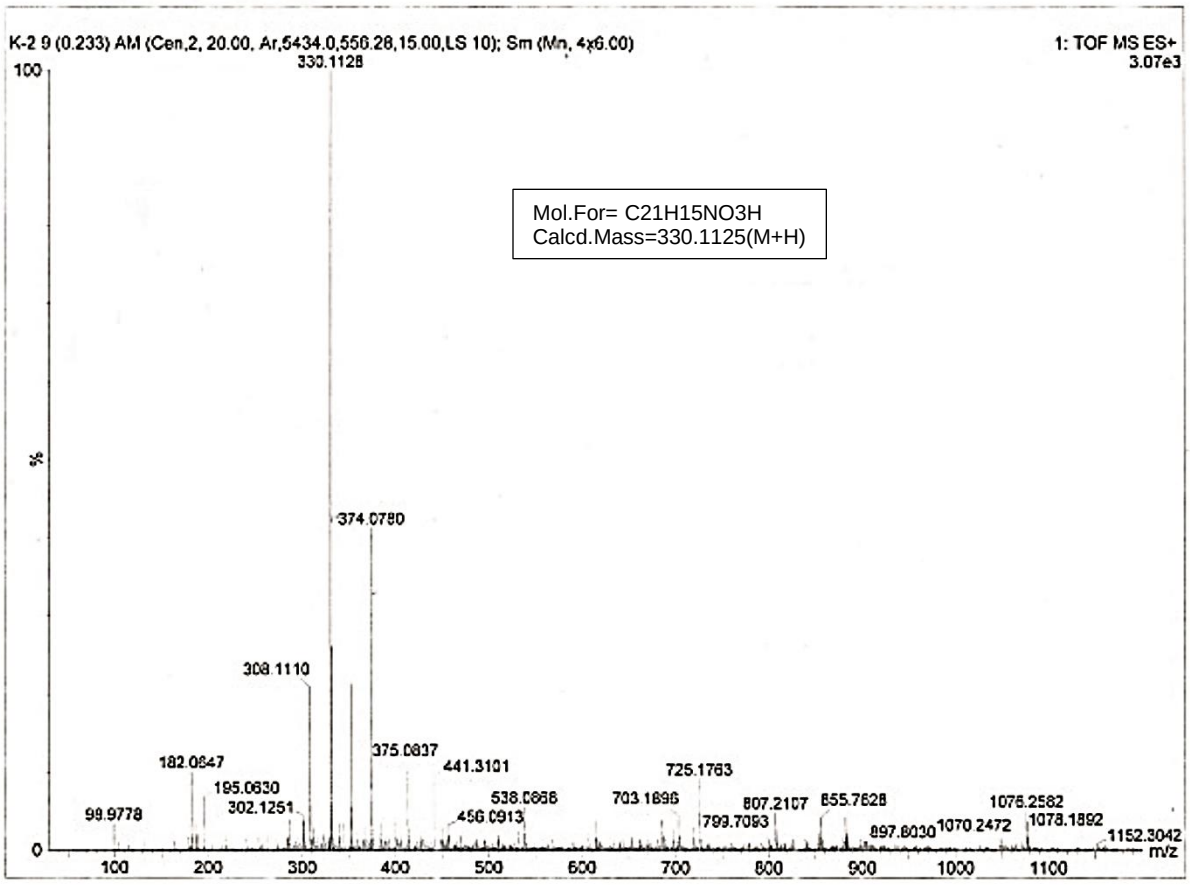

Figure S63: HRMS of **10a** showing molecular ion peak at 330.1128 (m/z) which corresponds to $[M+H]^+$.

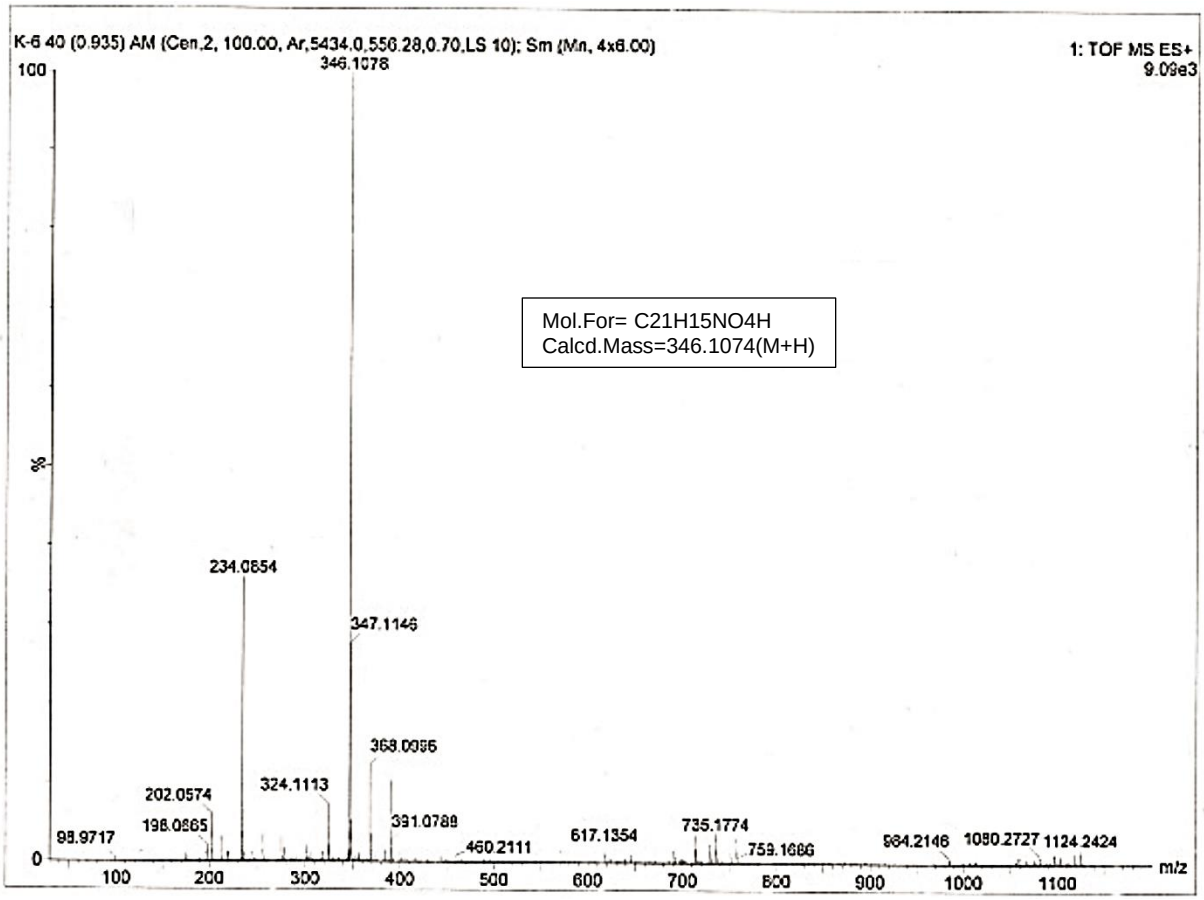

Figure S64: HRMS of **10b** showing molecular ion peak at 346.1078 (m/z) which corresponds to $[M+H]^+$.

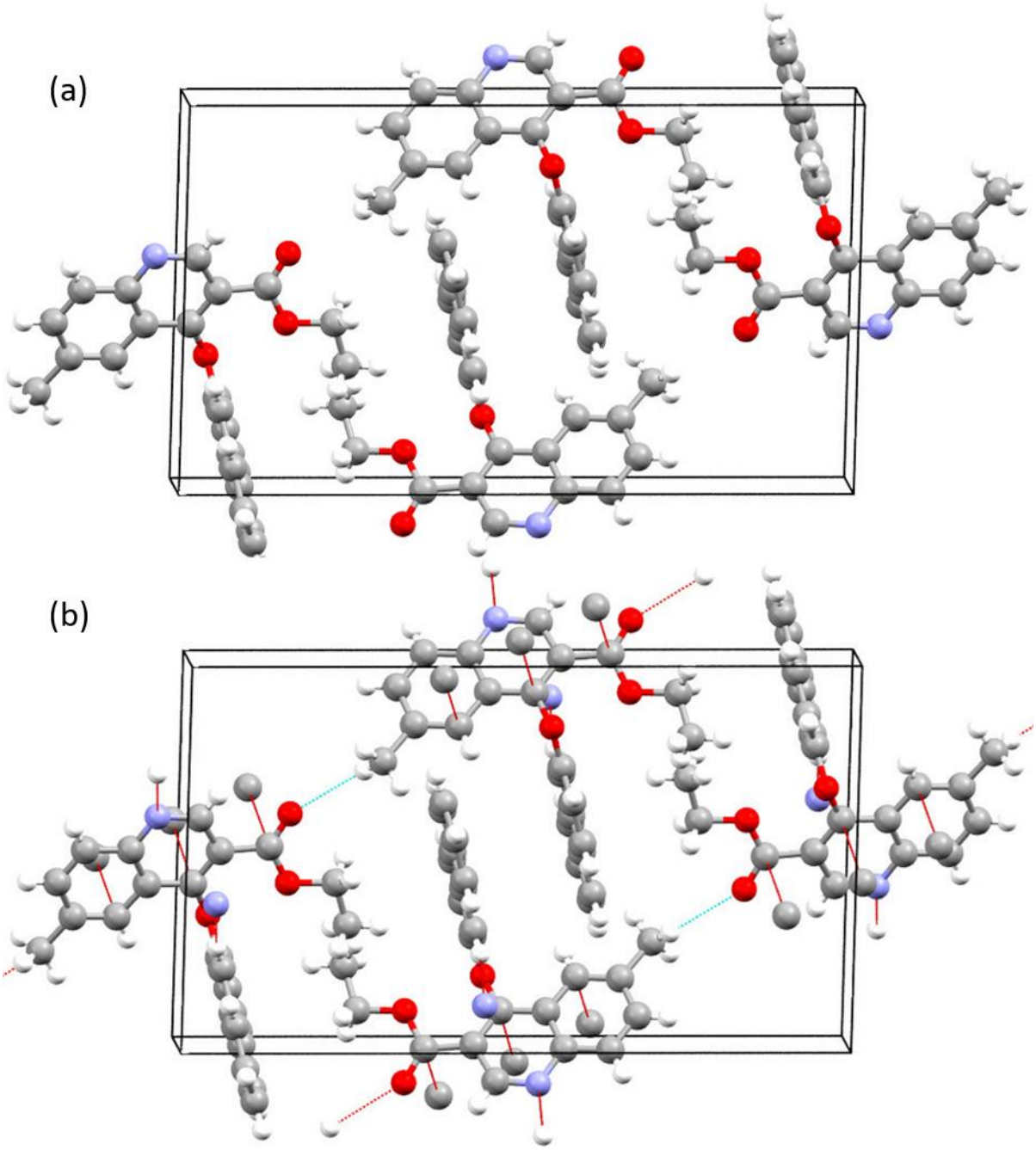

Figure S65: Unit cell packing diagram (a) and showing short contact bonding (b) of ethyl 6-methyl-4-(naphthalen-2-yloxy)quinoline-3-carboxylate (9a). Color code: N, blue; C, black; O, red; H, white.

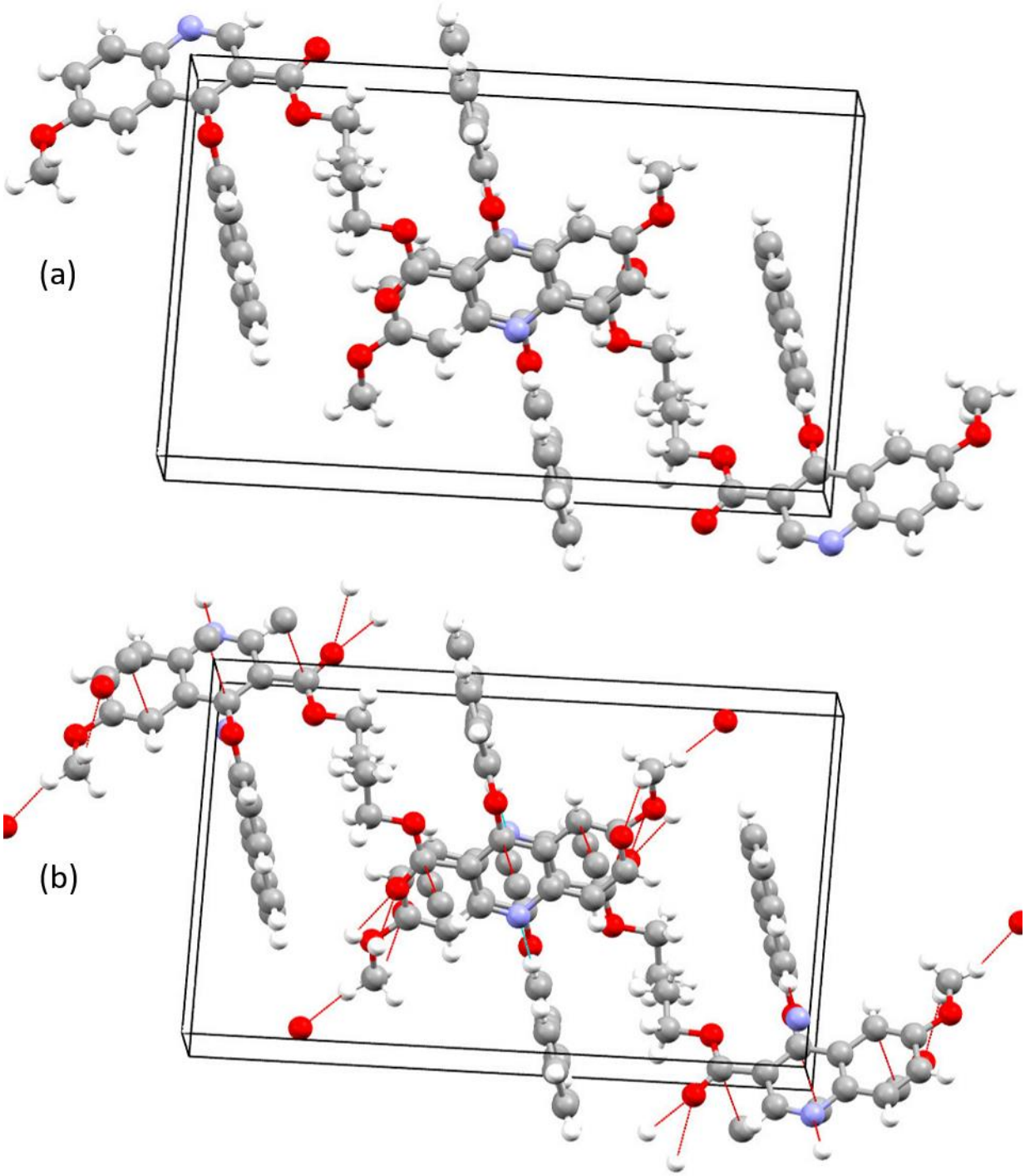

Figure S66: Unit cell packing diagram (a) and showing short contact bonding (b) of ethyl 6-methoxy-4-(naphthalen-2-yloxy)quinoline-3-carboxylate (9b). Color code: N, blue; C, black; O, red; H, white.

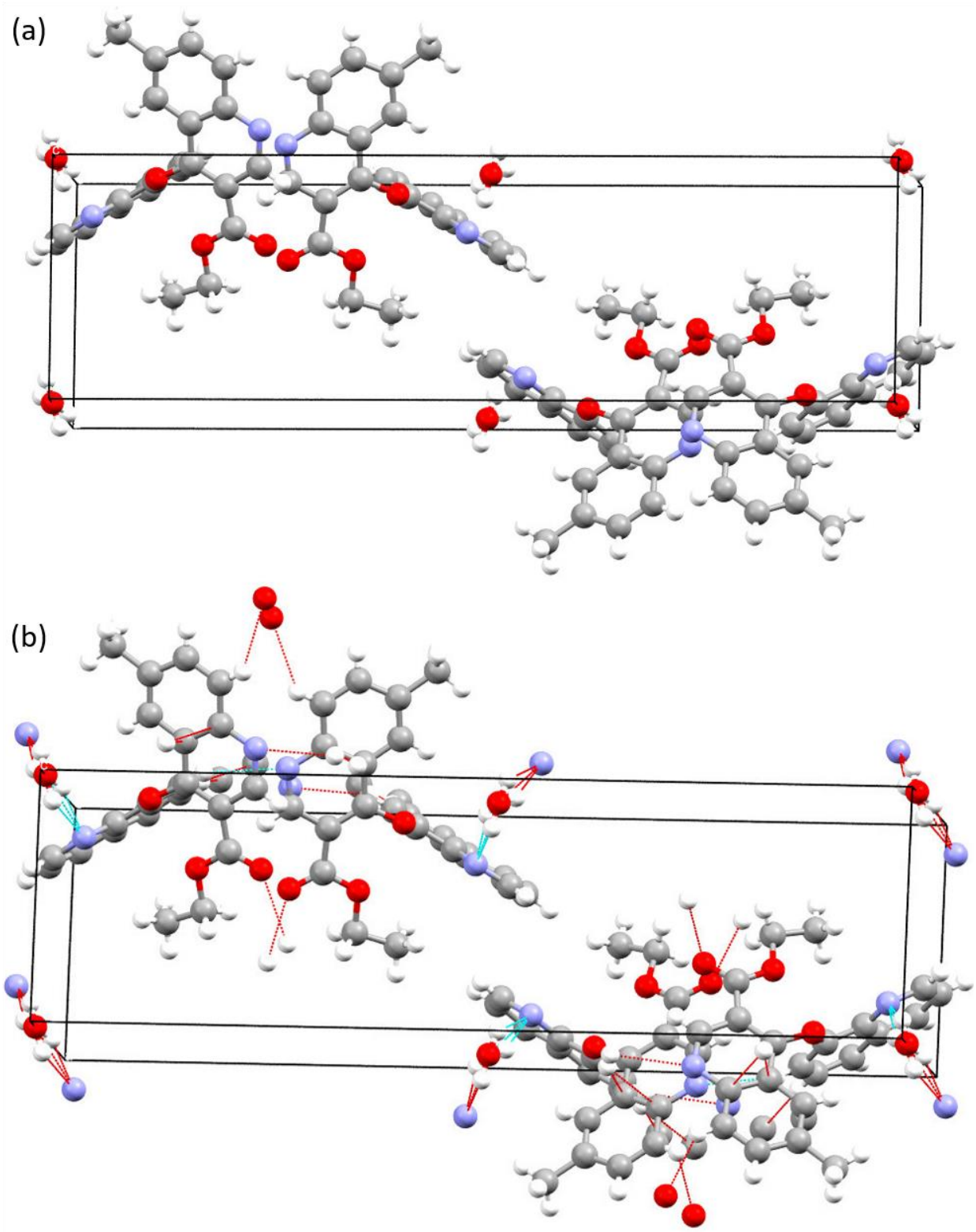

Figure S67: Unit cell packing diagram (a), showing short contact bonding (b) and hydrogen bonding (c) of ethyl 6-methyl-4-(quinolin-8-yloxy)quinoline-3-carboxylate (9c). Color code: N, blue; C, black; O, red; H, white.

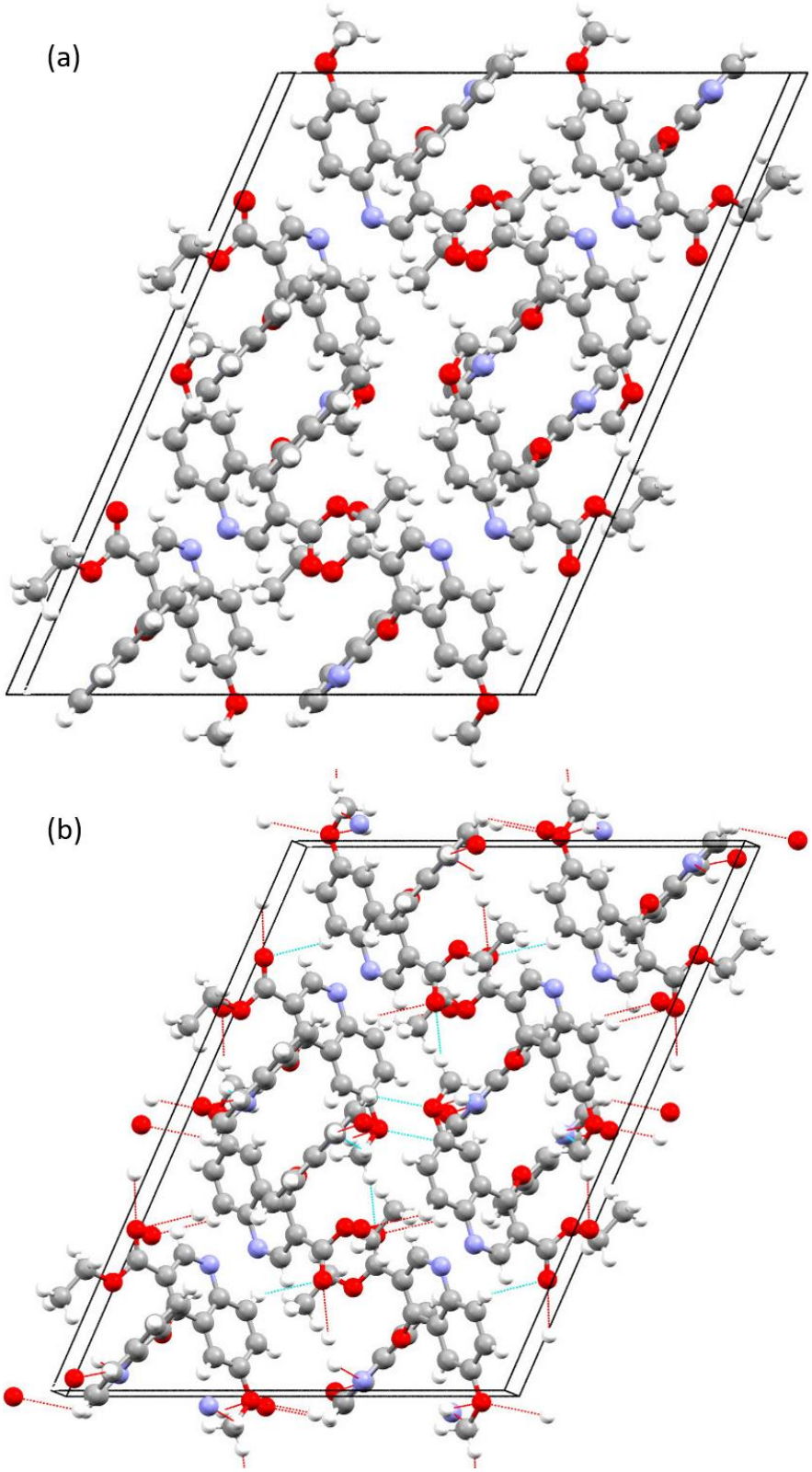

Figure S68: Unit cell packing diagram (a) and showing short contact bonding (b) of ethyl 6-methoxy-4-(quinolin-8-yloxy)quinoline-3-carboxylate (9d). Color code: N, blue; C, black; O, red; H, white.

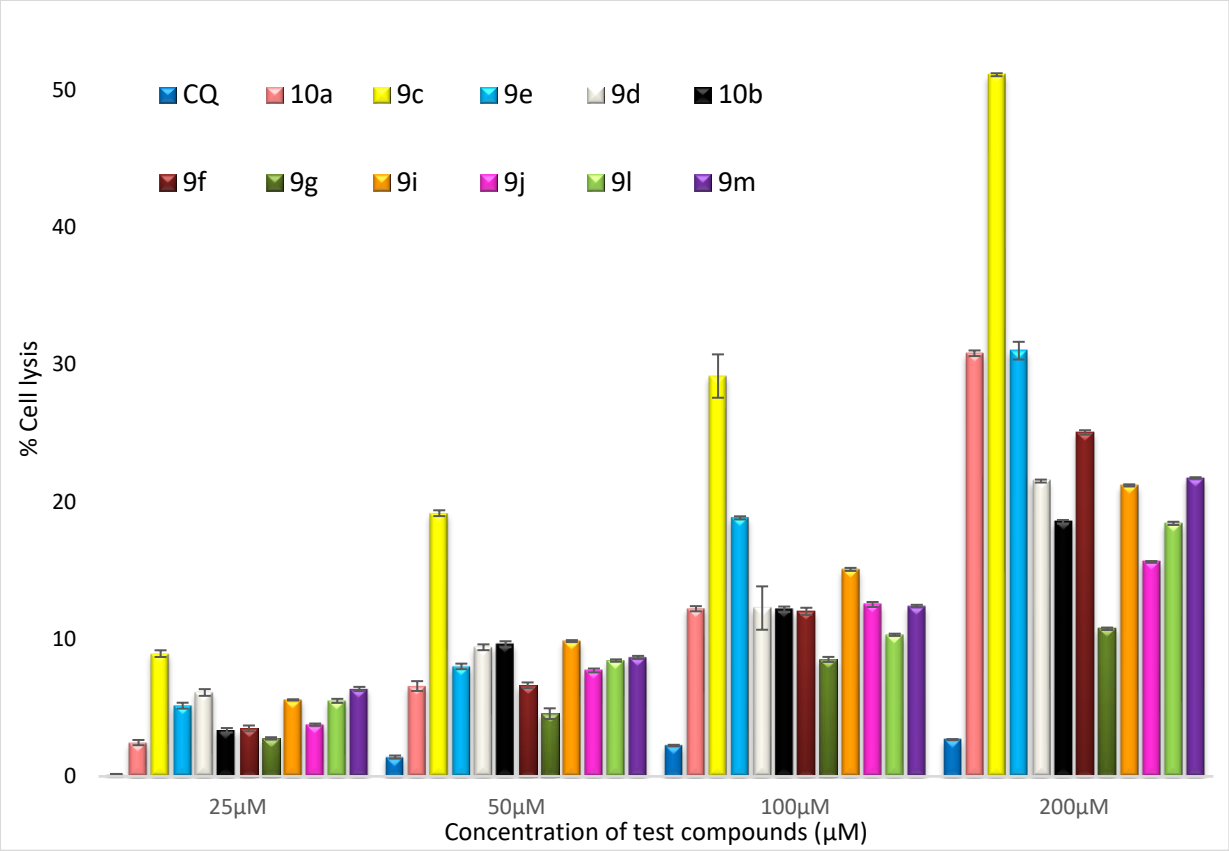

Figure S69: Hemolysis caused by CQ and test compounds. Hemolysis was determined by recording absorption at 450 nm and comparing to hemolysis achieved with 1% Triton X-100 (reference for 100% hemolysis). This data is a mean of triplicate experiments. The student's t-test was used to verify statistical significance ($p < 0.05$).

Table S4: Molecular Dynamics Simulation Details

S.No.	System	No. of Na ions	No. of water molecules	Cubic Box size Length (nm)	Total simulation time (ns)	Number of core used for simulation
1.	4BBH	2	43831	11.24	100	32
2.	4BBH_9a	2	43832	11.24	100	64
3.	4BBH_E	1	43831	11.24	100	64

Hardware Configuration:
Processor: Intel Skylake (Intel(R) Xeon(R) Gold 6130 CPU @ 2.10GHz), 32 Cores per node
RAM: 96GB
Graphics: MGA-G200 graphics chi
Operating System: CentOS Linux release 7.9.2009 (Core)